Thermophoresis of synthetic and biological systems

Inaugural-Dissertation

zur

Erlangung des Doktorgrades

der Mathematisch-Naturwissenschaftlichen Fakultät

der Universität zu Köln

vorgelegt von

Zilin Wang

aus Xuzhou

Berichterstatter:	Prof. Dr. A. Schmidt
(Gutachter)	PD Dr. S. Wiegand

Tag der mündlichen Prüfung: 08.07.2014

ABSTRACT

This work focuses on the thermal diffusion behavior of biological and synthetic bio-compatible systems using a holographic grating technique Thermal Diffusion Forced Rayleigh Scattering (TDFRS). Most biological systems are water-based and the thermodiffusion behavior of aqueous systems is less understood than organic systems, which can often be described by empirical correlations. Therefore, our study focuses on the investigation of four different aqueous systems in order to get a deeper microscopic understanding of the thermophoretic behavior. The thesis starts with small bio-molecules nucleotides, the building blocks of nucleic acids. Five nucleotides with systematically varied structures are investigated to make the connections between the thermodiffusion and their physical properties such as acidity, solubility, hydrophobicity and their capability to form hydrogen bonds. We find a correlation between the thermal diffusion coefficient and the ratio of the thermal expansion coefficient and the kinematic viscosity. Besides the capability to form hydrogen bonds, the charge effect is another important parameter that complicates the situation in aqueous systems. In this context aqueous electrolyte solutions are a simple model system, which can be investigated by computer simulations and experimentally. We study alkali halide aqueous solutions ($Na^+/K^+ - Cl^-$) by both non-equilibrium molecular dynamics simulations and TDFRS measurements. We find that the Soret coefficient decreases with increasing concentration at temperatures higher than 315 K, whereas it increases at lower temperatures. In agreement with previous experiments, we find a sign inversion. We use computer simulations as a microscopic approach to establish a correlation between sign and magnitude of the Soret coefficient and ionic solvation and hydrogen bond structure of the solutions. Additionally, the analysis of heat transport in ionic solutions by quantifying the thermal conductivity as a function of concentration is provided. The simulations accurately reproduce the decrease of

the thermal conductivity with increasing salt concentration that is observed in experiments. Charged colloids and proteins in aqueous electrolyte solutions are always surrounded by an electric double layer. Their contribution to the thermodiffusion of colloids and proteins have also to be considered. We investigate the charge effect using a charge stabilized rod-like colloid (*fd*-virus), which can be modeled theoretically. The Soret coefficient of the charged rods is measured as a function of the Debye screening length, as well as the rod-concentration. The Soret coefficient of the rods increases monotonically with increasing Debye length, while there is a relatively weak dependence on the rod-concentration when the ionic strength is kept constant. An existing theory for thermodiffusion of charged spheres is extended to describe the thermodiffusion of long and thin charged rods, leading to an expression for the Soret coefficient in terms of the Debye length, the rod-core dimensions, and the surface charge density. The thermal diffusion coefficient of a charged colloidal rod is shown to be accurately represented, for arbitrary Debye lengths, by the thermal diffusion coefficient of a superposition of spherical beads with the same diameter and the same surface charge density as the colloidal rod. Additionally, a *fd*-virus grafted with a water soluble polymer polyethylene oxide (PEO) is investigated as a function of ionic strength. For a low ionic strength corresponding to a large Debye length we find the same behavior as in the case of the bare virus, while with increasing ionic strength the Soret coefficient increases, which is the opposite trend compared to the bare *fd*-virus. PEO is a non-ionic water soluble, biocompatible polymer with the capability to form hydrogen bonds with water. Only low molar mass ethylene oligomer is soluble in ethanol, while water is a good solvent for the whole molar mass range. To study the solvent quality effect we investigate the thermodiffusion of ethylene oxide oligomers and PEO at different temperatures in water, ethanol and in a water/ethanol mixture with a water content of 70% in a molar mass range from monomer up to $M_{\mathrm{w}} = 180000$ g/mol. The specific water/ethanol concentration has been chosen, because the thermal diffusion coefficient of the water/ ethanol mixture vanishes, so that the system can be treated as a pseudo binary mixture. In pure ethanol, a sign change of the Soret and thermal diffusion coefficient as a function of molar mass from positive to negative is found for a molar mass around 2200 g/mol. In water/ethanol mixtures, PEO of all molar masses accumulate at the warm side, while in pure water they all enrich at the cold side. The interaction energies ε_s (solvent-solvent) and ε_p (polymer-solvent) are determined from a theoretical model derived by Würger [*Phys. Rev. Lett.*, **102**, 078302, 2009]. ε_s and ε_p are positive under good solvent conditions and negative otherwise.

KURZZUSAMMENFASSUNG

In dieser Arbeit wird das Thermodiffusionsverhalten von biologischen und synthetischen biokompatiblen Systemen mit einer holographischen Gittertechnik, der sogenannten *Thermal Diffusion Forced Rayleigh Scattering* (TDFRS) Methode untersucht. Die meisten biologischen Systeme enthalten Wasser, wobei gerade das Thermodiffusionsverhalten von wässrigen Systemen schlecht verstanden ist, da es in diesem Fall nicht einmal empirische Zusammenhänge, wie im Fall von organischen Systemen, gibt. In dieser Arbeit untersuchen wir systematisch die Thermodiffusion von vier verschiedenen wässrigen Modellsystemen, um Ansätze für ein besseres mikroskopisches Verständnis zu entwickeln. Im ersten Teil der Arbeit betrachten wir Nukleotide, die die biologischen Bausteine der Nukleinsäuren bilden. Das Thermodiffusionsverhalten von fünf verschiedenen Nukleotiden mit systematisch veränderter Struktur wird experimentell untersucht, um auf diese Weise Korrelationen zwischen dem Thermodiffusionsverhalten und den physikalischen Eigenschaften wie Säuregrad, Löslichkeit und Hydrophobie abzuleiten. Darüber hinaus beobachten wir einen linearen Anstieg des Thermodiffusionskoeffizienten mit dem Verhältnis des Wärmeausdehnungskoeffizienten und der kinematischen Viskosität. Neben der Möglichkeit der Ausbildung von Wasserstoffbrückenbindungen, spielen auch Ladungseffekte eine wichtige Rolle und beeinflussen das Thermodiffusionsverhalten von wässrigen Systemen. Hier stellen die Elektrolytlösungen ein interessantes einfaches Modellsystem da, dass sowohl in Simulationen als auch experimentell untersucht werden kann. Hierzu haben wir wässrige Salzlösungen ($\mathbf{Na^+/K^+ - Cl^-}$) sowohl in Nichtgleichgewichts-Molekulardynamik-Simulationen als auch durch TDFRS-Messungen untersucht. Es zeigt sich, dass für Temperaturen über 315 K der Soretkoeffizient mit zunehmender Konzentration sinkt, während er bei niedrigeren Temperaturen ansteigt. In Übereinstimmung mit älteren Arbeiten zeigt sich eine Vorzeichenumkehr des Soretkoeffizienten.

Die Computersimulationen dienen als mikroskopischer Ansatz, um Korrelationen zwischen dem Vorzeichen und dem Betrag des Soretkoeffizienten mit der Solvatation der Ionen und der Wasserstoffbrückenstruktur der Lösungen zu eruieren. Zusätzlich analysieren wir den Wärmetransport in ionischen Lösungen und bestimmen die Wärmeleitfähigkeit als Funktion der Konzentration. In Übereinstimmung mit den Experimenten beobachten wir auch in den Simulationen eine Abnahme der Wärmeleitfähigkeit mit steigender Salzkonzentration. Geladene Kolloide und Proteine in wässrigen Elektrolytlösungen sind immer von elektrischen Doppelschichten umgeben, deren Beitrag zur Thermodiffusion berücksichtigt werden muss. In diesem Kontext haben wir ladungsstabilisierte stabförmige Kolloide sogenannte *fd*-Viren untersucht, die sich auch theoretisch modellieren lassen. Hierzu haben wir den Soretkoeffizienten des geladenen *fd*-Virus als Funktion der Debye-Länge und der Stäbchenkonzentration bestimmt. Es zeigt sich, dass der Soretkoeffizient der *fd*-Viren monoton mit zunehmender Debye-Länge ansteigt, während er nur eine relativ schwache Abhängigkeit von der Stäbchenkonzentration bei festgehaltener Ionenstärke zeigt. Eine bestehende Theorie, die die Thermodiffusion geladener Kugeln beschreibt, kann entsprechend erweitert werden, um auch die Thermodiffusion von langen und dünnen Stäbchen zu beschreiben. Dieser Ausdruck hängt lediglich von der Debye-Länge, dem Kerndruchmesser und der Oberflächenladungsdichte der Stäbchen ab. Weiter zeigt sich, dass der Thermodiffusionskoeffizient eines geladenen kolloidalen Stäbchens sich für beliebige Doppelschichten als Überlagerung des Thermodiffusionskoeffizienten von Kugeln ausdrücken lässt, deren Durchmesser und Oberflächenladungsdichte mit dem des Stäbchens übereinstimmt. Darüber hinaus haben wir auch das Thermodiffusionsverhalten von *fd*-Viren, die mit niedermolekularen, wasserlöslichen Polyethylenoxidketten (PEO) beschichtet sind, als Funktion der Ionenstärke untersucht. Für eine niedrige Ionenstärke, die einer großen Debye-Länge entspricht, finden wir das gleiche Verhalten wie im Fall des nicht beschichteten Virus. Mit zunehmender Ionenstärke steigt der Soretkoeffizient an und zeigt damit den umgekehrten Trend im Vergleich zum unbeschichteten *fd*-Virus. PEO ist ein nicht-ionisches, wasserlösliches, bio-kompatibles Polymer, das Wasserstoffbrücken ausbildet. Nur niedermolekulare Oligomere sind auch in Ethanol löslich, während Wasser im gesamten Molekulargewichtsbereich ein gutes Lösungsmittel ist. Um den Einfluss der Lösungsmittelqualität auf das Thermodiffusionsverhalten systematisch zu untersuchen, haben wir Ethylenoxidoligomere und PEO bis zu einer Molmasse von $M_w = 180000$ g/mol bei verschiedenen Temperaturen in Wasser, in Ethanol und in einer Wasser/Ethanol-Mischung mit einem Wassergehalt von 70% untersucht. Die Konzentration der Wasser/Ethanol-Mischung wurde so gewählt, dass der Thermodiffusionskoeffizient des Wasser/Ethanol-Gemisches ver-

schwindet und das System als pseudo-binäre Mischung behandelt werden kann. In reinem Ethanol haben wir einen Vorzeichenwechsel des Soret- und Thermodiffusionskoeffizienten als Funktion der Molmasse bei einer Molmasse von 2200 g/mol von positiv nach negativ beobachtet. In Wasser/Ethanol-Mischungen finden wir für alle Molmassen eine Anreicherung auf der warmen Seite, während wir in reinem Wasser eine Anreicherung auf der kalten Seite beobachten. Weiter zeigt sich, dass die Wechselwirkungsenergien $\boldsymbol{\varepsilon}_s$ (Lösungsmittel-Lösungsmittel) und $\boldsymbol{\varepsilon}_p$ (Polymer-Lösungsmittel) nach einem Modell von Würger [*Phys. Rev. Lett.*, **102**, 078302, 2009] unter guten Lösungsmittelbedingungen positiv und unter schlechten Bedingungen negativ sind.

CONTENTS

CHAPTER

ONE

INTRODUCTION

1.1 Introduction to thermodiffusion

1.1.1 Thermodiffusion and its applications

Thermodiffusion, also known as Ludwig-Soret effect or thermophoresis, describes the mass transport in response to a temperature gradient. For a multi-component fluid mixture under a temperature gradient ∇T, the flux of the solute can be described by:

$$J = -\rho D \nabla c - \rho c(1-c) D_T \nabla T \tag{1.1}$$

where D is the mass diffusion coefficient, D_T the thermal diffusion coefficient, ρ the mass density, and c the mass concentration of the solute. In a stationary state, the flux is counter balanced by the ordinary Fickian diffusion. The ratio of the concentration gradient and the temperature gradient in such stationary state is equal to the Soret coefficient $S_\mathrm{T} = D_\mathrm{T}/D$.

The Soret coefficient quantifies the tendency for a mixture to separate under the thermal gradient.

Since the first observation of the thermodiffusion phenomena by Ludwig more than 150 years ago [53], it has been used in various industrial and scientific applications.

The first mentioned application is the isotope separation demonstrated by Clusius and Dickel in 1939 [17] and in 1944 it was used for uranium isotope separation in the Manhattan Project [77]. Furthermore thermodiffusion influences the distribution of different crude oil components in hydrocarbon reservoirs [32].

In the second half of the twentieth century the effect was utilized in the Thermal Field-Flow Fractionation (Th-FFF) to characterize and fractionate polymers. In this method a temperature gradient is applied perpendicular to a flow. Already in 1967 Thompson *et al.* reported a successful fractionation of polystyrene (PS) [86]. Since then Th-FFF has been applied to many different synthetic polymers and colloids [18, 36, 83]. For big colloidal suspensions a micro-Th-FFF has been developed to shorten the measurement time [43]. The disadvantage of this technique is that for the low molar mass polymers with small thermal diffusion coefficient, a high temperature gradient of the order of 10^6 K/m is required [9].

Recently, applications in life science and modern biotechnology increased the interest in thermophoresis and it has been discussed as a key parameter in the origin of life puzzle [3, 8]. Lately, a new method MicroScale Thermophoresis (MST) emerged, combining the fluorescence microfluidic imaging technique and a temperature gradient. By monitoring the movement of fluorescent molecules as a respond to the temperature gradient [28, 29], biomolecular interactions can be characterized and parameters like binding or dissociation constants can be determined [85, 99].

The applications show that thermodiffusive or thermophoretic processes depend strongly on a variety of molecular properties such as molar mass, size, charge, hydration shell or conformations, but so far there exists no microscopic understanding in fluid mixtures.

1.1.2 Theoretical description and simulations

The first theoretical approach for thermodiffusion was developed for gas mixtures based on kinetic theory [16]. It predicts that the heavier or larger component move to the cold.

However, this theory is a purely kinetic approach and neglects two driving forces. The first one stems from the thermal fluctuations of solute and solvent molecules. The second one relies on the solute-solvent interactions such as electric double layer and dispersion forces. This is mostly relevant for colloidal suspensions and polymer solutions [88].

1.1.2.1 Theoretical concepts: molecular mixture

For molecular mixtures where the components are comparable in size, it is hard to apply hydrodynamics. Therefore, most theories of molecular mixtures are based on the concepts of transport-heat, transport-enthalpy or activation energies related to the mass transport [2, 10, 34]. Based on Haase's work [37], Kempers derived an expression consisting of two terms [45]. The first term is the kinetic term calculated from the kinetic theory of ideal gas state. The other term is the thermodynamic term obtained from an imaginary setup with two connected bulbs containing a mixture. The mass can interchange between bulbs due to the temperature difference. The concentration difference between two bulbs at the steady state is calculated from the maximization of the partition function of the total subsystem. Another method, based on the work of Prigogine *et al.* [73] assumes the activation energy of molecular motion to be the same as the activation energy of viscous flow. Then the self-diffusion activation energy can be calculated by the equilibrium molecular dynamic simulation (EMD). This model gives a good prediction of the sign change of Soret coefficient for water/ethanol mixture, but the values are underestimated [2].

The physics of thermodiffusion in associating mixtures such as alcohol/water systems are much more complicated than in non-associating mixtures due to the presence of the hydrogen bonding and the strong interaction between the alike and unlike molecules. Eslamian and Saghir developed a model that correlates the net heat of transport and the activation energy, then the activation energy is directly obtained from the experimental viscosity data [30]. The same authors used an example of water/alcohol mixture to differentiate associating and non-associating mixtures. Most molecules in the water/alcohol mixture are associated due to the hydrogen bonds, while only a few water and alcohol molecules are isolated. The activation energies needed to move the associated molecules are larger than for the free molecules. The strength of the association depends on the water content of the mixture. Therefore, for non-associating systems, the activation energy depends only on the viscosity, but in aqueous

mixtures the activation energy is proportional to the rate of change in the natural logarithm of mixtures viscosity with respect to concentration [31].

1.1.2.2 Theoretical concepts: colloids

The thermodiffusion of a colloidal suspension consists of two contributions, *i. e.* specific interactions between surface groups of the colloidal particles with the solvent and the inter-colloidal interactions. Inter-colloidal interactions are often neglected for very dilute suspensions and the system can be regarded as a single particle undergoing Brownian motion in a solvent exposed to an external temperature gradient [67].

Bringuier and Bourdon proposed an equation containing two forces between the colloidal particle and the solvent [12]. The first one is a chemical force that pushes the colloid from the place of high to low interaction energy. The second term is the local disequilibrium of the medium induced force, proportional to the temperature gradient, *i.e.* thermophoretic force. In the work of Dhont, expressions of the collective and thermal diffusion coefficient are given on the basis of statistical thermodynamics and force balance on the Brownian time scale. He divided the system into "boxes" and calculate the heat exchange and the work needed to move colloids among neighboring boxes of different temperatures. Note that he described only the concentration dependence of the thermophoresis up to 10% volume fraction, treating the single particle effect as a fitting parameter [22, 23].

Colloids often need to be charge stabilized in polar solvents and it has been experimentally shown that the charge and the electric double layer has a large impact on the thermodiffusion behavior of colloids [61, 66]. The theoretical approaches can be sub-divided into two categories.

Within the first approach the temperature-induced deformation of the electric double layer is neglected [11, 25, 29, 33, 93]. Along this direction, Dhont derived the expression of Soret coefficient based on his work for non-charged colloids [25] and extended this theory for arbitrary double-layer thickness [24]. The theory for thin double layers, where the electric double layer and the charged surface of the colloidal particle are considered analogue as a capacitor has been derived by two other groups, independently [29, 33].

In the second category where the double-layer structure and the resulting flow within the double layer are included. Within the same framework [57,64], a colloidal particle is assumed

to interact with the surrounding solvent and this force can lead to a solvent flow around the colloid. Then the thermophoretic force is considered equal to minus the total force of the colloids acting onto the surrounding fluid plus the friction force resulted from the solvent flow. For charged colloids the force from the electric double has to be considered. This force is related to the surface charge of colloids and the ionic density of the solvent. In the work of Parola and Piazza, it has been found that the linear Debye-Hückel and the Poisson-Boltzmann treatments lead to very different results, which need to be investigated in further experimental studies [64].

In this work we extend a theoretical concept derived for charged spherical colloids [24,61] to very long and thin colloidal rods. This theory predicts that the thermal diffusion coefficient of a rod is equal to that of a spherical bead with a diameter equal to that of the rod-core, and with the same surface charge density, multiplied by the number of beads. Such a superposition of spherical beads to calculate the thermal diffusion coefficient of a rod is valid for arbitrary Debye lengths. So far only rigid rod-like particles have been studied. The role of flexibility of rods on thermodiffusion has not been included in theoretical concepts, but simulations show that the flexibility has an effect [96].

1.1.2.3 Theoretical concepts: polymers

The thermodiffusion effect in polymer solutions has been originally investigated by Brochard and de Gennes [13]. They predicted the independence of thermal diffusion coefficient at infinite dilution on polymer chain length and branching. They argue that for thermodiffusion the long-range interactions between monomers are negligible and therefore a polymer chain could move under a temperature gradient with the same velocity as separated monomer. Later Schimpf and Semenov derived an expression of the thermal diffusion coefficient for very dilute non-polar polymer solutions ignoring all interactions between monomers [84]. This expression is based on the bead-spring model in which the polymer consisting of n beads are connected by springs. The distance between the beads are large enough so that the hydrodynamic interactions between the beads can be neglected. If such a polymer chain moves through a viscous fluid, the effective friction of the whole chain should be proportional to the number of monomers, *i.e.* the molar mass of the polymer.

However, the hydrodynamic approach treats the solvent as a continuous medium and the solute as a macroscopic body. This approach is only applicable for big particles and high

molecular polymers, whose size and gyration radius are much larger than the length scales set by the interaction and by the solvent molecular structure [93]. Würger included in his model the Brownian motion of both solute and solvent [92] and derives the following expression for the thermal diffusion coefficient at infinite dilution:

$$D_T = \frac{\beta \varepsilon_p}{6\pi\eta a} - \frac{\beta \varepsilon_s + (\varepsilon_s - \varepsilon_p)/T}{\kappa \eta R} \tag{1.2}$$

where ε_s and ε_p are the polymer-solvent and solvent-solvent interaction parameters, a is the radius of the monomer and R is the radius of gyration of polymer. For a single bead one can put $\kappa R = 6\pi a$. With increasing R, the second term vanishes, which means the thermal transport of high polymers is only contributed by the solute-solvent interactions. This equation bridges the gap between the single bead model and the macroscopic hydrodynamic model for high polymers.

1.1.2.4 Simulations

In recent years, computer simulations, especially the molecular dynamics (MD) simulations have become a powerful tool in the investigation of thermodiffusion. There are two main categories of MD simulation methods: equilibrium molecular dynamics (EMD) simulations and non-equilibrium methods (NEMD). EMD simulations use Green-Kubo formalism to derive the corresponding transport coefficients of homogeneous systems. The main advantage of EMD is that the properties of systems are well defined. But also because of that, it's not applicable for heterogeneous systems. Furthermore, the simulated systems are not directly related to real experiments with external forces driving the transport process. NEMD methods contain synthetic NEMD (S-NEMD), which works for homogeneous systems, and boundary-driven NEMD (BD-MEND), where the external force stem from perturbation of the system boundaries [38].

There have been several simulations to compute the Soret coefficient in molecular liquid mixtures. Using MD simulation, Zhang and Müller-Plathe compute the concentration and temperature dependence of the Soret coefficient of benzene/cyclohexane mixtures. Their simulations show the same trend as the experimental values an decreasing absolute value of S_T with higher benzene content. However, the magnitude of simulated S_T is too large [97].

Besides organic mixtures, aqueous molecular mixtures also have been simulated. Nieto-

Draghi *et al.* use BD-NEMD computed water/alcohol mixtures and find a sign reversion of Soret coefficient with composition, which is in good agreement with experimental data [59].

It is also possible to simulate big particle system like polymer solutions. Zhang and Müller-Plathe use a bead-spring model to simulate thermodiffusion in dilute polymer solutions by NEMD. A sign change has been observed when the solvent quality switches from good to poor. They also find that the thermal diffusion coefficient of the flexible polymer chain reaches a constant value at a shorter chain length than the rigid polymer, which also corresponds to some experimental data [48, 96].

Many other simulation works also show that computer simulation techniques in the last years enabled extensive systematic investigations, providing a route to the microscopic interpretation of thermodiffusion [1, 72, 94].

1.1.3 Experimental studies

Numerous experimental studies of thermodiffusion have been performed for many different systems *e.g.* polar and non-polar low molecular weight systems, polymer solutions and colloidal suspensions [47, 51, 61, 71]. In the following we will summarize recent relevant studies.

1.1.3.1 Organic system

Organic systems are usually non-polar mixtures with primarily Van-der-Waals interaction. There are some rules of thumb for simple binary mixtures. Typically the heavier or denser component moves to the cold side, and the Soret effect becomes stronger if the mixture is less miscible [89].

One way to vary the physical properties systematically is using isotope substitutions. From the measurements of cyclohexane and its isotope substitutes mixed with other organic compounds, two distinct contributions to the Soret coefficient could be identified. In addition to the contribution stemming from the difference between the molar mass δM and the moment of inertia δI [39, 80], the chemical differences between the two components also used to be considered [21, 91]:

$$S_T = S_T^0 + a_M \delta M + b_I \delta I \tag{1.3}$$

where S_T^0 is shown to be concentration dependent, while the part from the isotopic effect does not depend on concentration. The Soret coefficient of the chemically similar organic mixtures like bromo-/fluoro- and bromo-/chlorobenzene is concentration independent [39], as it is also observed for isotopes. Besides the isotope substances, the study of n−alkane in organic solvent mixtures with different branching indicates a dependence of the Soret coefficient on the difference of moment of inertia between two components [69]. This study shows that with increasing degree of branching the heptane isomers have a stronger tendency to go to the cold side. For this mixture the effect of branching on the Soret coefficient is larger than that of the molar mass [69]. On the other hand, the chemical contribution cannot be easily measured or calculated. Therefore a prediction of thermodiffusion for liquid binary mixtures using Eq. 1.3 is not straightforward.

In a benchmark test the three binary mixtures of a heavier n−alkane, a one-ring and a two-ring organic compound have been investigated by various methods [68]. For these mixtures the component with the largest density moves to the cold side, but not the one with largest mass. However, so far even for these simple liquid mixtures without specific interactions there is no clear relation between the Soret coefficient and physical properties.

1.1.3.2 Aqueous system

The situation becomes more complicated for aqueous system, where specific interactions like hydrogen bond, polarity or charge effect take place. The simple aqueous mixture ethanol/water is a well known example. The water molecules move to the cold side at water weight fractions below 0.7 and a sign change occurs at higher water fractions. This sign change occurs for all temperatures at the same concentration [47, 50]. Sign changes as function of concentration occur also for many other aqueous mixtures containing organic compounds such as methanol, acetone, DMSO or isopropanol [62, 71]. Also aqueous electrolyte solutions with NaCl or KCl [35] show a sign change of the thermodiffusion behavior and a minimum of the Soret coefficient. In contrast to ethanol/water mixture, the sign change concentration for electrolyte solutions varies with temperature and so does the position of the minimum [35].

Contrary to the organic mixtures, there is no clear correlation between thermodiffusion behavior and the molecular structure for aqueous systems. Some of aqueous monosaccharide solution show a trend with their molecular structure, but not all. For the low concentration

a linear dependence of S_T on the ratio of the thermal expansion coefficient and the kinematic viscosity of different saccharides is found. For higher concentration deviations from the linear behavior are observed due to the interaction between saccharide molecules [5].

1.1.3.3 Polymers and colloids

In contrast to simple liquid mixtures, Brownian motion and hydrodynamic interactions are important for polymer solutions and colloidal dispersions.

For the thermophoresis of polymer many studies focus on the independence of D_T on the chain length of polymers [15, 76, 89]. The first systematic demonstration of this independence is a study of 17 different polymer-solvent systems by ThFFF [83]. This independence is confirmed not only by polymers in organic solvents such as polystyrene (PS) in ethyl acetate [79] or in ethyl benzene [82], but also by the water soluble polymer poly(ethylene oxide) (PEO) [15,48]. Nonetheless another study of PS in toluene shows that the molar mass independence of D_T holds only for polymers with more than 10 repeating units due to the influence of the end groups [76].

Besides the molar mass effect, another important aspect of thermodiffusion of polymers is their dependence on solvent properties. Hartung *et al.* studied PS in several different solvents and found that D_T is inversely proportional to the solvent viscosity [41], which cannot be found for low molecular mixtures. Another study of PEO in water/ethanol solvents shows a sign change of S_T from negative to positive with increasing water content, due to the fact that water is a better solvent than ethanol for PEO [47]. Often the accumulation of polymers at the cold side corresponds to a good solvent quality.

For colloidal suspensions the surface properties of particles are important. Colloids can either be stabilized by an electric double layer or sterically by surface grafting. In both scenarios we observe an influence on the thermodiffusion behavior of particles. There have been several systematic studies of the charge dependence [29, 61, 65]. For instance a study of spherical PS particles in water shows an increase of S_T with increasing Debye length and PS spheres move to the cold side [29]. In another study of Ludox silica particles in water the particles tend to go to the warm side and the absolute value of S_T decreases with increasing Debye length [61]. Besides the study of spherical particles, charge effect on the thermodiffusion of rod-like particles mutant *fd*-virus have been investigated as well. The results show a sign

change of S_T at low ionic strength of solution at low temperature [4], which leads to another interesting and common feature of thermodiffusion in aqueous systems, the temperature dependence.

The temperature dependence of the thermodiffusion has been extensively studied for proteins [42], polymers [46] and colloids [75]. The general temperature trend is that particles diffuse to the cold region if the temperature is sufficiently high and they turn to the warm side if the temperature decreases to a certain temperature T_{inv}. This dependence can be described by an empirical equation proposed by Iacopini and Piazza [42]:

$$S_T(T) = S_T^{\infty}\left[1 - \exp\left(\frac{T_{inv} - T}{T_0}\right)\right] \tag{1.4}$$

Here S_T^{∞} is the saturation value of S_T at high temperatures, T_{inv} is the temperature at which the sign inversion occurs, T_0 indicates the degree of the temperature dependence. The observation of this temperature dependence is especially interesting for bio-molecules since the general temperature always plays an important role in biological functions.

1.2 Method

1.2.1 Experimental methods: Overview

Over decades according to various demands like to reach large separation ratio or to serve as analytical purpose, different experimental methods have been developed. Depending on their working principles, these methods can be divided into convective and convection-free.

1.2.1.1 Convective method

One example of a convective method is a thermogravitational (TG) column. A TG column can consist two vertical concentric cylinders with an annular gap filled with a gaseous or fluid mixture. From the inner and outer walls a temperature gradient can be applied across the gap. An overlaying convection which drives the gas or liquid at the hot wall to the top and at the cold wall to the bottom enhances the separation ratio if the denser component

of the mixture diffuses to the cold side. For some mixtures like cyclohexane/toluene, the concentration density gradient is opposite to the temperature density gradient and only a poor separation ratio can be achieved [89]. The sample is withdrawn from several taps placed along the column and analyzed in order to determine the concentration as a function of height. To do the analysis a concentration curve for a property such as density or refractive index have to be measured independently. If two properties are known, it is possible to analyze also ternary systems [6]. Furthermore a TG microcolumn with an interferometric contactless detection system has been developed [58]. It reduces the required sample amount from several milliliters to 50 μL and allows a continuous analysis of the concentration profile by measuring the phase difference between two different heights. Disadvantages of TG technique is the long equilibration time of several hours even for low molecular mixture and only D_{T} can be determined.

1.2.1.2 Non-convective methods

Often the non-convective methods are combined with an optical detection system. The classical experimental configurations are thermal diffusion cells and thermal lens setup.

A conventional thermal diffusion cell is heated from above and cooled from below and the concentration changes induced by the temperature gradient can be probed by the deflection of a laser beam [51, 95]. Using an additional read-out beam with another wavelength, it is possible to investigate ternary mixtures by using the dispersion of two laser beams [52]. The time to reach steady state is determined by the thickness of the gap, which is typically 1-2 mm and limited by the beam waist of the focused laser beam. This results in equilibrium time of several hours for low molecular weight mixtures, which is fairly high, and requires an excellent temperature stability. Due to the limited angular range of the deflected beam, this technique works better with aqueous suspensions with rather low thermal expansion coefficient than in organic mixtures [67].

In contrast to the thermal diffusion cell with boundary heating and cooling, there are also methods, which use the laser beam for heating and detection simultaneously. The thermal lens method belongs to this group of experiments and has a very simple optical design. A focused laser creates a thermal lens due to partial absorption by the sample cell. In a mixture due to the Soret effect additionally an heterogeneous concentration profile is generated. Both process the temperature and the concentration change due to the thermodiffusion

alter the refractive index profile in the sample cell, which influence the laser beam. By detecting changes of the central beam intensity, the Soret coefficient and the thermal diffusion coefficient can be determined [67,89]. The thermal lens method is a fairly fast and inexpensive method. On the other hand, its high sensitivity to convection makes it impossible to measure very slow diffusing particles, for which the convection happens before the equilibration time is reached. Another problem is the astigmatism resulted distortion of the probing beam, which makes the analysis very difficult. There are some other variations of thermal lens method, which use a laser for writing the lens and another laser for detecting [14].

As mentioned in Sec. 1.1.1 the fluorescence microscopy has been developed, which makes the single-particle tracking of fluorescent labeled particles possible. The temperature gradient is generated by focusing an IR laser on a microfluidic channel and the movements of the fluorescent labeled particles are recorded by a microscope [29]. Thanks to the high sensitivity of the fluorescent detection, even extremely low sample concentrations can be detected. Due to the fact that only the labeled particles are visible, multi-component mixtures such as buffered solutions can be investigated. However, this method works only for particles that are intrinsically fluorescent or fluorescently labeled. The fluorescence dyes are usually quite big molecules, therefore this method cannot be applied to low molecular weight solutions. Furthermore bleaching is a common problem for fluorescence dyes and accurately monitoring of the temperature profile is difficult and necessary in order to obtain quantitative results.

The method used in this work is the Thermal Diffusion Forced Rayleigh Scattering (TDFRS) technique, which is a holographic grating technique. The working principle and setup details will be discussed in Sec. 1.2.2. Compared to the above mentioned methods, this technique is suitable for low molecular weight mixtures and colloidal particles up to 100 nm. As the measured quantity in this method is the refractive index change, it's sensitive to every component in the solution. Therefore it is difficult to measure multi-component mixtures unless the size scale or diffusion velocity of components differ by orders of magnitude or two read out beams with different wavelengths are used.

1.2.2 Description of the used setup IR-TDFRS

1.2.2.1 Working principle

The experimental setup used in this work is Thermal Diffusion Forced Rayleigh Scattering (TDFRS). The schematic illustration of the setup is shown in Fig. 1.1. The basic principle of a TDFRS, is to generate a vertical intensity and thereby temperature grating inside the sample volume by interference of two laser beams. This is technically realized by splitting up one laser beam into two beams which intersect inside the sample cell. An interference grating created by the intersection of two split laser beams is directly converted into a temperature gradient due to the absorption of the laser light. In the classical TDFRS an inert dye is used to reach a sufficient absorption. The setup used in this work uses an infrared laser (980 nm) as writing beam which is absorbed by water without the requirement of additional dye. The absorption generated temperature grating causes in turn a concentration grating by the effect of thermodiffusion. Both gratings contribute to the induced refractive index grating, which is read out by the diffraction of a HeNe laser beam (632.8 nm). The diffracted intensity of HeNe laser is detected by an avalanche diode.

In order to determine the grating vector, the Excitation function is measured by reflecting a small fraction ($< 10\%$) of the IR beam with semitransparent mirror in front of the sample cell. The reflected beams interfere at a reticle and the interference grating gets optically magnified by a microscope objective. The magnified light grating and the magnified reticle are mapped by the camera. Another partially reflecting mirror is placed behind the objective which reflects approximately 10% of the light to a fiber coupler connected with another avalanche diode.

The sample cell is fixed in a custom built cell-holder which is thermostated with a stability of 0.1 K by an external thermostat. The temperature is measured inside the holder by a PT100 temperature sensor and the thermostat can be controlled by the measurement software.

The measured quantity of TDFRS is the heterodyne diffraction intensity of the read out beam. The working principle in detail can be found in literature [49]. The normalized heterodyne scattering intensity $\zeta_{\mathrm{het}}(t)$, assuming an ideal excitation with a step function, is

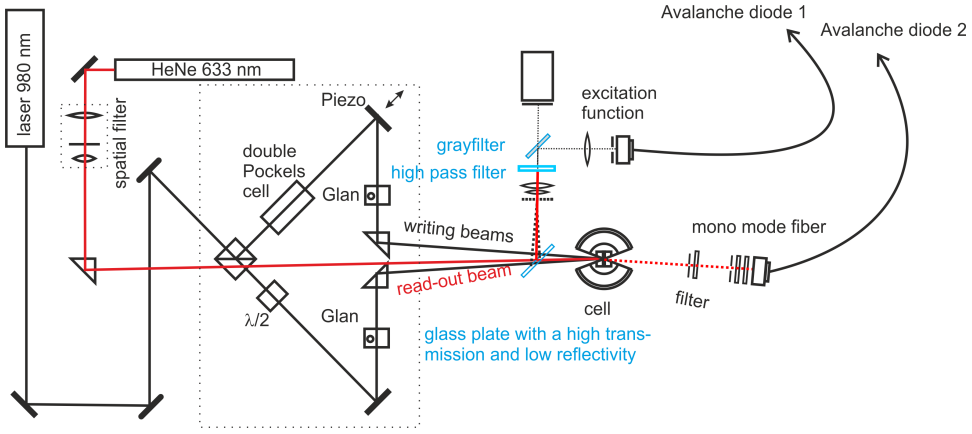

Figure 1.1: *Schematic drawing of an IR Thermal Diffusion Forced Rayleigh Scattering setup.*

given by

$$\zeta_{\text{het}}(t) = 1 - \exp\left(-\frac{t}{\tau_{\text{th}}}\right) - A(\tau - \tau_{\text{th}})^{-1}$$
$$\left\{\tau\left[1 - \exp\left(-\frac{t}{\tau}\right)\right] - \tau_{\text{th}}\left[1 - \exp\left(-\frac{t}{\tau_{\text{th}}}\right)\right]\right\}$$

with the steady state amplitude A

$$A = \left(\frac{\partial n}{\partial c}\right)_{p,T}\left(\frac{\partial n}{\partial T}\right)_{p,c}^{-1} S_{\text{T}} c(1-c) \tag{1.5}$$

where c is the mass fraction, τ_{th} the heat diffusion time, τ the mass diffusion time, $(\partial n/\partial c)_{p,T}$ and $(\partial n/\partial T)_{p,c}$ are refractive index contrast factors with respect to mass concentration at constant pressure and temperature, and referring to temperature at constant pressure and mass concentration, respectively.

The equilibration time for the temperature grating τ_{th} can be used to calculate the thermal diffusivity, $D_{\text{th}} = \kappa/\rho c_p$, which describes the heat transport in the solution, and corresponds to the ratio of the thermal conductivity, κ, over the product of density, ρ, and specific heat capacity at constant pressure, c_p.

The mass diffusion coefficient can be calculated from the relaxation time of the concentration signal τ and the grating vector q.

$$D = \frac{1}{\tau_c q^2} \tag{1.6}$$

1.2.2.2 Contrast factors

The refractive index contrast factors $(\partial n/\partial c)_{p,T}$ and $(\partial n/\partial T)_{p,c}$ are the refractive index change with respect to mass concentration at constant pressure and temperature, and with respect to temperature at constant pressure and mass concentration, respectively. They are measured separately. $(\partial n/\partial c)_{p,T}$ is determined by taking the slope of the linear interpolation of refractive index as a function of concentration of at least 3 samples with concentrations around the desired concentration. All the refractive indices are measured by an Abbe refractometer. The refractive index increments with temperature $(\partial n/\partial T)_{p,c}$ is measured interferometrically, in a temperature range of 1 K around the temperature of interest.

1.3 Outline of the thesis

In this thesis we investigated four different systems nucleotides, salts, a rod-like colloidal model system and a bio-compatible polymer.

As mentioned above, thermodiffusion has been applied to many biological systems. In the prebiotic evolution, high concentrations of nucleotide monomer are necessary for the formation of biopolymers like DNA or RNA. Recent experiments have simulated the scenario of natural thermophoretic setting in pores of rocks near hot springs on the floor of the ocean [7,8]. It is shown that by the effect of spatially confined thermal gradient and convection, the polymerization can be initiated [56].

The molecular evolution is driven by a combination of various effects. It is important to study separately the thermodiffusion behavior of the nucleotide monomers. As building blocks of nucleic acids, nucleotides contain nitrogenous base, a five-carbon sugar, and one or more phosphate groups. The polarity and hydrophobicity of nucleotides depend on the base and the number of phosphate groups, which allows a systematic study as a function of their structures. Furthermore, nucleotides dissociate with water, so that their surface charge depend on the pH value of the solution. It has been shown that the thermodiffusion

behavior of synthetic particles are influenced by surface charge [60]. The open question here is, for such small bio-molecules like nucleotides whether the surface charge also plays a role in thermodiffusion.

Besides changing the pH value of the solution, adding salt is often used to tune the surface charge of colloids. NaCl and KCl as monovalent water soluble salt are the most common choices. As shown in previous studies [19, 35], salts themselves have also strong thermophoretic effect. Therefore, it is necessary to understand their thermodiffusion behavior and the concentration and temperature dependence of it. Furthermore, salts associate in water, but don't form hydrogen bond with water. They are good models to investigate the role that water plays in determining the thermophoretic response of solutions and suspensions, especially with the help of computer simulations.

The *fd*-virus is widely used as mono-disperse model systems for colloidal rods. The wild type *fd*-virus has a molecular weight of 1.64×10^7 g/mol, a contour length L of 880 nm, a radius a of 3.4 nm, and persistence length L_P of 2.2 μm. Due to the high aspect ratio, various liquid-crystalline phases can be observed. Above pH 4 these particles are negatively charged and interact via a combination of electrostatic repulsion and hard-core interactions. The net surface charge can be increased or decreased by increasing or decreasing the solution pH, respectively. Each virus consists of a single-stranded DNA molecule of 2700 copies of coat proteins. With the surface amino groups of the coat proteins polymers with modified end such as N-hydroxysuccinimide (NHS) esters, isothiocyanates and aldehydes can be grafted onto the virus [98]. By grafting polymers, the surface property of *fd*-virus is changed. If the grafting polymers are neutral, the interaction of *fd*-virus with water change from electric to steric. Using this model system we were able to study the thermodiffusion of rod-like colloids with different surface properties and build theoretical models including charge and steric effects.

Synthetic polymers are often used as steric stabilizer for colloidal suspensions. Especially those which are bio-compatible can be used for protein surface modification and drug delivery. It has been found that the average temperature difference between nucleus and cytoplasm is 0.96 °C for many cell samples and this temperature difference is related to fundamental cellular processes [63]. Therefore investigation of thermodiffusion behavior of bio-compatible polymers needs to be included in order to understand processes in the cell. In this work we studied the thermodiffusion behavior of the water soluble polymer poly(ethylene oxide) (PEO), which is also used in *fd*-virus grafting as mentioned above.

CHAPTER

TWO

THERMAL DIFFUSION OF NUCLEOTIDES

THE JOURNAL OF PHYSICAL CHEMISTRY B

Article

pubs.acs.org/JPCB

Thermal Diffusion of Nucleotides

Zilin Wang,* Hartmut Kriegs, and Simone Wiegand*

ICS-Soft Condensed Matter, Forschungszentrum Jülich GmbH, D-52428 Jülich, Germany

ABSTRACT: We investigate the thermal diffusion behavior of aqueous solutions of nucleotides using an infrared thermal diffusion forced Rayleigh scattering (IR-TDFRS) setup. In this work we study 5 nucleotides: cyclic nucleotides adenosine and guanosine monophosphate, 5′-adenosine and 5′-cytidine monophosphate, and also adenosine diphosphate in water. The structures of nucleotides vary systematically, which results in different physical properties such as acidity, solubility, hydrophobicity, and melting point. We discuss the connection between the thermal diffusion behavior and the properties of the different nucleotides. Additionally, as in the case of the alkanes and monoscaccharides, we find a correlation between the thermal diffusion coefficient and the ratio of the thermal expansion coefficient and the kinematic viscosity.

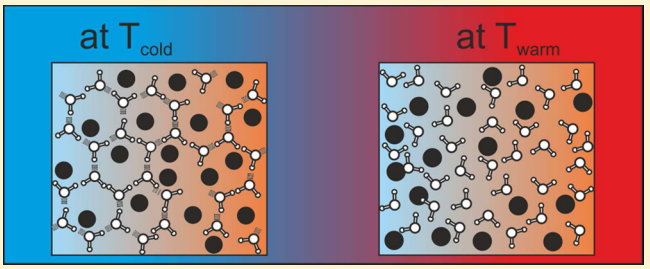

INTRODUCTION

Thermal diffusion, i.e., the mass transport caused by a temperature gradient, influences many processes in multicomponent systems. Lately, the effect has been used in the analysis of protein interactions.[1] But it is also used in polymer analysis and plays an important role in the distribution of crude oil components in geological fields. Recent simulations suggest that nucleotides and nucleic acid oligomers can be concentrated in prebiotic deep-sea alkaline vents by means of the thermal gradients originated between the warm volcanic rock and cold ocean water.[2] Further, it has experimentally been demonstrated that protocells like vesicles can be concentrated in narrow channels with a thermogravitational configuration;[3] i.e., the thermal gradient is applied perpendicular to the gravity field into a vertical narrow cavity. A microthermal focusing field flow fractionation technique has been used to separate different bacteria.[4] Braun and co-workers found that DNA molecules can be trapped by means of thermal diffusion[5] and that DNA self-replicates in a temperature gradient.[6] An all-optical microfluidic fluorescence method has been used to determine the thermal diffusion properties of DNA.[7,8]

For many biological and synthetic systems the influence of charge by varying salt concentration or pH has been experimentally studied[9−12] and theoretically analyzed.[13−15] For all systems studied so far an increase of the Soret coefficient, S_T, with increasing Debye length, λ_{DH}, has been found. Although there has been a lot of research activities on aqueous synthetic and biological systems, there are still many open questions.

We still lack a microscopic description which relates shape, size, charge and hydration shell of the molecules to the thermal diffusion properties of aqueous systems, in a similar way as it has been done for alkane.[16] First systematic studies on the thermal diffusion behavior of aqueous systems have been performed for aqueous solutions of mono- and oligosaccharides.[17,18] Some important results for the monosaccharides are that the thermal diffusion coefficient, D_T, increases linearly with the ratio of the thermal expansion coefficient and the kinematic viscosity,[17] and D_T decreases with increasing sugar length and approaches a plateau value.[18]

Although empirical correlations between the thermal diffusion properties of nonpolar organic mixtures and the structure and size of the constituents are known,[16,19,20] those concepts fail for aqueous mixtures. The only correlation, which has been found also for some aqueous mixtures is the linear dependence of D_T on the ratio of the thermal expansion coefficient and the viscosity. Moreover, a universal temperature dependence of the Soret coefficient has been found for many aqueous systems[9,21] except for poly(*N*-isopropylacrylamide) in water. For many system the temperature dependence of the Soret coefficient can be described by an empirical law,[9]

$$S_T(T) = S_T^{\infty}\left[1 - \exp\left(\frac{T^* - T}{T_0}\right)\right] \quad (1)$$

with the parameters S_T^{∞}, T^*, and T_0.

We assume that the physical mechanism behind this universal temperature dependence of S_T is related to the formation of hydrogen bonds in aqueous solutions. In order to gain better intuitive feeling for this observation, we try to adopt a free energy minimization concept, which is often used to explain the closed loop phase diagrams under isothermal conditions to this nonisothermal condition. Strictly speaking, a free energy is not defined under nonisothermal conditions. However, experimental and theoretical studies have shown that local thermodynamic equilibrium can be successfully applied to describe thermophoresis.[22,23] As illustrated in Figure 1a, the system can locally minimize its free energy $F = U - TS$ by the

Received: April 5, 2012
Revised: May 22, 2012
Published: June 4, 2012

   dx.doi.org/10.1021/jp3032644 | *J. Phys. Chem. B* 2012, 116, 7463−7469

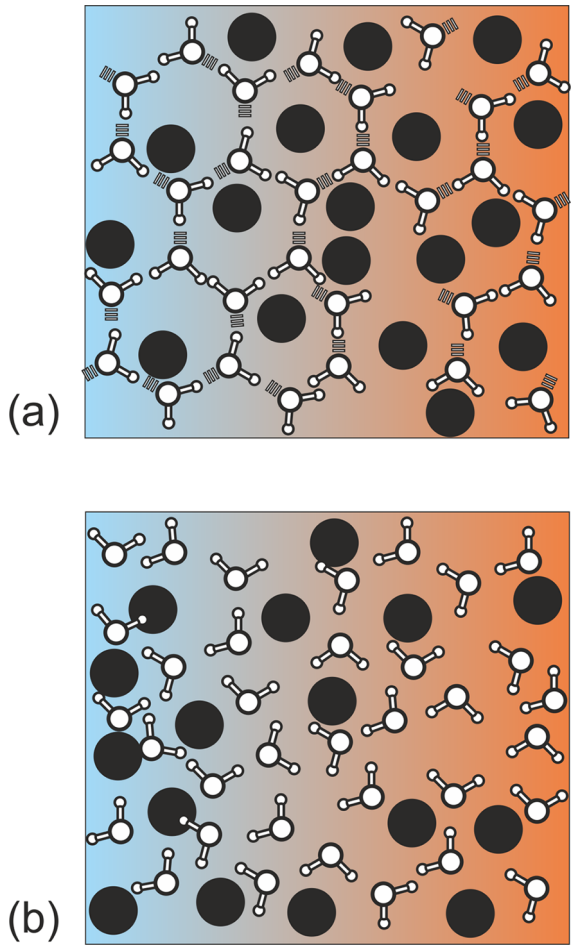

Figure 1. (a) At low overall temperatures the system reduces inner energy by forming hydrogen bonds on the cold side. (b) At higher overall temperatures, the system minimizes free energy by increasing the translational and orientational entropy.

formation of hydrogen bonds, so that at lower overall temperature the water molecules accumulate on the cold side and the solute molecules on the warm side. At high overall temperatures the energy gain due to the formation of hydrogen bonds becomes less important, therefore the system minimizes its free energy by maximizing the orientational entropy as illustrated in Figure 1b. Thus, it is favorable for the small water molecules to be on the warm side in order to maximize their orientational and translational entropy. The influence of hydrogen bonds on the thermodiffusive properties has also been used to explain sign changes of the thermophoretic motion in aqueous solutions and binary mixtures.[24,25] In these studies, a direct correlation between the breakdown of the hydrogen bond network and the sign change concentration has been observed.

Studying the thermal diffusion behavior of nucleotides, which are the building blocks of DNA and RNA is another important step toward a better understanding of biological systems and to validate the hypothesis that thermal gradients are essential for the origin of life. On the basis of the phosphorylated nucleoside structure, the conformation of nucleotides can be varied by the chain length of phosphate and the type of bases. The study of nucleotides in aqueous solution is of particular interest since it offers the possibility to tune the number of charges on the molecules[26] or the base ring-phosphate interactions by changing the pH value.[27] NMR studies show that a decreasing pH, which causes deprotonation of phosphate, increases the probability for the *anti* conformation of 5′-adenosine monophosphate (AMP). On the other hand, a temperature change also affects the conformation.[27,28] Unfortunately, the nucleotides cannot not be modified so systematically in their shape variation, and the variety of the nucleotides is much larger compared to the saccharides. An additional important aspect for the investigation of nucleotides is the presence of charges, so that we can study charge effects on a low molecular weight level, which will also influence the thermal diffusion behavior of large biomolecules such as DNA and proteins.

In this work we investigate the thermal diffusion phenomena of cyclic nucleotides adenosine and guanosine monophosphate (cAMP and cGMP), 5′-adenosine and 5′-cytidine monophosphate (AMP and GMP) and also adenosine diphosphate (ADP) in water. For all five systems we perform temperature and pH dependent measurements of the thermal diffusion properties with the infrared thermal diffusion forced Rayleigh setup (IR-TDFRS). Additionally, we perform also temperature dependent density measurements to examine the correlation between the thermal diffusion coefficient and the ratio of the thermal expansion coefficient and the viscosity.The structures are shown in Figure 2.

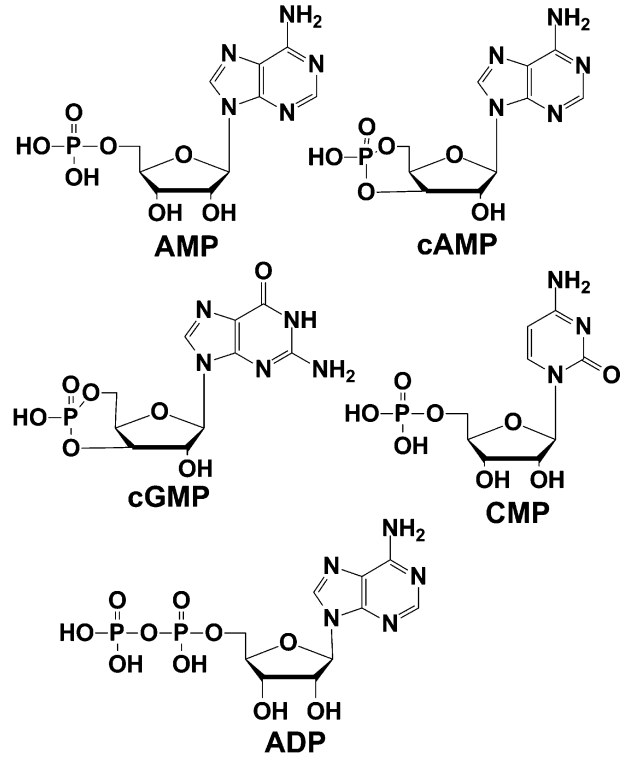

Figure 2. Structure of investigated nucleotides.

EXPERIMENTAL SECTION

Sample Preparation and Characterization. cAMP (≥98.5%), AMP(≥97%), cGMP(≥98%), ADP(≥95%), and CMP(≥99%) were purchased from Sigma-Aldrich and were used without further purification. Deionized water from a Millipore filter unit (0.22 μm) was used to prepare all aqueous solutions.

dx.doi.org/10.1021/jp3032644 | J. Phys. Chem. B 2012, 116, 7463−7469

Approximately 2 mL of the prepared solutions were filtered through a 0.2 μm filter (Whatman Anotop 10) before filling them into an optical quartz cell (Hellma) with an optical path length of 0.2 mm. At least two measurements with different cells and freshly prepared samples were done for each system.

The refractive index increments with the mass concentration $(\partial n/\partial c)_{p,T}$ was measured by an Anton Paar RXA 156 refractometer, whose accuracy is 0.00002 nD with a temperature control of $\Delta T = \pm 0.03$K. For each nucleotide, the refractive index has been measured for at least three concentrations around the desired concentration. The slope of the linear interpolation of the refractive index as a function of the concentration gives $(\partial n/\partial c)_{p,T}$. The refractive index increments with temperature $(\partial n/\partial T)_{p,c}$ was measured interferometrically,[29] in a temperature range of 1 K around the temperature of interest. The refractive index varied linearly with temperature and concentration in the investigated range. The refractometer uses the sodium line with a wavelength of 589.3 nm, which is roughly 40 nm shorter than the HeNe-laser of 632.8 nm used as read-out beam in the IR-TDFRS. This causes a small systematic error in the refractive index increment in the order of 0.5−1%.[30,31]

All measurements are performed in the temperature range of 30 and 70 °C, since below 30 °C the solubility of the nucleotides is too low to get a good signal and above 70 °C the nucleotides start to decompose.

Infrared Thermal Diffusion Forced Rayleigh Scattering. A detailed description of the recently modified IR-TDFRS can be found in the paper by Blanco et al.[12] This setup is optimized for aqueous systems and has been used to study the transport properties in different aqueous systems of nonionic surfactants,[32,33] saccharide solutions[17,18] and anisotropic biocolloids.[12]

The normalized heterodyne scattering intensity $\zeta_{het}(t)$, assuming an ideal excitation with a step function, is given by

$$\zeta_{het}(t) = 1 - \exp\left(-\frac{t}{\tau_{th}}\right) - A(\tau - \tau_{th})^{-1} \left\{\tau\left[1 - \exp\left(-\frac{t}{\tau}\right)\right] - \tau_{th}\left[1 - \exp\left(-\frac{t}{\tau_{th}}\right)\right]\right\} \quad (2)$$

with the steady state amplitude A

$$A = \left(\frac{\partial n}{\partial c}\right)_{p,T}\left(\frac{\partial n}{\partial T}\right)_{p,c}^{-1} S_T c(1-c) \quad (3)$$

where c is the mass fraction, τ_{th} the heat diffusion time, and $(\partial n/\partial c)_{p,T}$ and $(\partial n/\partial T)_{p,c}$ are refractive index contrast factors with respect to mass concentration at constant pressure and temperature and referring to temperature at constant pressure and mass concentration, respectively. The equilibration time for the temperature grating τ_{th} can be used to calculate the thermal diffusivity, D_{th}, which describes the heat transport in the solution. It is related to the thermal conductivity, κ, specific heat capacity, c_p and density, ρ by

$$D_{th} = \frac{\kappa}{\rho c_p} \quad (4)$$

The Soret coefficient, $S_T = D_T/D$, can be expressed as ratio of the thermal diffusion coefficient, D_T, and the collective diffusion coefficient, D. Whereas the diffusion coefficient $D = 1/(q^2\tau)$ can be calculated from the diffusion time, τ (cf. eq 2), using the magnitude of the grating vector q, which is given by $q = (4\pi)/\lambda_w \cdot \sin(\theta/2)$. Here θ is the angle between the two writing beams and λ_w is the wavelength of the laser beam. The transport coefficients are determined by fitting eq 2 to the measured heterodyne signal and deconvoluting the excitation function.[34,35]

Figure 3 shows the normalized heterodyne signals of only 100 mM TRIS buffer and of cAMP (wt = 0.5%) in 100 mM TRIS buffer. It is obvious that the buffer solution itself contributes to the concentration part of the heterodyne signal. This leads to some uncertainty in the data analysis of the nucleotides in buffer solutions, which makes it difficult to draw significant conclusions. Therefore, we decided to perform all measurements in pure water, which leads to more reliable results. This shows that reproducible measurements of the thermal diffusion behavior by methods, which rely on refractive index contrast, become difficult, if biomolecules are dissolved in buffer or nutrient solutions. In these cases, often methods using fluorescent labeling are superior, but the investigation of nucleotides by fluorescent methods is also a difficult task, because the typical fluorescent marker are comparable in mass and size and will influence the transport properties of the nucleotides. Also methods such as thermogravitational columns, which can handle multicomponent solutions, are not feasible due to fairly large sample volumes in the order of typically 20 mL and the high costs of the nucleotides.

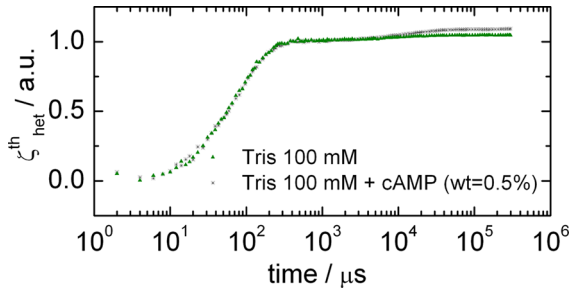

Figure 3. Normalized heterodyne signal ζ^{th}_{het} of TDFRS measurements for 100 mM TRIS buffer and a solution of cAMP (wt = 0.5%) in 100 mM TRIS buffer.

RESULTS AND DISCUSSION

First of all, we discuss the temperature dependence of S_T, D, and D_T for aqueous solutions of various nucleotides, which are shown in Figure 4 in the investigated temperature range. Both diffusion coefficients D and D_T increase with temperature. This indicates that nucleotides diffuse faster at higher temperature, which is related to the decreasing viscosity of water with increasing temperature. S_T, which describes the separation between the nucleotide and water, at first glance shows a weaker temperature dependence compared to DNA and other biomolecules. But actually this is a matter of the regarded temperature range. Looking at the overal trend of the temperature dependence of S_T expressed by eq 1, we find for higher temperatures in general a weaker temperature dependence. As shown in Figure 5, S_T of DNA (6.7 kbp) and one of the nucleotides CMP are both normalized to S_T(30 °C). Although we have only two measured temperatures, which overlap with the temperature range of DNA measurement, it is possible to extrapolate the fitted curve in the high temperature

dx.doi.org/10.1021/jp3032644 | J. Phys. Chem. B 2012, 116, 7463−7469

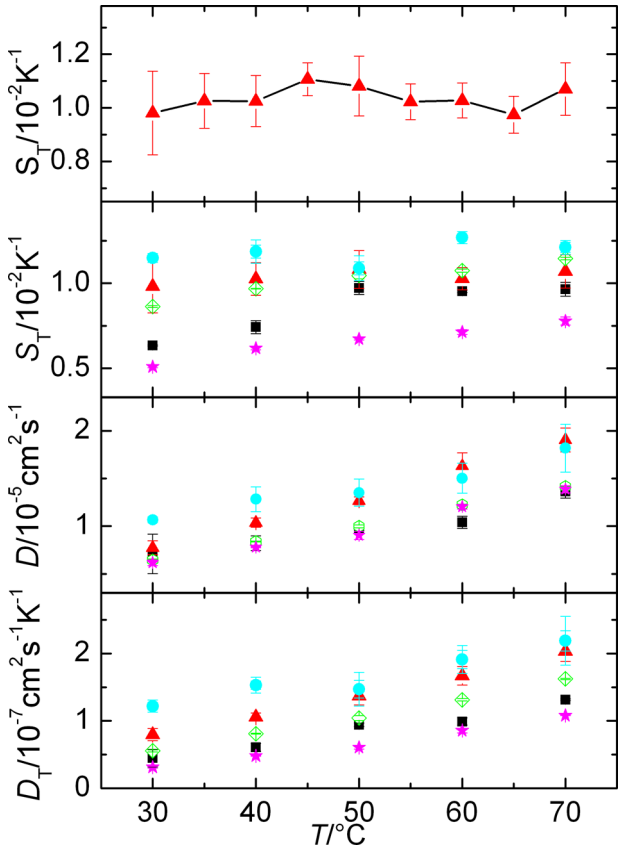

Figure 4. S_T, D, and D_T for CMP (pink star), AMP (black box), cAMP (green diamond), cGMP (red triangle) and ADP (blue circle) with a concentration of 0.5 wt % in water. S_T of cGMP is plotted separately with a better temperature resolution. The solid line is the guide to the eye. The error bars correspond to the standard deviation of repeated measurements. Because of the absence of a buffer solution the pH was around 2.

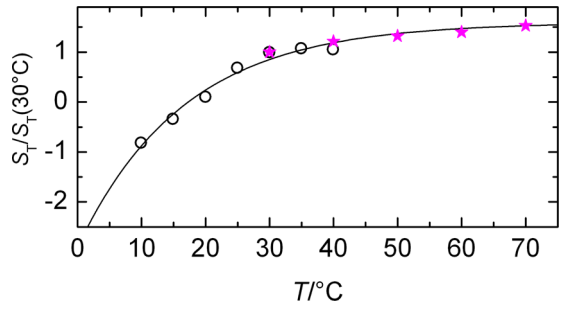

Figure 5. S_T of DNA (black ring) fitted by eq 1. Data are obtained by digitizing figures of original paper.[9] S_T of CMP (pink star) is also shown as comparison. All the S_T are normalized at 30 °C.

regime by fitting only the DNA data with eq 1. As expected, S_T of DNA increases rapidly with temperature in the cold regime, while in the high temperature regime, it shows a temperature dependence as weak as for the nucleotides. The absence of the buffer solution can lead to a change of the pH value with increasing temperature. However, the nucleotides contain both phosphate and amino groups, which release positive or negative charges, respectively. This helps to balance the pH value. The pH values of different nucleotide solutions differ slightly due to the presence of different chemical groups. The pH value of AMP and CMP solutions is around 2.6, slightly higher than the values for the other nucleotide solutions, which are 2.2 for cAMP and 1.6 for cGMP and ADP. We measured the temperature dependence of the pH value for cAMP and CMP, exemplary. The pH value declines 0.02 and 0.05 units for cAMP and CMP, respectively, when the temperature is rised by 10 K. This pH change enhances the temperature effect of S_T, which could explain the stronger temperature dependence of CMP and AMP compared to the other nucleotides.

For many systems the Soret coefficient increases steadily with temperature. In contrast, some of the nucleotides show a "dip" in S_T at temperatures around 60 °C, specifically ADP and cGMP. According to earlier publications by Son et al.[28] and Wang et al.,[27] NMR studies indicated that there is a conformational change between *syn* and *anti* conformers. In order to quantify this we performed NMR and microcalorimetry measurements in the relevant temperature range. None of our results are conclusive enough to confirm this conformational change. This might indicate that the energy difference between the two conformational statuses is below kT, so that both conformations are occupied and no clear transition can be observed.

Additionally, we analyze also the thermal diffusivity, D_{th}, and calculate the specific heat capacity, C_p, according to eq 4, whereas we use the value of thermal conductivity of pure water and the measured density of the nucleotide solutions. The measured D_{th} and calculated C_p are shown in Figure 6, parts a and b, respectively. D_{th} of all nucleotides increase linearly with temperature, but the heat capacity of the nucleotides shows no clear monotonic trend, which is however not correlated with the variation of S_T. In comparison, water does not show any

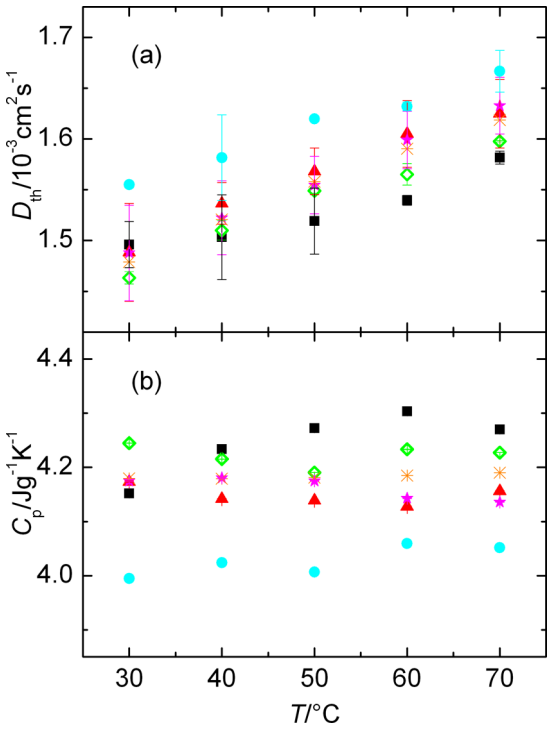

Figure 6. Measured thermal diffusivity and calculated heat capacity of nucleotides as a function of temperature. Thermal conductivity of water[37] was used to calculate the heat capacity. For nucleotides we used the same symbols as in Figure 4. For comparison, we added water (brown asterisk). Error bars are included in both thermal diffusivity and heat capacity and are too small to be seen in the latter case.

dx.doi.org/10.1021/jp3032644 | J. Phys. Chem. B 2012, 116, 7463−7469

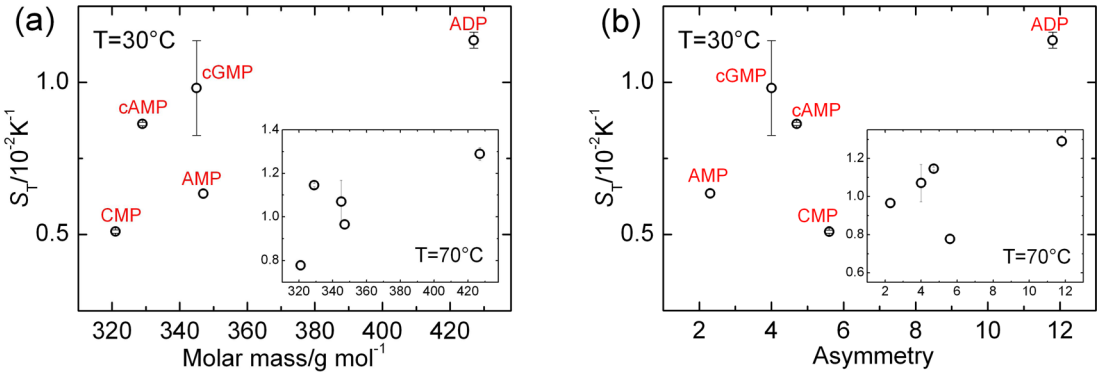

Figure 7. Soret coefficient of nucleotides in water with a weight fraction c = 0.5% at T = 30 and 70 °C as a function of (a) mass and (b) asymmetry of the molecules, defined by ratio of the principle moments of inertia. For further details, see the text.

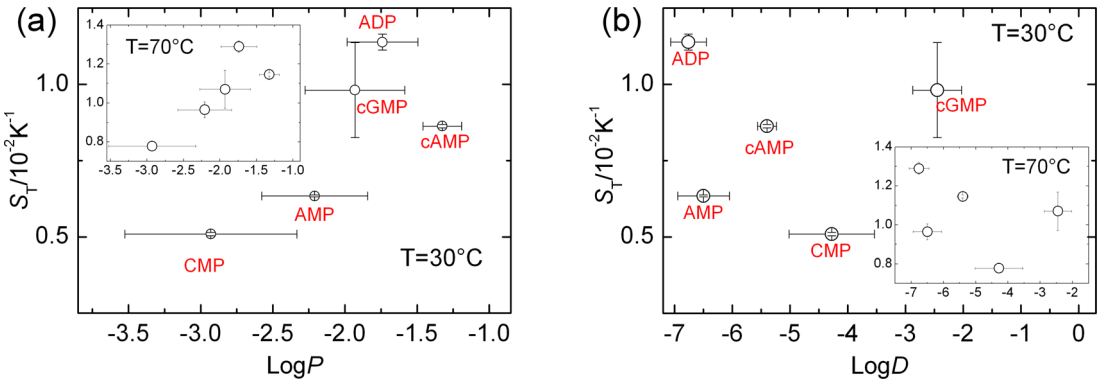

Figure 8. Soret coefficient of nucleotides in water with a weight fraction c = 0.5% at T = 30 and 70 °C as a function of (a) log p, partition coefficient, (b) log d, distribution coefficient.

temperature dependence in the investigated temperature range. None of the thermophysical properties confirm our hypothesis of the conformational change. This is in contrast with the measurements by Braun's group, who found a clear signature in the thermal diffusion behavior, when a conformational change for proteins occurred.[36]

The next question we raised is, whether there is a correlation between the structure of the nucleotides and their thermophysical properties. There are several examples in the literature, where a correlation between structure and thermal diffusion behavior has been observed, but preferentially for nonpolar systems.[16,38] In order to investigate whether the measured S_T relates with the mass or symmetry of the nucleotides, we plotted Soret coefficients as a function of mass and asymmetry at 30 and 70 °C in Figure 7, parts a and b. Here, asymmetry is defined as the ratio of the principle moments of inertia of x-direction and z-direction, which are calculated by an atomistic model for single molecules in vacuum.[39]The Soret coefficients show no clear correlation with mass and asymmetry. Only the heaviest and most asymmetric nucleotide ADP always stays at the top.

Former studies showed that formation of hydrogen bond plays a very important role in aqueous system.[24] Therefore, we tried to find a criterion, which describes the hydrophobicity of the nucleotides. One concept often used for drug compounds is the partition coefficient, P and the distribution coefficient D, which are defined as the ratio of concentrations of a compound dissolved in the two phases of a mixture of water and organic solvent at equilibrium. The most commonly used organic solvent is octanol. The partition coefficient consists of the concentrations of the un-ionized solute, while the calculation of distribution coefficient contains also the ionized solute concentration of water and is pH dependent. The logarithmic expressions $\log p = \log([\text{solute}]_{\text{octanol}})/([\text{solute}]^{\text{un-ionized}}_{\text{water}})$ and $\log d = \log([\text{solute}]_{\text{octanol}})/([\text{solute}]^{\text{ionized}}_{\text{water}} + [\text{solute}]^{\text{neutral}}_{\text{water}})$ are often used to quantify the hydrophobicity of a compound. Positive log$p$ and log$d$ values are found for hydrophobic compounds, while negative values are observed for hydrophilic substances. The partition coefficients of nucleotides can be calculated by adding the contributions of the different chemical groups present in the molecule.[40] The calculation of the distribution coefficient, log$d$, includes further terms depending on the ionization at different pH value. On the basis of literature values[41,42]the obtained log p and log d values differ considerably, which leads to fairly large error bars. Figure 8a displays that S_T shows an increasing trend with an increasing log p value, which means that S_T becomes larger, when the nucleotide is more hydrophobic and is thus less soluble in water. We expect that log d should be the better coefficient to describe the behavior of the nucleotides due to the ionization of water. However, log d values show no correlation with Soret coefficients. A possible reason could be that the calculation of the pH value based on the dissociation constant of individual chemical groups is not sufficient to describe the experimental situation.

In order to investigate the charge influence we performed additional measurements at pH 5.2 and 10.2 with cAMP. As shown in Figure 9, for all pH values the coefficients increase with increasing temperature. S_T shows a strong pH dependence, while the collective diffusion coefficient has almost no pH

dx.doi.org/10.1021/jp3032644 | J. Phys. Chem. B 2012, 116, 7463−7469

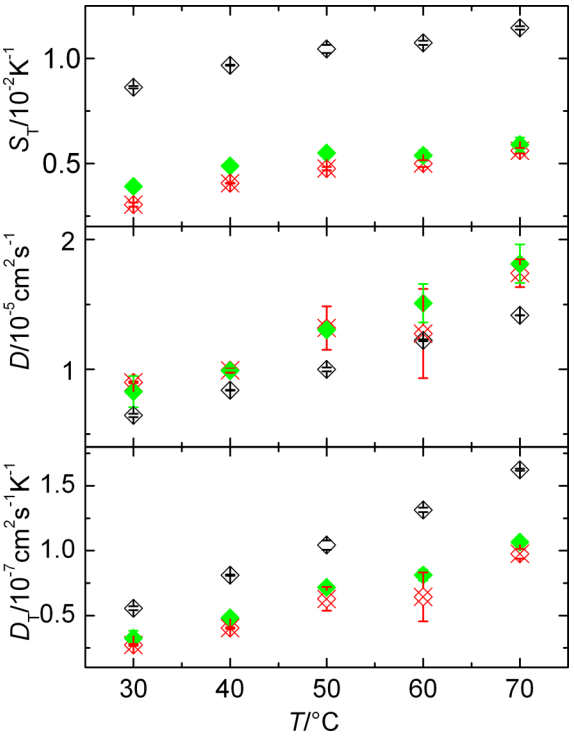

Figure 9. S_T, D, and D_T for cAMP at pH 2.2 (black diamond), pH5.2 (green diamond), and pH 10.2 (red crossed diamond) as a function of temperature.

dependence. At pH 2.2, the protonation of the amino group from the base should be more than the deprotonation of the phosphate group. At pH 5.2, which is the isoelectric point of cAMP, the molecules have the same amount of positive and negative charge. S_T increases rapidly from pH 2.2 to 5.2, but only slightly from 5.2 to 10.2. This is due to the definition of pH value. Also the ionic strength shows a much weaker pH-dependence at high pH values compared to low pH, which results in a linear dependence of the Soret coefficient on the ionic strength. Also the ammonium hydroxide added to adjust the pH value increases the ionic strength of the solution, which means a decline of the Debye length. This effect, that S_T increases with Debye length, has already been observed by Ning et al.[10] and Blanco et al.[12] with Ludox colloidal particles and fd-virus, respectively.

The last point we want to study in this work is the correlation between D_T and the thermal expansion coefficient α. Brenner derived the expression $D_T \propto \alpha D$ in his elementary theory of thermal diffusion. As D is inversely proportional to the kinematic viscosity ν, we can deduce that D_T is proportional to α/ν. As indicated in Figure 10 for all the nucleotides, a linear dependence of D_T on the ratio of the thermal expansion coefficient α, and the kinematic viscosity ν is found. In this case, we use α and ν of water. This is justified because our solutions are very dilute. For the same α/ν of nucleotides, ADP, which has the largest hydrophobicity, has the strongest tendency to go to the cold side, while CMP is at the other end. The same linear α/ν dependence has already been observed for diluted aqueous monosaccharides solutions, but not for concentrated solutions.[17] This correlation is often found if one stays in one system class, as long as the system is isotropic and no phase changes occur. Therefore, this simple correlation is not valid for micellar systems.[43]

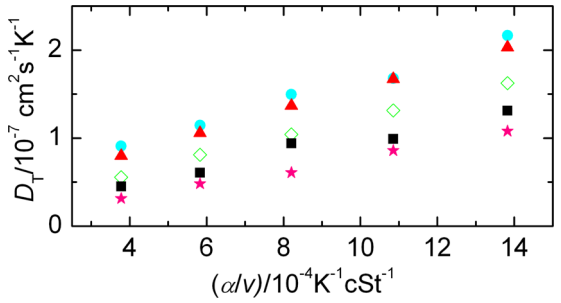

Figure 10. D_T of nucleotides as a function of the ratio of the thermal expansion coefficient, α, and the kinematic viscosity, ν. All the symbols are consistent with Figure 4.

CONCLUSION

In this work, thermal diffusion properties of aqueous solutions of nucleotides are presented at different temperatures. The Soret coefficients of the nucleotides increase with increasing temperature in the measured temperature range. The obtained Soret coefficients and their temperature dependence are comparable to large biomolecules, such as DNA. However, compared to other systems with a similar molar mass, like oligosaccharide, the thermal diffusion coefficients of the nucleotides are 1 order of magnitude larger. The diffusion coefficients remain in the same range, which shows that we do not have aggregation problems.

We find a correlation between the thermal diffusion properties and hydrophibicity represented by the partition coefficient, log p. However, it is difficult to correlate the Soret coefficient to structure and mass. Furthermore, the pH value has a strong influence on the thermal diffusion behavior of nucleotides, and the results are comparable with those found for charged colloids.[10,12] Additionally, we also find that the thermal diffusion coefficient is proportional to the ratio of the thermal expansion coefficient and kinematic viscosity.

Further research is needed to investigate whether thermal diffusion coefficients of nucleotides are large enough to support an origin of life scenario in temperature gradients.

AUTHOR INFORMATION

Corresponding Author

*E-mail: (Z.W.) zil.wang@fz-juelich.de; (S.W.) s.wiegand@fz-juelich.de.

Notes

The authors declare no competing financial interest.

ACKNOWLEDGMENTS

We appreciate many fruitful discussions with Dieter Braun and Pablo Blanco. We express our gratitude to Jan Dhont for his generous support. We thank Sabine Willbold for performing the NMR measurements and Doris Vollmer for her help with the micro calorimetry experiments. Financial support due to the Deutsche Forschungsgemeinschaft Grant Wi 1684 is gratefully acknowledged.

REFERENCES

(1) Wienken, C. J.; Baaske, P.; Rothbauer, U.; Braun, D.; Duhr, S. *Nat. Commun.* **2010**, *1*, 100.

(2) Baaske, P.; Weinert, F. M.; Duhr, S.; Lemke, K. H.; Russell, M. J.; Braun, D. *Proc. Natl. Acad. Sci. U.S.A.* **2007**, *104*, 9346−9351.

(3) Budin, I.; Bruckner, R. J.; Szostak, J. W. *J. Am. Chem. Soc.* **2009**, *131*, 9628−9629.

(4) Kasparkova, V.; Halabalova, V.; Simek, L.; Ruzicka, J.; Janca, J. *J. Biochem. Bioph. Methods* **2007**, *70*, 685−687.
(5) Braun, D.; Libchaber, A. *Phys. Rev. Lett.* **2002**, *89*, 188103.
(6) Mast, C. B.; Braun, D. *Phys. Rev. Lett.* **2010**, *104*, 188102.
(7) Duhr, S.; Arduini, S.; Braun, D. *Eur. Phys. J. E* **2004**, *15*, 277−286.
(8) Duhr, S.; Braun, D. *Proc. Natl. Acad. Sci. U.S.A.* **2006**, *103*, 19678−19682.
(9) Iacopini, S.; Rusconi, R.; Piazza, R. *Eur. Phys. J. E* **2006**, *19*, 59−67.
(10) Ning, H.; Dhont, J. K. G.; Wiegand, S. *Langmuir* **2008**, *24*, 2426−2432.
(11) Reineck, P.; Wienken, C. J.; Braun, D. *Electrophoresis* **2010**, *31*, 279−286.
(12) Blanco, P.; Kriegs, H.; Lettinga, M. P.; Holmqvist, P.; Wiegand, S. *Biomacromolecules* **2011**, 1602−1609.
(13) Dhont, J. K. G.; Wiegand, S.; Duhr, S.; Braun, D. *Langmuir* **2007**, *23*, 1674−1683.
(14) Dhont, J. K. G.; Briels, W. J. *Eur. Phys. J. E* **2008**, *25*, 61−76.
(15) Würger, A. *Langmuir* **2009**, *25*, 6696−6701.
(16) Polyakov, P.; Luettmer-Strathmann, J.; Wiegand, S. *J. Phys. Chem. B* **2006**, *110*, 26215−26224.
(17) Blanco, P.; Wiegand, S. *J. Phys. Chem. B* **2010**, *114*, 2807−2813.
(18) Blanco, P.; Kriegs, H.; Arlt, B.; Wiegand, S. *J. Phys. Chem. B* **2010**, *114*, 10740−10747.
(19) Blanco, P.; Bou-Ali, M. M.; Platten, J. K.; Urteaga, P.; Madariaga, J. A.; Santamaria, C. *J. Chem. Phys.* **2008**, *129*, 174504.
(20) Wittko, G.; Köhler, W. *J. Chem. Phys.* **2005**, *123*, 014506.
(21) Kishikawa, Y.; Wiegand, S.; Kita, R. *Biomacromolecules* **2010**, *11*, 740−747.
(22) Duhr, S.; Braun, D. *Phys. Rev. Lett.* **2006**, 96.
(23) Astumian, R. D. *Am. J. Phys.* **2006**, *74*, 683−688.
(24) Kita, R.; Wiegand, S.; Luettmer Strathmann, J. *J. Chem. Phys.* **2004**, *121*, 3874−3885.
(25) Ning, H.; Wiegand, S. *J. Chem. Phys.* **2006**, *125*, 221102.
(26) Saenger, W. *Principles of nucleic acid structure*; Springer: New York, 1984.
(27) Wang, P. M.; Izatt, R. M.; Oscarson, J. L.; Gillespie, S. E. *J. Phys. Chem.* **1996**, *100*, 9556−9560.
(28) Guschlbauer, W.; Son, T. D. *Nucleic Acids Res.* **1975**, *2*, 873−86.
(29) Becker, A.; Köhler, W.; Müller, B. *Ber. Bunsen-Ges. Phys. Chem. Chem. Phys.* **1995**, *99*, 600−608.
(30) Camerini-Otero, R. D.; Franklin, R. M.; Day, L. A. *Biochemistry* **1974**, *13*, 3763−3773.
(31) Sechenyh, V. V.; Legros, J.; Shevtsova, V. *J. Chem. Thermodyn.* **2011**, *43*, 1700−1707.
(32) Ning, H.; Datta, S.; Sottmann, T.; Wiegand, S. *J. Phys. Chem. B* **2008**, *112*, 10927−10934.
(33) Arlt, B.; Datta, S.; Sottmann, T.; Wiegand, S. *J. Phys. Chem. B* **2010**, *114*, 2118−2123.
(34) Wittko, G.; Köhler, W. *Philos. Mag.* **2003**, *83*, 1973−1987.
(35) Ning, H.; Kita, R.; Kriegs, H.; Luettmer-Strathmann, J.; Wiegand, S. *J. Phys. Chem. B* **2006**, *110*, 10746−10756.
(36) Wienken, C.; Baaske, P.; Duhr, S.; Braun, D. *Nucleic Acids Res.* **2011**, *39*, 1−10.
(37) Kreith, F. *The CRC Handbook of Thermal Engineering*; CRC Press: Boca Raton, FL, 2000.
(38) Köhler, W.; Debuschewitz, C. *Phys. Rev. Lett.* **2001**, *87*, 055901.
(39) CambridgeSoft: Chem3d, V.12. 2010.
(40) ChemAxon: Marvin 5.9.0. 2012.
(41) Viswanadhan, V. N.; Ghose, A. K.; Revankar, G. R.; Robins, R. K. *J. Chem. Inf. Comput. Sci.* **1989**, *29*, 163−172.
(42) Klopman, G.; Li, J.-Y.; Wang, S.; Dimayuga, M. *J. Chem. Inf. Comput. Sci.* **1994**, *34*, 752−781.
(43) Arlt, B. Thermal diffusion in binary surfactant systems and microemulsions. Ph.D. Thesis, Universität zu Köln: Cologne, Germany, 2011.

CHAPTER

THREE

ALKALI HALIDE SOLUTIONS UNDER THERMAL GRADIENTS: SORET COEFFICIENTS AND HEAT TRANSFER MECHANISMS

Römer, F., Wang, Z., Wiegand, S. and Bresme, F., Alkali halide solutions under thermal gradients: Soret coefficients and heat transfer mechanisms, *J. Phys. Chem. B*, 117(27), 8209-8222, 2013.

THE JOURNAL OF PHYSICAL CHEMISTRY B

Article

pubs.acs.org/JPCB

Alkali Halide Solutions under Thermal Gradients: Soret Coefficients and Heat Transfer Mechanisms

Frank Römer,[†,∥] Zilin Wang,[‡] Simone Wiegand,*[,‡] and Fernando Bresme*[,†,§]

[†]Department of Chemistry, Imperial College London, SW7 2AZ, London, United Kingdom

[‡]Forschungszentrum Jülich GmbH, ICS-3 − Soft Condensed Matter, D-52428 Jülich, Germany

[§]Department of Chemistry, Norwegian University of Science and Technology, Trondheim, Norway

Supporting Information

ABSTRACT: We report an extensive analysis of the non-equilibrium response of alkali halide aqueous solutions (Na^+/K^+-Cl^-) to thermal gradients using state of the art non-equilibrium molecular dynamics simulations and thermal diffusion forced Rayleigh scattering experiments. The coupling between the thermal gradient and the resulting ionic salt mass flux is quantified through the Soret coefficient. We find the Soret coefficient is of the order of 10^{-3} K^{-1} for a wide range of concentrations. These relatively simple solutions feature a very rich behavior. The Soret coefficient decreases with concentration at high temperatures (higher than $T \sim 315$ K), whereas it increases at lower temperatures. In agreement with previous experiments, we find evidence for sign inversion in the Soret coefficient of NaCl and KCl solutions. We use an atomistic non-equilibrium molecular dynamics approach to compute the Soret coefficients in a wide range of conditions and to attain further microscopic insight on the heat transport mechanism and the behavior of the Soret coefficient in aqueous solutions. The models employed in this work reproduce the magnitude of the Soret coefficient, and the general dependence of this coefficient with temperature and salt concentration. We use the computer simulations as a microscopic approach to establish a correlation between the sign and magnitude of the Soret coefficients and ionic solvation and hydrogen bond structure of the solutions. Finally, we report an analysis of heat transport in ionic solution by quantifying the solution thermal conductivity as a function of concentration. The simulations accurately reproduce the decrease of the thermal conductivity with increasing salt concentration that is observed in experiments. An explanation of this behavior is provided.

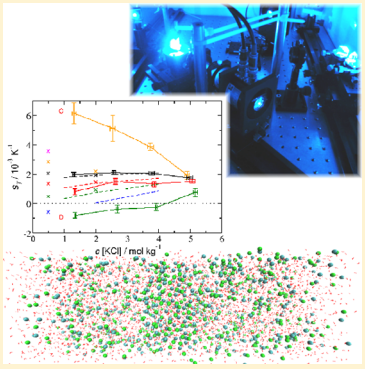

INTRODUCTION

Thermal gradients are responsible for a whole range of transport phenomena. They can induce the motion of solute particles in suspensions (thermophoresis),[1−5] the separation of mixtures, and thermal diffusion in aqueous solutions, where the concentration becomes inhomogeneous, normally increasing in the colder region (thermodiffusion).[6−8] This phenomenon was observed for the first time in liquid mixtures at the end of the 19th century, and investigated systematically by Soret around that time. The *Soret coefficient* quantifies the tendency for a mixture to separate under the thermal gradient. Despite the early discovery of this phenomenon, there is not yet a full microscopic explanation and therefore not a full theory that can successfully predict the magnitude and sign of the Soret coefficient in a wide range of situations. Notwithstanding significant efforts are being devoted to achieve a microscopic explanation of the Soret effect. Part of this activity is motivated by the practical importance of the Soret effect in determining the composition of oil reservoirs, and the possibility of manipulating small liquid volumes or solutes, which provides a route to design microscale and nanoscale thermophoretic devices with technological applications (e.g., bioanalytical assays[9,10]). A correlation between the Soret effect in binary mixtures and the recently found thermomolecular orientation effects has also been established very recently,[11,12] highlighting the complexity of this phenomenon.

Many situations of practical interest in thermodiffusion and thermophoresis involve aqueous solutions. Water is known to feature many thermodynamic and dynamic anomalies.[13] The thermal conductivity of water, a relevant variable in thermophoretic and thermodiffusive processes, is the highest observed in any liquid (except for liquid metals), and features an anomalous increase with temperature. The response of aqueous suspensions to thermal gradients is also peculiar. Experiments of charged nanoparticle suspensions have reported an inversion in the sign of the Soret coefficient at 320 K.[14] Similar changes in sign have been reported in thermophoretic experiments of DNA suspensions,[1] polypeptide solutions (see, e.g., refs 15 and 16), and polymer solutions.[17] It has been suggested that this behavior might be connected to the anomalous thermal expansion coefficient of water.[15] Nevertheless, the direct relationship between the thermal expansion coefficient and the Soret coefficient sign inversion has been challenged by experiments with proteins and biopolymers,

Received: April 18, 2013
Revised: June 12, 2013
Published: June 12, 2013

   dx.doi.org/10.1021/jp403862x | J. Phys. Chem. B 2013, 117, 8209−8222

highlighting other factors such as solute−solvent interactions. Indeed, the role of the hydration entropy in defining the sign of the Soret coefficient has been suggested recently.[18]

The peculiar change in the Soret coefficient discussed above has also been observed in aqueous electrolyte solutions. These systems are simpler in comparison with colloids and biomolecules and provide an interesting theoretical and experimental model to advance in the understanding of the microscopic origin of the sign inversion. The first experimental systematic investigations of aqueous solutions under thermal gradients were reported by Soret.[19] Later studies reported positive Soret coefficients in a wide range of salt concentrations and salts, indicating that the concentration of salt increases in the cold region, and that the Soret coefficient is of the order of 10^{-3} K^{-1}, i.e., about 2 orders of magnitude smaller than the values normally observed in colloidal and polymer aqueous suspensions.[20−24] Alexander[25] and later Gaeta et al.[21] reported sign inversion in the Soret coefficient upon decreasing the average salt concentration of the solution. This work was performed with thermogravitational columns, where the concentration gradient is formed by a combination of a convective and thermal diffusion process. Advancing the discussion, we show in this Article that such inversion is also present in our experiments, both in NaCl and KCl. Our experiments are performed using state of the art techniques (thermal diffusion forced Rayleigh scattering (TDRFS)) which has been validated in a benchmark test.[26] Gaeta et al. also reported a minimum in the Soret coefficient of different alkali halide salts. More recent studies of LiCl solutions[27] have reported a minimum too. We note however that experiments in the concentration regime where the minimum is observed are difficult. Gaeta et al. used a method that combines thermal diffusion and convective processes and very large temperature differences (∼30 K),[28] 1 order of magnitude larger than that employed in earlier experiments.[29] Both the combination of large temperature gradients and convection effects might affect the Soret coefficient estimates. Indeed, in the past, disagreements between the Soret coefficients obtained from TDRFS and thermogravitational column experiments have been observed.[30] These discrepancies have been resolved using specially designed thermogravitational columns, which validate the results obtained with the TDRFS approach.[31] Several authors,[21,27,32] who have employed convective methods, have reported a minimum in the Soret coefficient as a function of concentration and at very low salt contents. Unfortunately, this minimum could not be confirmed by convection free methods, because the achieved concentration differences are smaller in the absence of convection. The discussion above shows that the Soret coefficient measurements are not trivial, and the results should be considered with care.

The phenomenology discussed above for aqueous solutions and suspensions is in contrast with the simple behavior observed in organic mixtures, where clear correlations between the shapes of the molecules and the Soret coefficient have been established; e.g., in heptane/benzene mixtures, the linear alkane becomes more thermophobic with increasing degree of branching.[33] Similar effects regarding the influence of the molecular shape on aqueous sugar and nucleotide solutions could not be confirmed.[34−36] While for organic mixtures *sign changes are an exception*,[37] aqueous systems feature readily sign changes with concentration and with temperature.[15,38,39] It has been suggested that the sign change with concentration is connected to the perturbation (break) of the hydrogen bond network.[38] Hence, the inversion would be connected to a diminishing influence of the hydrogen bonds and an increasing importance of the entropy maximization at higher temperatures.[36] This explanation relies on the specific structural properties of water, but there is evidence that hydrogen bonding is not always required to drive the sign inversion effect. Indeed, in binary mixtures, e.g., liquid−liquid mixtures, it has been shown that strong cross interactions between different molecules can also lead to a sign reversal.[40,41]

Summarizing, considering all the different experimental observations, we can conclude that the thermal diffusion of organic mixtures is influenced to a greater extent by the shape of the molecules and intermolecular interactions, while in the case of aqueous solutions structural changes in the solvent, in particular the hydrogen bonding network, may influence the thermophoretic/thermodiffusive response. The high sensitivity of the thermal diffusive mobility to structural changes in aqueous solutions has been used as a physical principle to monitor protein ligand reactions under thermal gradients,[42] and to develop analytical devices.

The discussion above shows that ionic solutions are useful experimental systems to investigate the role that water plays in determining the thermodiffusive/thermophoretic response of solutions and suspensions. Computer simulation techniques have evolved significantly in the last years, and now they enable extensive systematic investigations of thermal transport phenomena in aqueous environments,[12] providing a route to advance in the microscopic interpretation of these phenomena. Computer simulations of aqueous mixtures have also been considered, showing good agreement with experimental studies.[43] The investigation of alkali halide aqueous solutions using computer simulations has not been attempted before to the best of our knowledge, although previous computations of Soret coefficients in molten salts have been reported,[44] showing the possibility of polarizing the sample with a thermal gradient when the ionic charges are significantly screened. In this work, we implement an aqueous solution model to quantify via classical computer simulations the Soret coefficient of ionic solutions. Given the uncertainty in the experimental available data, we have also performed new thermodiffusion experiments using state of the art techniques that are convection-free. In particular, we employ the infrared thermal diffusion forced Rayleigh scattering (IR-TDFRS) technique,[45] which uses a natural absorption band of water in the near-infrared to generate a thermal gradient in the solution and that requires no dye.

The paper is structured as follows. First, we discuss the simulation and experimental approaches employed in this work. A discussion of the thermal diffusion results for alkali halides as a function of temperature and concentration follows. The main conclusions and final remarks close the paper.

METHODOLOGY

Background. We consider our electrolyte solution as a binary system consisting of solvent and salt. Following non-equilibrium thermodynamics, three non-convective transport processes may be observed: diffusive mass flux, $\mathbf{J}_k$, heat flux $\mathbf{J}_q$, and a charge flux, $\mathbf{I}$. We shall ignore the latter, as there are no external electrostatic fields present, and consider the electrolyte solution as a binary mixture with two components, salt and water. Under these conditions, the entropy production can be written as[46]

dx.doi.org/10.1021/jp403862x | J. Phys. Chem. B 2013, 117, 8209−8222

$$\sigma = -\frac{1}{T^2}\mathbf{J}_q \cdot \nabla T - \frac{1}{T}\sum_{k=1}^{2}\mathbf{J}_k \cdot \nabla_T \mu_k \quad (1)$$

where $\nabla_T \mu_k$ represents the chemical potential gradient of component k at constant temperature, ∇T is the thermal gradient, and $\mathbf{J}_q$ and $\mathbf{J}_k$ are the heat and mass flux for component k, respectively. In this equation, we ignore external magnetic fields and viscous forces and it is assumed that no chemical reactions take place.

The phenomenological equations follow from eq 1

$$\mathbf{J}_q = -L_{qq}\frac{\nabla T}{T^2} - L_{q1}\nabla_T(\mu_1 - \mu_2) \quad (2)$$

$$\mathbf{J}_1 = -L_{1q}\frac{\nabla T}{T^2} - L_{11}\frac{\nabla_T(\mu_1 - \mu_2)}{T} \quad (3)$$

where $L_{\alpha\beta}$ represent the phenomenological coefficients, which fulfill Onsager reciprocal relations.

The investigation we are interested in corresponds to zero mass flux in the stationary state, hence

$$\frac{\nabla_T(\mu_1 - \mu_2)}{\nabla T} = \frac{-L_{1q}}{L_{11}T} = -s_T\frac{\mathrm{d}\mu_1}{\mathrm{d}\ln w_1} \quad (4)$$

where s_T is the Soret coefficient we want to quantify in this work and w_1 is the weight fraction of component 1. The Soret coefficient can be written alternatively as

$$s_T = \frac{-1}{T}\left(\frac{\nabla \ln(w_1/w_2)}{\nabla \ln T}\right)_{\mathbf{J}_1=0} = \frac{-1}{x_1 x_2}\left(\frac{\nabla x_1}{\nabla T}\right)_{\mathbf{J}_1=0} \quad (5)$$

The Soret coefficient can be simplified in the case of dilute solutions, taking component 1 as the solute, $s_T \simeq -1/x_1(\mathrm{d}x_1/\mathrm{d}T)_{\mathbf{J}_1=0}$, where x_1 is the molar fraction of solute. In the computations, we employed the exact eq 5.

It is clear from the discussion above that all that is needed to quantify the Soret coefficient is to establish a thermal gradient and measure the resulting concentration gradient. In the following, we discuss the simulation and experimental approaches we have employed to set up the thermal gradient in the aqueous solutions.

Non-Equilibrium Computer Simulations. The computer simulations involved an alkali halide aqueous solution under an explicit temperature gradient. With this purpose, we employed boundary driven non-equilibrium molecular dynamics simulations by setting appropriate thermostatting regions in the simulation box so that the simulation cell remains fully periodic.[44,47,48] The simulations were performed using orthorhombic periodic cells with dimensions $\{L_x, L_y, L_z\}/L_x = \{1, 1, 2.5\}$, with L_x between 3.73 and 3.88 nm depending on the conditions. The simulation box contained 5000 water molecules and different amounts of ion pairs 90−540 depending on the concentration.

For the integration of Newton's equations of motion, we employed the leapfrog[49] algorithm with a time step of 2 fs. Data were written every 1000 steps in order to obtain statistical averages. The short-range Lennard-Jones (LJ) interactions were truncated at a cutoff distance of r_c = 1.9 nm, corresponding to $\sim 6\sigma_{OW}$. This cutoff is long enough to reproduce the properties of the full potential; hence, no long-range corrections were applied. It has been noted that the thermal conductivity slightly depends on whether long-range Coulombic interactions are included or not.[50] To address this issue, Coulomb interactions were computed using the particle-mesh[51] (PME) variant of the Ewald method, with a mesh width of 0.12 nm and an interpolation order of 4. The real space cutoff was the same employed in the LJ potential. The potential parameters for SPC/E were taken from the original publication.[52] The water molecules were maintained rigid by using the SETTLE[53] algorithm.

The modeling of ionic solutions requires some care, as different models/approaches may overemphasize some effects, e.g., polarization. We have recently performed an extensive investigation of alkali halide aqueous solutions using point charge potentials, where we have justified the choice of these models to simulate simple ionic solutions.[54] In that work, an intrinsic analysis of the interfacial structure has been introduced for the first time, which provides a detailed view of the arrangement of ions at the interface as well as a new approach to compute interfacial free energy profiles, and an efficient approach to test the performance of different force fields. The force fields used to model ion−ion and ion−water interactions in that paper and in this Article are the same. Specifically, our primary force field parameters are taken from Dang et al. (DGS).[55−58] We have considered also a second force field, which has been derived recently by Deublein et al. (DVH),[59] as an approach to assess the impact of the force field details on the thermodiffusive response. In both cases, the parameters have been specifically derived for the SPC/E water model. The cross-interaction parameters were obtained by using the Lorentz−Berthelot's mixing rules.[60] Full details of the models employed in this work are compiled in Table 1.

Table 1. Lennard-Jones Parameters for SPC/E[52] Water and for the Ions

atom type	σ (nm)	ε (kJ mol^{-1})	q (e)
OW	0.3166	0.65021	−0.8476
HW	0.0000	0.00000	+0.4238
Na^+ [a]	0.2350	0.54392	+1.0000
K^+ [a]	0.3332	0.41868	+1.0000
K^+ [b]	0.2770	0.83145	+1.0000
Cl^- [a]	0.4401	0.41868	−1.0000
Cl^- [b]	0.4410	0.83145	−1.0000

[a]From Dang, Garrett, and Smith (refs 55−58), respectively. [b]From Deublein, Vrabec, and Hasse (ref 59).

To perform the non-equilibrium molecular dynamics (NEMD) simulations, we have followed the method discussed in our recent study of the thermal conductivity of water.[61] The computations were performed using boundary driven molecular dynamics simulation, following refs 44, 47, and 48. First, we add ions at the desired concentration to a pre-equilibrated box containing water at 1 g/cm^3, which is then equilibrated for ∼1 ns in the canonical ensemble (NVT) at a temperature equal to the desired average temperature of the NEMD run, i.e., $T_{ave} = (T_{hot} + T_{cold})/2$, where T_{hot} and T_{cold} are the temperatures of the hot and cold thermostats. Then, hot and cold thermostats at the edges and in the middle of the box are set up by defining layers with thicknesses of ∼0.1 nm. For the NEMD simulation, we employ as a starting configuration the NVT equilibrated system. We first identify those water molecules inside the thermostatting regions. During the simulations, the translational motion of ∼80% of these thermostatting molecules is restrained by applying a harmonic potential on the oxygen atom. These water molecules are free to rotate and exchange

dx.doi.org/10.1021/jp403862x | J. Phys. Chem. B 2013, 117, 8209−8222

momentum with the unrestrained molecules. The thermostatting layers are then set at the desired temperatures T_{hot} and T_{cold}, setting in this way the thermal gradient and the heat flux across the simulation box. For the thermostatting process, we employ the v-rescale algorithm,[62] which preserves the momentum of the system. As the thermostatting process does not affect the particle coordinates, the change in the internal energy is given (classically) by[61]

$$\Delta U(\mathbf{r}, \mathbf{p}) = \Delta V(\mathbf{r}) + \Delta K(\mathbf{p}) \tag{6}$$

$$\Delta V(\mathbf{r}) = 0 \tag{7}$$

$$\Delta K(\mathbf{p}) = \frac{1}{2} \sum_{i=2}^{N \in TL} m_i v_i^2 \tag{8}$$

where ΔV and ΔK represent the change in the potential and kinetic energies associated to the thermostatting process and $N \in TL$ indicates the sum runs over all thermostatted molecules (hot or cold thermostats). The heat flux can then be obtained from the continuity equation

$$\mathbf{J}_U = \left[0, 0, \pm\frac{\langle \Delta U \rangle}{2\delta t A}\right] \tag{9}$$

where A is the cross-sectional area of the simulation box in the plane (x, y) perpendicular to the heat flux vector, δt is the time step, and $\pm\langle \Delta U \rangle$ is the average change in internal energy in the cold $(-)$ and hot $(+)$ thermostatting layers. A more detailed description of the method and its implementation can be found in refs 48 and 61.

A typical NEMD simulation involved 4 ns to ensure the stationary state is reached. We then performed simulations for a further 14 ns in order to collect averages. The density and temperature profiles were computed locally, by dividing the simulation box in layers (typically 120) along the direction of the temperature gradient, z-axis. The simulations were performed with a modified version of the Gromacs code.[63]

EXPERIMENTAL METHODS

Infrared Thermal Diffusion Forced Rayleigh Scattering. To measure the thermal diffusion properties of the salt solutions, we used an infrared thermal diffusion forced Rayleigh (IR-TDFRS) scattering setup. A detailed description can be found in the paper by Blanco et al.[64] This setup is optimized for aqueous systems and has been used to study the transport properties in different aqueous systems of nonionic surfactants,[65,66] saccharide solutions,[34,35] and anisotropic biocolloids.[64]

The normalized heterodyne scattering intensity $\zeta_{het}(t)$, assuming an ideal excitation with a step function, is given by

$$\zeta_{het}(t) = 1 - \exp\left(-\frac{t}{\tau_{th}}\right) - A(\tau - \tau_{th})^{-1} \times \left\{\tau\left[1 - \exp\left(-\frac{t}{\tau}\right)\right] - \tau_{th}\left[1 - \exp\left(-\frac{t}{\tau_{th}}\right)\right]\right\}$$

with the steady state amplitude A

$$A = \left(\frac{\partial n}{\partial c}\right)_{p,T}\left(\frac{\partial n}{\partial T}\right)_{p,c}^{-1} s_T c(1 - c) \tag{10}$$

where c is the mass fraction, τ_{th} is the heat diffusion time, and $(\partial n/\partial c)_{p,T}$ and $(\partial n/\partial T)_{p,c}$ are refractive index contrast factors with respect to mass concentration at constant pressure and temperature, and referring to temperature at constant pressure and mass concentration, respectively. The equilibration time for the temperature grating τ_{th} can be used to calculate the thermal diffusivity, D_{th}, which describes the heat transport in the solution. It is related to the thermal conductivity, κ, specific heat capacity, c_p, and density, ρ, by

$$D_{th} = \frac{\kappa}{\rho c_p} \tag{11}$$

The Soret coefficient, $s_T = D_T/D$, can be expressed as a ratio of the thermal diffusion coefficient, D_T, and the collective diffusion coefficient, D. Whereas the diffusion coefficient $D = 1/(q^2\tau)$ can be calculated from the diffusion time, τ (cf. eq 10), using the magnitude of the grating vector q, which is given by $q = (4\pi)/\lambda_w \sin(\theta/2)$. Here θ is the angle between the two writing beams and λ_w is the wavelength of the laser beam. The transport coefficients are determined by fitting eq 10 to the measured heterodyne signal and deconvoluting the excitation function.[67,68]

Figure 1 shows the normalized heterodyne signals of a 0.5 M potasium chloride solution at temperatures of 15 and 35 °C.

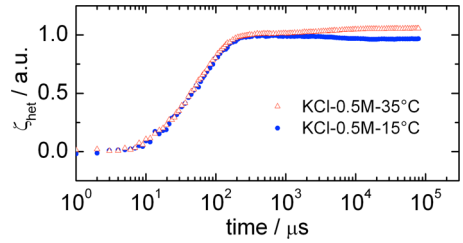

Figure 1. The normalized heterodyne signal ζ_{het} of IR-TDFRS measurements for 0.5 M KCl solution at temperatures of 15 and 35 °C.

Both curves show a thermal plateau around 200 μs and a concentration plateau at 20 000 μs. This shows clearly that the equilibration of the thermal plateau is 3 orders of magnitude faster than the equilibration of the concentration. While the concentration part of the signal decays at the lower temperature, it increases at higher temperatures. This indicates that the salt diffuses at lower temperatures toward the warm side, while it accumulates at higher temperatures at the cold side, pointing toward a sign reversal in the Soret coefficient.

Sample Preparation and Characterization. Sodium chloride (NaCl) (≥98.5%) and potasium chloride (KCl) (≥98.5%) were purchased from Merck and were used without further purification. Deionized water from a Millipore filter unit (0.22 μm) was used to prepare all aqueous solutions.

Approximately 2 mL of the prepared solutions were filtered through a 0.2 μm filter (Whatman Anotop 10) before filling them into an optical quartz cell (Hellma) with an optical path length of 0.2 mm. At least two measurements with different cells and freshly prepared samples were done for each system. All measurements are performed in the temperature range of 25 and 65 °C. The 0.5 M KCl solution was also measured at 15 °C, since the sign change in the Soret coefficient is expected at that temperature.

The refractive index increments with the mass concentration $(\partial n/\partial c)_{p,T}$ was measured by an Anton Paar RXA 156

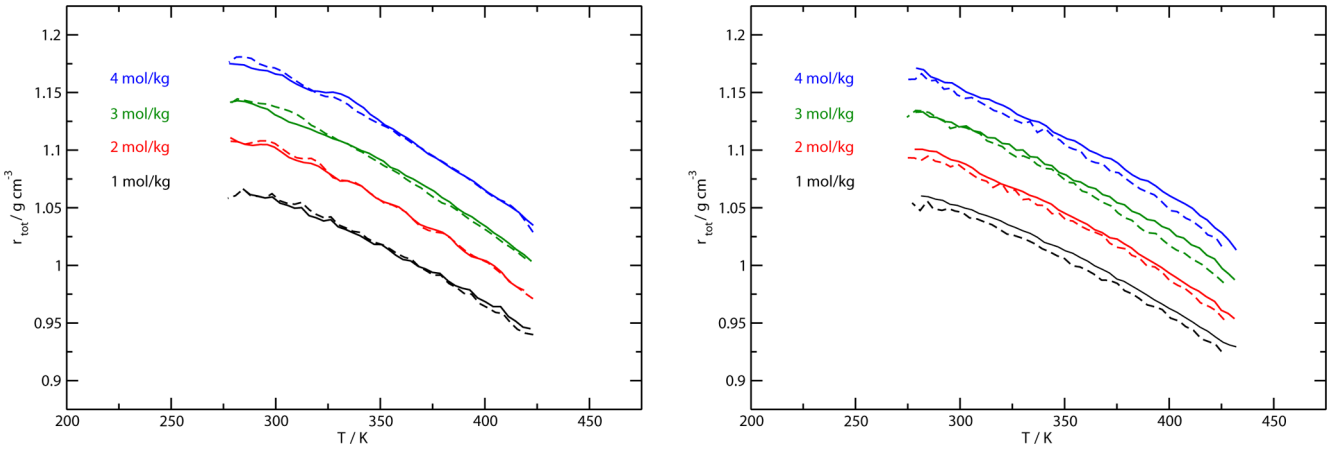

Figure 2. Equation of state of (left) KCl at 500 bar and (right) NaCl solutions at 100 (dashed lines) and 500 (full lines) bars. The left panel (KCl) shows results obtained using the DGS (full line) and DVH (dashed lines) force fields. The right panel (NaCl) presents results for the DGS force field only. All the simulations were performed at an average temperature of 350 K and a thermal gradient of ∇T = 3.7 K/Å.

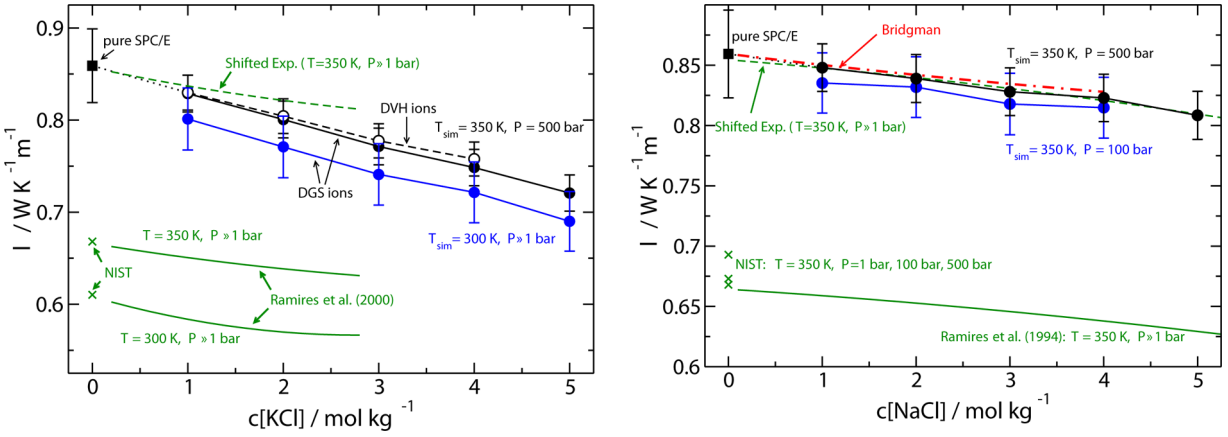

Figure 3. Thermal conductivities of (left) KCl, using the DGS (full lines) and DVH (dashed line) force fields and (right) NaCl (DGS force field only) solutions from non-equilibrium molecular dynamics simulations (black and blue lines) as a function of salt concentration. The data for pure SPC/E water correspond to 350 K and 500 bar. Experimental data for KCl and NaCl (full green lines) at different temperatures and at 1 bar are also shown. These data were taken from refs 74–76. The crosses represent experimental results (NIST database[74]) of the thermal conductivity of pure water at different thermodynamic conditions. T_{sim} denotes the average temperature employed in the NEMD simulations. The green dashed lines are experimental values shifted in order to fit to the thermal conductivity of pure SPC/E, and enable a direct comparison of the experimental and simulation data as the salt concentration increases. The dashed dotted line labeled "Bridgman" in the right panel is the thermal conductivity predicted by the Bridgman equation as discussed in the text. See the Supporting Information for numerical data.

refractometer, whose accuracy is 0.00002 nD with a temperature control of $\Delta T = \pm 0.03$ K. For both salts, the refractive index has been measured for at least three concentrations around the desired concentration. The slope of the linear interpolation of the refractive index as a function of the concentration gives $(\partial n/\partial c)_{p,T}$. The refractive index increments with temperature $(\partial n/\partial T)_{p,c}$ were measured interferometrically,[69] in a temperature range of 1 K around the temperature of interest. The refractive index varied linearly with temperature and concentration in the investigated range. The refractometer uses the sodium line with a wavelength of 589.3 nm, which is roughly 40 nm shorter than the He/Ne laser of 632.8 nm used as a read-out beam in the IR-TDFRS. This causes a small systematic error in the refractive index increment of the order of 0.5–1%.[70,71]

We note that using a buffer can be problematic at low salt concenctrations, because the buffer itself will contribute to the refractive index profile. We also note that in our experiments the influence of external sources, which lead to pH change due to solvation of CO_2, is unlikely because the cells were sealed during the measurements. The pH of the solutions was always around 8.0 ± 0.3 and did not show a systematic trend with concentration.

RESULTS AND DISCUSSION

Equations of State and Thermal Conductivities. Before we start our discussion, we note that our simulations and experiments were performed at relatively high concentrations, >0.5 M. At these concentrations, the electrostatic interactions are significantly screened; hence, the ion–ion and ion–solvent dispersive interactions play an increasingly important role.

We first report our results of the simulated equation of state and thermal conductivities of the solutions, as a first step to validate the accuracy of the force fields employed in this work. Figure 2 shows the equations of state of KCl and NaCl solutions at different average salt concentrations. The equations of state were obtained from a direct analysis of the non-equilibrium simulation data. In our NEMD approach, the thermal gradient results in a concomitant density gradient.

dx.doi.org/10.1021/jp403862x | J. Phys. Chem. B 2013, 117, 8209–8222

These two gradients develop preserving mechanical equilibrium, i.e., $\nabla P = 0$, where P is the pressure along the simulation box. By considering pairs of density and temperature at the same position on the simulation box, we can then reconstruct the equations of state shown in Figure 2. This idea has been tested before for pure water and other simple fluids, and the equations of state obtained in this way showed excellent agreement with the equilibrium results.[44,61,72]

The equation of state of KCl is fairly insensitive to the force field employed to simulate the ion−water interactions in the concentration interval 1−4 M (see Figure 2, left). This is an important result, as different force fields may predict large differences in other properties (e.g., interfacial adsorption[54]). Our results show that the force fields are robust in predicting the solution densities in the concentration range we are interested in. Similar conclusions are expected at lower concentrations, as in this case the dependence of the equation of state with temperature will be dominated by the solvent properties.

We have investigated the impact of the pressure on the equation of state (see Figure 2, right). The NEMD simulations do not allow a very fine control of the pressure, as they are normally performed at constant volume; hence, this analysis is necessary to assess the impact of the simulation conditions when comparing simulation and experimental Soret coefficients. The pressure has a minor impact on the density of the ionic solution. It increases ∼1% in going from 100 to 500 bar. Similar variations in density with pressure were observed in the KCl solutions (not shown). We note that, for the pressure range considered here, SPC/E water does not feature significant changes in its hydrogen bond structure either (see ref 73 for an extensive discussion). Advancing the discussion below, we also find that the pressure does not have a significant effect on the magnitude of the Soret coefficient.

The thermal conductivity is a relevant property in heat transport applications, and it is connected to the thermal diffusivity measured in the optical experiments (see eq 11). Non-equilibrium molecular dynamics simulations provide a direct route to quantify the thermal conductivity by using Fourier's law

$$J_q = -\lambda \nabla T \tag{12}$$

In using eq 12, we have followed the approach discussed in our previous investigations in water, and the thermal conductivity was extracted from the local derivative of the temperature gradient (see ref 61 for further details). Figure 3 shows the thermal conductivity for representative temperatures and pressures using both the DVH and DGS force fields for KCl and the DGS force field for NaCl salts. Numerical results are reported in the Supporting Information. The experiments show that the thermal conductivity of the solution decreases with salt concentration. This trend is reproduced by the simulations using both force fields, DGS and DVH, showing that this physical behavior is independent of the details of the force fields employed.

It is well-known that water has the highest thermal conductivity of any liquid, with the exception of metals. It has been assumed that the liquid tetrahedral structure plays an important role in determining this high thermal conductivity, and it is known from computer simulations that the dominant mechanism for heat transport in water is through intermolecular interactions (see ref 72). Alkali cations tend to generate robust solvation shells around them; hence, the tetrahedral structure should be perturbed as the salt concentration increases. To quantify the degree of orientational order, we have computed the radial distribution function of NaCl aqueous solutions for one of the thermodynamic states considered in Figure 3 (350 K and 500 bar). These *equilibrium* simulations were performed in the isothermal−isobaric ensemble.

Figure 4 shows the radial distribution functions for NaCl solutions at 0, 2, and 4 M concentrations. The largest changes

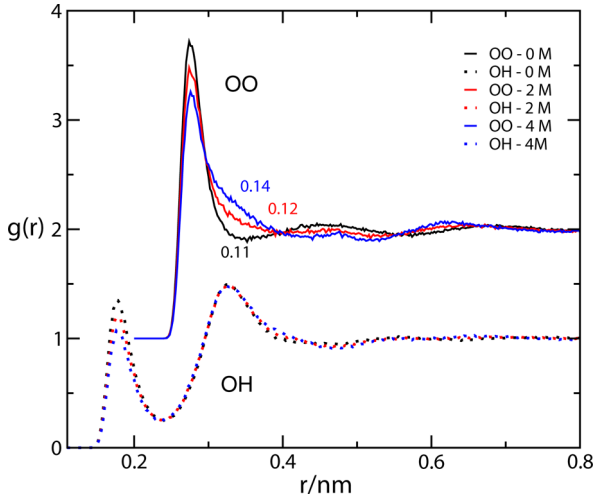

Figure 4. OO and OH radial distribution functions of NaCl solutions at 500 bar and 350 K and concentrations 0, 2, and 4 M. The numbers in the graph indicate the tetrahedral order parameter (see eq 13 and the main text for details). The OO radial distribution function has been shifted vertically 1 unit. All the simulations were performed with the DGS model.

induced by the ions are more apparent in the OO radial distribution functions, which features a clear perturbation in the region 3−5 Å, which is characteristic of the water tetrahedral structure. In contrast, the modification of the OH correlations is minor. The modifications of the tetrahedral structure can be further quantified through the tetrahedral order parameter[77]

$$S_g = \frac{3}{32} \sum_{i=1}^{3} \sum_{j=i+1}^{4} \left(\cos \phi_{ijk} + \frac{1}{3} \right)^2 \tag{13}$$

where the sum runs over the four nearest neighbors around a given water molecule and ϕ_{ijk} is the angle between two "bonds" joining two of those molecules to the central one. The order parameter is normalized and is equal to 0 for a perfect tetrahedral structure and 1/4 when the bond orientation is random. The typical value of the order parameter for SPC/E liquid water at 300 K and 1 bar is 0.1, that for SPC/E hexagonal ice near the melting temperature is 0.012, and that for a typical Lennard-Jones liquid is ∼0.15. The order parameters we obtain for the solutions are higher than the reference value for SPC/E, indicating that the water tetrahedral structure is indeed disrupted as the salt concentration increases. For 2 and 4 M concentrations, the order parameter is similar to that obtained for water at high temperatures or very high pressures (see, e.g. ref 73 for an extensive discussion). We have shown so far that ions have a strong impact on the tetrahedral water structure. A direct link between the disruption of the hydrogen bond network and the change in thermal conductivity is tempting,

but it is not supported in general by observations in pure water under extreme conditions. Indeed, it has been shown that the thermal conductivity of water can increase upon a disruption of the hydrogen bond network, an effect that is particularly noticeable at extreme pressures.[73] Hence, this suggests that the disruption of the hydrogen bond network induced by the ions might not necessarily be the main factor behind the reduction in thermal conductivity. As indicated above, in water, and in general in any liquid, intermolecular interactions provide the main mechanism for heat transfer; hence, the fluid density plays an important role in determining the final thermal conductivity, and the latter can feature a strong dependence with the fluid density. The analysis of our computer simulations shows that the number density, ρ, decreases with increasing salt concentration: ρ = 99.2, 96.2, and 93.8 particles/nm^3 for 0, 2, and 4 M concentrations, respectively. Following earlier theories on the thermal conductivity of pure liquids,[78] this reduction in density should result in a reduction of the thermal conductivity, as the mean interparticle distance increases as the density decreases and henceforth less energy is being transported per unit volume. We can test this notion by considering Bridgman's equation,[78] $\lambda = 2\alpha v\delta^{-2}$, where, using Bridgman's notation, α is the gas constant, v is the speed of sound, and δ is the average distance between atoms, i.e., $\delta = \rho^{-1/3}$. Retaining the density as a leading term in determining the thermal conductivity, we expect that $\lambda(c) \approx (\rho(c)/\rho(c))^{2/3}\lambda(0)$, where $\lambda(0)$ and $\rho(0)$ correspond to pure water and c indicates the salt concentration. To perform the analysis, we fitted our simulated densities, $\rho(c)$, to a second degree polynomial in c. We have represented in Figure 3 the expected dependence of the thermal conductivity with salt concentration according to the correlation that follows from the Bridgman equation, using for $\rho(0)$ = 99.2 nm^{-3} the density of SPC/E water at 500 bar and 350 K and for $\lambda(0)$ = 0.859 the thermal conductivity of SPC/E water at the same temperature and pressure, which corresponds to the point represented in Figure 3. We find that the Bridgman correlation reproduces very well the reduction in the thermal conductivity with salt concentration, underlying the importance of the number density as the main factor determining the reduction. We note again that, in deriving the correlation, $\lambda(C) \approx (\rho(C)/\rho(c))^{2/3}\lambda(0)$, we have assumed that the speed of sound is independent of salt concentration.

So far, we investigated the qualitative dependence of the thermal conductivity of water as a function of concentration, and we showed that this can be understood by considering the changes in density undergone by the solutions; i.e., there is no need to consider the peculiar hydrogen bond structure explicitly.

In the following, we investigate the performance of the models in predicting the thermal conductivity of aqueous solutions. Our simulated thermal conductivity increases with temperature (in the interval 300−350 K), in agreement with the experimental results for pure water and ionic solutions. This result also indicates that the anomalous increase of the thermal conductivity which is characteristic of pure water is preserved in ion solutions too, despite the fact the ions considerably disrupt the water tetrahedral structure (see Figure 2). A closer comparison of our simulation data and the available experiments shows that the force fields employed in this work overestimate the thermal conductivities by about 20% (see Figure 3). This overestimation can be traced back to the SPC/E water model, which already overestimates the thermal conductivity of pure water at ∼300 K by that amount (see ref 61 for an extensive investigation). Rescaling of the experimental data to match the simulation thermal conductivity of pure water allows a direct comparison of the experimental and simulation results for ionic solutions (see Figure 3). We find that the salt force fields very accurately account for the experimental trends; indeed, the general dependence of the thermal conductivity with salt concentration is well captured, even at a quantitive level by the models employed in this work.

Soret Coefficients. The Soret coefficients were calculated by quantifying the derivative dx_1/dT (see eq 5), which can be obtained directly from both experiments and simulations. Figure 5 shows a representative molar fraction profile for KCl

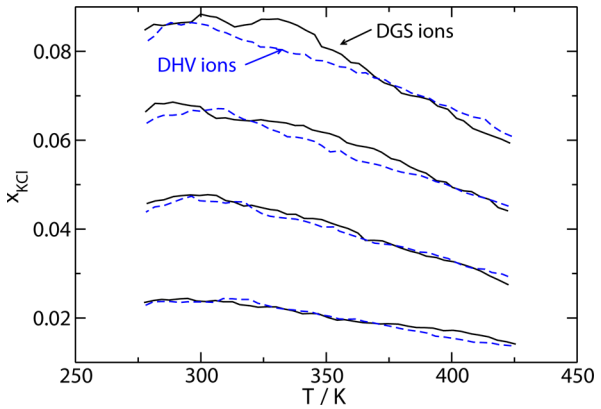

Figure 5. Dependence of the molar fraction of KCl with temperature, obtained from NEMD simulations using the DGS model (black solid line) and the DHV model (blue dashed−dotted line). The different pairs of lines represent different average salt concentrations, from bottom to top, 1, 2, 3, and 4 mol/kg. See the Supporting Information for numerical results.

obtained from NEMD simulations using the DGS and DHV force fields. Numerical results are provided in the Supporting Information. We find that both force fields predict the same results with some noticeable differences at high concentrations (4 M) and in the low temperature range. As we will show below, these differences have an impact on the simulated Soret coefficients. The most noticeable feature of these profiles is the maximum in the molar fraction, which appears at about 300 K. At this point, the Soret coefficient is zero, and our simulations therefore indicate the existence of sign inversion in this coefficient. As discussed in the Introduction, the origin of the sign inversion has been linked by some authors to the unusual behavior of the thermal expansion coefficient in water (water density maximum), which changes sign at about 277 K in real water. For the SPC/E water model, such correlation is not at all evident, as the density maximum appears at much lower temperatures, ∼241 K and 1 bar,[79] which is well below the temperature at which we observe the sign inversion in our NEMD simulations. Although our simulations are performed at pressures higher than 1 bar (100−500 bar), we note that an increase in pressure would reduce even more the temperature of the density maximum, which would be shifted to temperatures below 241 K.[80] Overall, our results for the SPC/E solutions do not support the existence of a correlation between the sign inversion and the water density maximum.

We have employed eq 5 to calculate the Soret coefficient, and to investigate its dependence with the thermodynamic state and salt concentration. The simulated Soret coefficients were obtained by calculating the local derivative ∼10 data points

dx.doi.org/10.1021/jp403862x | J. Phys. Chem. B 2013, 117, 8209−8222

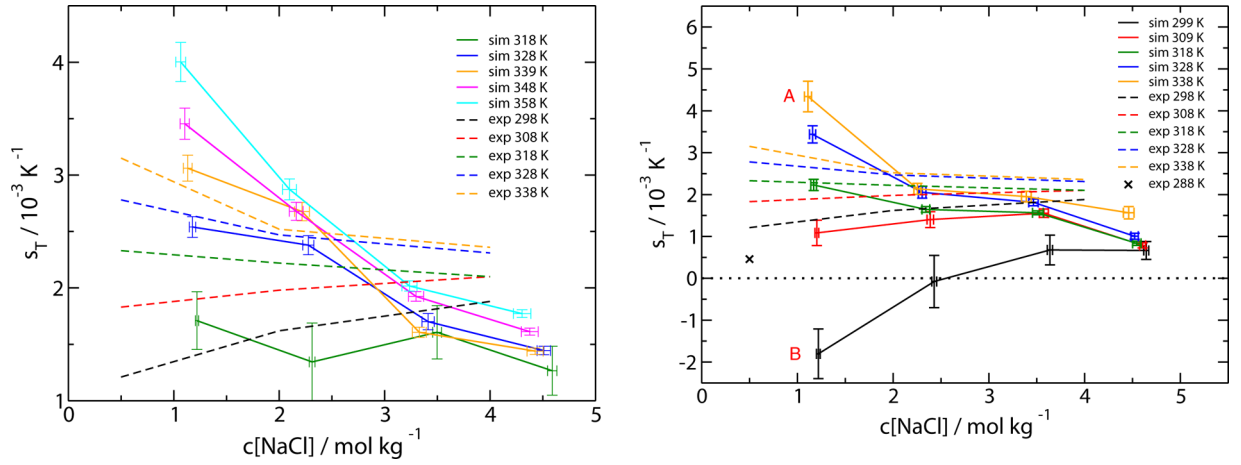

Figure 6. Soret coefficient of NaCl solutions at different temperatures and salt concentration: The dashed lines in both panels and the cross in the right panel represent experimental data obtained in this work and (symbols and solid line) NEMD simulations at (left panel) 500 bar and (right panel) 100 bar pressures. The simulations were performed with the DGS model, the thermal gradient was set to ∇T = 3.7 K/Å, and the average temperature was set to 350 K. The letters "A" and "B" in the right panel represent thermodynamic states for which additional analyses of the aqueous solution structure were performed. See the main text for details.

of the molar fraction profiles (see Figure 5). Then, the local temperature and local molar fractions were employed to extract the coefficient. In this way, we can obtain a range of Soret coefficients for an isobar using a single NEMD simulation. This method follows the approach employed previously by us to obtain the equation of state of water from a single NEMD simulation (see previous section in this paper and refs 44, 61, and 72). The experimental Soret coefficients were obtained using the infrared thermal diffusion forced Rayleigh scattering approach as discussed in the Methodology section.

Figure 6 shows our experimental and simulation results for the Soret coefficients of NaCl solutions. The experimental data correspond to 1 bar pressure, whereas the simulation results were obtained at 100 and 500 bar. We have shown above that the impact of this pressure change on the equation of state is small. We find that both the experimental and simulated Soret coefficients agree in the order of magnitude, $\sim 10^{-3}$ K^{-1}, which is in line with previous experiments of alkali halides.[21,27] Similar values for the Soret coefficient have been reported in mixtures of simple liquids modeled with Lennard-Jones potentials, or in experiments of nucleotide solutions,[36] water−alcohol mixtures,[45] and mixtures of organic liquids.[30]

Our simulation results show that the pressure has a small impact on the Soret coefficient (cf. Figure 6, left and right), which increases slightly in going from 100 to 500 bar. This effect is more noticeable at lower salt concentrations (see, e.g., the T = 318 K data set in Figure 6). Overall, the qualitative dependence of the Soret coefficient with salt concentration is not affected by the pressure, and this gives us confidence we can establish a direct comparison between experiments and simulation results.

The experimental Soret coefficients for NaCl are all positive for the concentration range 0.5−4 m and 298−338 K, indicating that the salt accumulates in the cold region; i.e., it is thermophobic. The Soret coefficient also features a very interesting dependence with temperature. At high temperatures of $T \geq 318$ K, the coefficient decreases with salt concentration; i.e., less salt is accumulated in the cold region, whereas below this temperature it increases with concentration. Hence, there is an isotherm at ∼313 K, where the Soret coefficient is independent of salt concentration. A similar invariance of Soret coefficient with temperature has been observed in polar and nonpolar systems, methanol/DMSO,[39] and cyclohexane/dibromohexane.[81]

In general, the Soret coefficient features a much stronger variation with temperature at low salt concentrations. This general behavior is reproduced qualitatively by our NEMD simulations. At high temperatures and pressures, we also find a monotonic decrease of the Soret coefficient with concentration (see Figure 6, left), whereas at low temperatures it increases with concentration (see Figure 6, right) following the experimental observations. Furthermore, our simulations, as advanced above, also predict a sign inversion in the Soret coefficient (see T = 299 K and P = 100 bar in Figure 3, right). This sign inversion is compatible with previous experimental reports on alkali halides,[21,27] although in these experiments the inversion was observed at lower concentrations of $\sim 10^{-2}$ M, much lower than the ones considered in our experiments of NaCl (0.5 m). We have performed an additional simulation to address the existence of the sign inversion in NaCl, and performed additional experiments at lower temperatures (see 288 K in Figure 6, right). We find that the Soret coefficient decreases with temperature and approaches 0, although it is still positive. Unfortunately, our experimental setup did not allow us to investigate lower temperatures, for which the sign inversion is expected to appear. When the concentration becomes very low, the amplitude, A (see eq 10), signal also becomes small because A is proportional to the concentration. Hence, we could not resolve properly the signal to determine the Soret coefficients. To estimate the sign inversion temperature, we have employed the correlation formula of Piazza et al.,[15] $s_T(T) = s_{T,\infty}[1 - \exp((T_0 - T)/c)]$, which has been used to model the temperature dependence of the Soret coefficient in a wide range of aqueous suspensions. The sign inversion temperature in the above formula is given by T_0. Figure 7 shows our experimental results for NaCl at 0.5 M and the corresponding fitting to the correlation formula. The empirical equation provides an excellent fit to our data, and we estimate that the sign inversion temperature at 0.5 M concentration should be 283 K. Comparison of this result with data obtained in previous works at different salt concentrations indicates that the

dx.doi.org/10.1021/jp403862x | J. Phys. Chem. B 2013, 117, 8209−8222

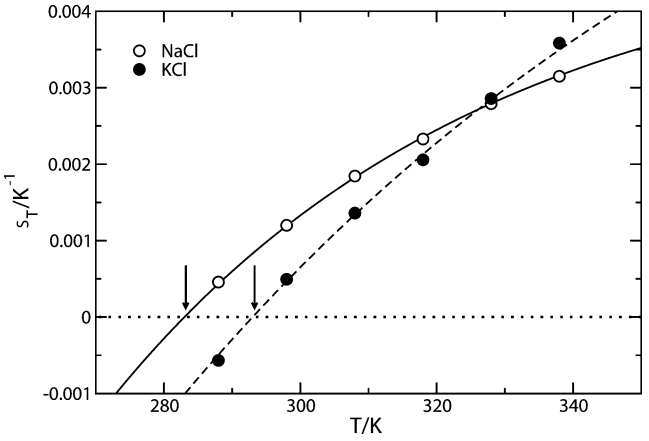

Figure 7. (symbols) Experimental Soret coefficient of NaCl and KCl solutions at 0.5 M concentration and different temperatures. (lines) Fitting to the correlation formula, $s_T(T) = s_{T,\infty}[1 - \exp((T_0 - T)/c)]$, where $s_{T,\infty}$ = 0.005 (NaCl), 0.0098 (KCl) K^{-1}, T_0 = 283 (NaCl), 293 (KCl) K, c = 55 (NaCl), 102 (KCl) K. See the text for details.

inversion temperature in alkali halide solutions increases with salt concentration.

We now discuss the dependence of the Soret coefficient with salt composition by considering a new set of experiments and simulations for KCl solutions. The Soret coefficient are of the same order as the ones obtained for NaCl. The qualitative dependence of the coefficient with temperature and concentration is very similar; namely, at high temperatures, the Soret coefficient decreases with concentration, whereas, at low temperatures, it increases. Our results for the Soret coefficient agree with previous experiments performed by Longsworth,[22] using a different experimental approach. The most important difference between the NaCl and KCl solutions is the location of the inversion temperature, which we can measure directly for KCl in our experiments, and it is shifted from 283 K (NaCl) to 293 K (KCl) at 0.5 m concentration. Similarly, the isotherm where the Soret coefficient is constant with concentration is shifted too, although to a lesser extent, to higher temperatures, from 313 to ∼318 K.

The simulation results for KCl using the DGS and DVH models (see Figure 8) reproduce the general experimental trends. Namely, they predict an increase in the Soret coefficient with concentration at high temperatures, sign inversion, and also in the case of the DVH model the decrease of the coefficient with concentration at high temperatures. The simulations for these two models were performed at different pressures, but we note that as shown above for the NaCl case (see Figure 3) the general behavior and magnitude of the Soret coefficient is fairly independent of the pressure for the simulation conditions considered here. The DVH model provides a more accurate prediction of the Soret coefficients, and in general, the results are in closer quantitative agreement with experiments. Overall, our results show that the dependence of the Soret coefficient with temperature and salt concentration is independent of the force field employed; however, the actual value of the Soret coefficient is very sensitive to the model employed. This is particularly evident in the shift observed in the concentration at which the Soret coefficient changes sign, which is shifted from ∼2 m (DGS) to ∼4 m (DVH). The sensitivity of the structure of ionic solutions to the force field parameters has been highlighted recently in an intrinsic analysis of the interfacial structure of ionic solutions.[54] It was shown that small variations in the cation and anion size have a strong impact on the adsorption behavior of the ions. These results reflect ultimately strong modifications of the ion solvation structure. To address this point, we have computed the radial distribution functions of the DGS and DVH at the same thermodynamic conditions. As shown in Figure 2, the equation of state is fairly insensitive to the force field; hence, we expect that the distribution functions reflect true changes in the local organization of water around the ions. Figure 9 shows the corresponding radial distribution functions for KCl at 1 M concentration and two different temperatures, 299 and 325 K, which correspond to negative and positive Soret coefficients, respectively. The DGS and DVH models use similar diameters for the anions, Cl^-, but the cation diameters differ, with the

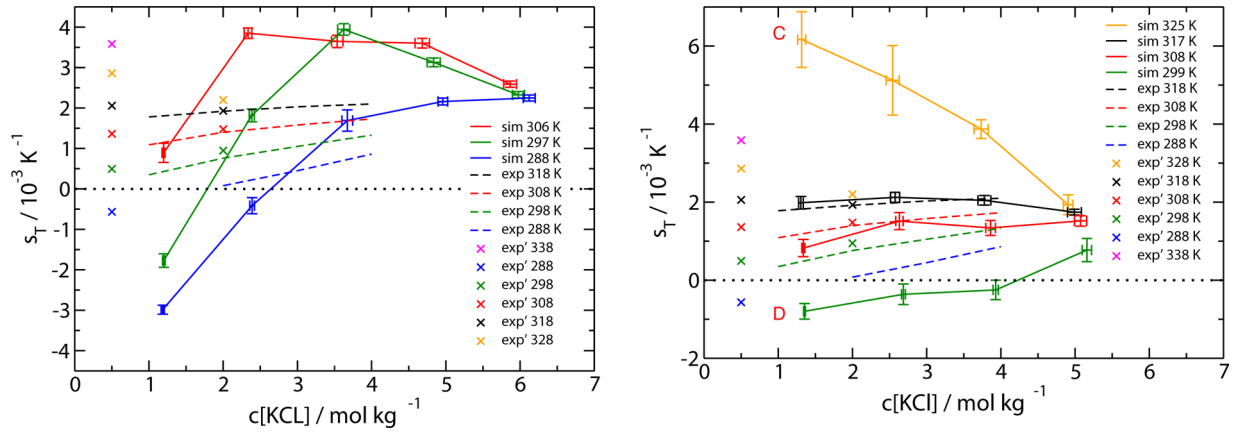

Figure 8. Soret coefficient of KCl solutions as a function of temperature and concentration. Symbols and full lines: NEMD simulations. Dashed lines: experiments performed by Longsworth.[22] Crosses: experiments performed in this work. The NEMD simulation data presented in the left panel were obtained NEMD with the DGS model at an average temperature and pressure of 300 K and 1 bar, respectively, and with a temperature gradient of ∇T = 1.8 K/Å. The NEMD results represented in the right panel were obtained with the DVH model at an average temperature and pressure of 350 K and 500 bar, and using a temperature gradient of 3.7 K/Å. The letters "C" and "D" in the right panel represent thermodynamic states for which additional analyses of the aqueous solution structure were performed. See the main text for details and the Supporting Information for numerical data of the simulated Soret coefficients.

dx.doi.org/10.1021/jp403862x | J. Phys. Chem. B 2013, 117, 8209−8222

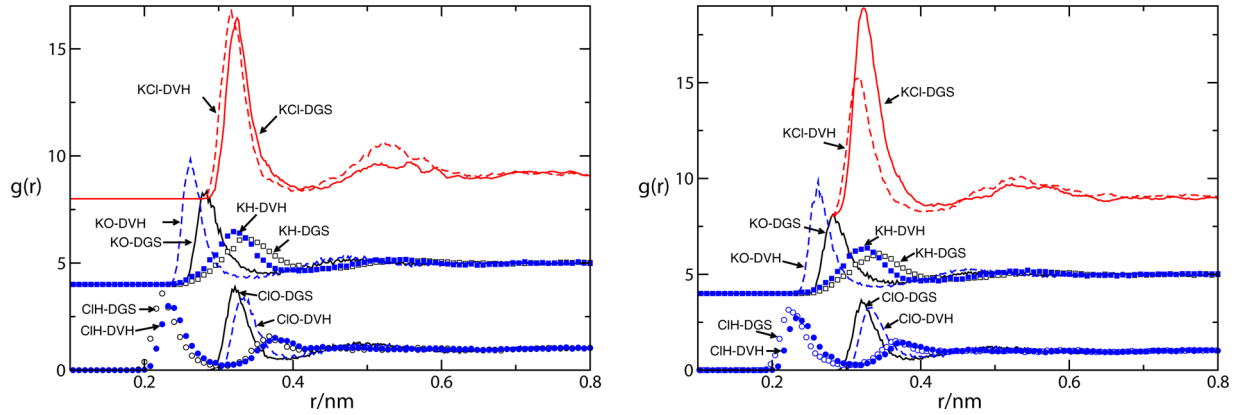

Figure 9. Radial distribution functions of KCl solutions at 1 M concentration at 299 K (left) and 325 K (right). All the simulations were performed at P = 500 bar using computer simulations in the isothermal−isobaric ensemble. The radial distribution functions for cation−water and KCl have been shifted vertically 4 and 8 units, respectively.

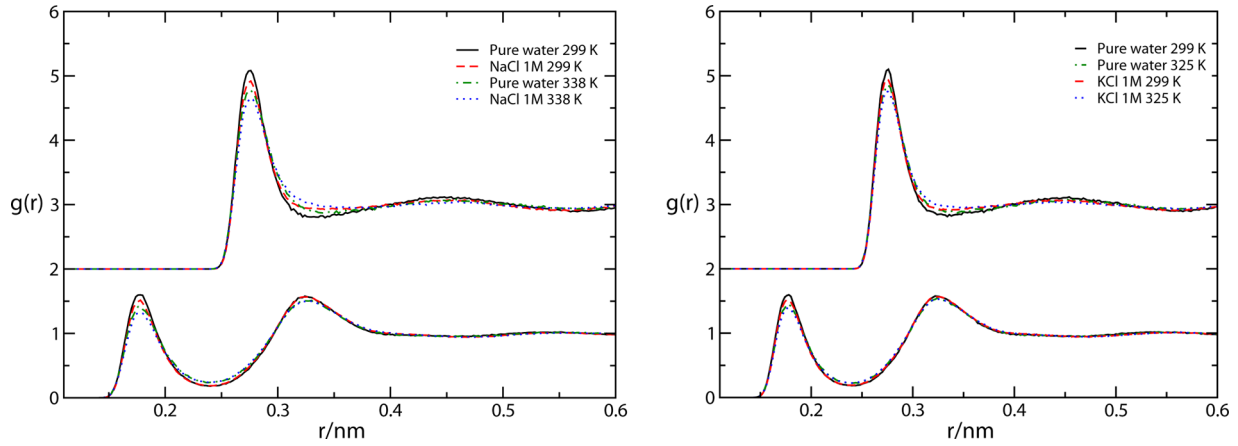

Figure 10. (left) Oxygen−oxygen and oxygen−hydrogen radial distribution functions of pure water and NaCl solutions at 1 M concentration at 299 and 338 K and 100 bar. (right) KCl solutions at 1 M concentration and T = 299 and 325 K and P = 500 bar. All the simulations were performed using equilibrium simulations in the isothermal−isobaric ensemble. The radial distribution functions for OO correlations have been shifted vertically by 2 units. The thermodynamic states investigated correspond to those denoted as "A, B, C, and D" in Figures 6 and 8.

DGS cation being about 20% bigger. These differences are well reflected in the local structure of water around the ions and in the ion−ion correlations. The bigger cation in the DGS model results in a coordination shell (see the KO and KH RDFs in Figure 9) that is shifted to longer distances, with a concomitant increase in the water coordination number (n_{KO} = 6.8 (DGS), 6.1 (DVH) at 299 K). The modifications of the Cl−O coordination shells are less important. We find that the coordination shell of the DVH anions is shifted to shorter distances, and these ions accumulate more water molecules around them (n_{KO} = 6.7 (DGS), 7.1 (DVH) at 299 K). The temperature, 299 or 325 K, has little effect on the water structure, which remains essentially the same, whereas we find larger modifications in the KCl local coordination in the DGS model, which features an enhanced structure in the first coordination shell.

What are the implications of these results to understand the magnitude of the Soret coefficients? First, at 299 K, the K-water solvation shell undergoes the largest perturbation upon modifying the force field parameters, and this is expected to affect to a greater extent the final value of the Soret coefficients. According to this, a less tight solvation shell (KO with DGS model) results in a more negative Soret coefficient (cf. Figure 8, left and right panels, and systems at ∼1 m concentration and 297 K (DGS) and 299 K (DVH)). Second, we find that the KO and ClO coordination shells at 299 and 325 K are very similar, *despite* the fact that the Soret coefficients have opposite signs, hence showing the lack of a clear correlation between the sign of the Soret effect and the ion−water solvation structure. Overall, the analysis above indicates that the ion−water correlations modify the strength of the Soret effect but they are not the primary factor in determining its sign at the thermodynamics conditions considered here.

The negative Soret coefficients that we obtain at low temperatures indicate that the salt accumulates in the warm region, whereas at higher temperatures the coefficient becomes positive, indicating the salt accumulates in the cold region. We note that the change of the sign of the Soret coefficient can also be induced by changing the salt concentration at constant temperature, negative for low concentrations and positive for higher concentrations. The sign inversion of the Soret coefficient with temperature has been discussed in terms of the perturbations undergone by the hydrogen bond network.[36] According to this at low temperatures, the formation of hydrogen bonds is favored and the system would minimize its free energy by accumulating water in the cold side. On the other hand, at high temperatures, the hydrogen bond formation would become less important and moving water molecules

dx.doi.org/10.1021/jp403862x | J. Phys. Chem. B 2013, 117, 8209−8222

toward the warm region would increase their entropy and therefore reduce the free energy. We can take advantage of the computer simulations to investigate to what extent the average hydrogen bond structure of water is modified in aqueous solutions featuring both negative and positive Soret coefficients. Such an analysis is possible, as our simulations show sign inversion. To advance in the analysis of the possible correlations between hydrogen bonding structure and the Soret coefficient, and therefore the origin of the sign inversion, we have performed additional simulations to compute the water−water radial distribution function for ionic solutions featuring Soret coefficients with opposite sign. We have chosen NaCl and KCl solutions at 1 M concentration and thermodynamic conditions corresponding to those represented by the states A, B, C, and D in Figures 6 and 8.

Figure 10 shows the pair correlation functions at different thermodynamic states (see Table 2 and Figures 6 and 8). The most noticeable result from this analysis is that the structure of water is perturbed very little by changes in temperature, pressure, or salt composition. The main structural changes are observed in the OO correlations, where the main peak decreases slightly in height upon increasing the temperature or the salt concentration. We note however that these changes in temperature in NaCl (left panel in Figure 10) and KCl (right panel in Figure 10) lead to a large modification in the magnitude of the Soret coefficient as well as to sign inversion. To explore further the lack of a strong correlation of the water average structure with the sign of the Soret coefficient, we have computed the OO and OH coordination numbers (see Table 2). First, as expected, addition of salt modifies the average OO and OH coordination which is reduced with respect to to pure water. We find that the changes in temperature (299 to 338 K in NaCl and 299 to 325 K in KCl) have a very small impact on the coordination number. Again, these numerical data show the lack of a clear correlation between the water average local structure (measured by the radial distribution function) and the sign of the Soret coefficient.

Table 2. Coordination Numbers Corresponding to the Radial Distribution Functions Represented in Figure 10[a]

		pure water		NaCl		KCl	
T (K)	P (bar)	OO	OH	OO	OH	OO	OH
299	100	4.61	1.84	4.42	1.74		
338	100	4.45	1.81	4.35	1.68		
299	500	4.58	1.88			4.42	1.75
325	500	4.56	1.84			4.39	1.72

[a]The coordination numbers were computed from integration of the pair correlation functions up to 0.334 nm for OO and 0.24 nm for OH correlations. These distances correspond to the first minimum of the radial distribution functions at 100 bar and 299 K. For the OH coordination number, we represent the intermolecular contribution only. The salt concentration is 1 M in all cases. DGS and DVH force fields were used for the NaCl and KCl salts, respectively.

CONCLUSIONS AND FINAL REMARKS

We have investigated the non-equilibrium response of alkali halide solutions (NaCl and KCl) to thermal gradients. State of the art experiments and computer simulations were employed to quantify the Soret coefficient of the ionic solutions. The Soret coefficient is of the order of 10^{-3} K^{-1}, which is within the range measured in earlier experiments using different approaches, and of the same order as the Soret coefficients measured in aqueous solutions containing nucleotides, water−alcohol mixtures, or organic liquid mixtures. This shows that the strength of the Soret effects in these systems is fairly independent of the specific composition. Despite the apparent simplicity of the alkali halide solutions, we find that their response to thermal gradients is very rich. From our experiments, we infer that the Soret coefficient does not depend on concentration (0.5−4 m) at $T^* \sim 318$ K for NaCl and $T^* \sim 313$ K for KCl solutions. Above these temperatures, the Soret coefficient decreases with salt concentration, whereas it increases with concentration below T^*. Most of the Soret coefficients reported in this work are positive, meaning that the salt accumulates in the cold side; i.e., it is thermophobic. However, we have found that at low enough temperatures the Soret coefficient reverses its sign. This observation agrees with previous investigations using different experimental setups. The sign inversion temperature depends on the solution composition, 283 K for NaCl and for 293 KCl at 0.5 M concentration.

To gain microscopic insight on this complex behavior, we have performed non-equilibrium molecular dynamics simulations of alkali halide solutions. Our models are atomistic, and consist of a combination of a rigid non-polarizable model for water (SPC/E) and two different non-polarizable models for the ions. The models were validated by computing the thermal conductivity of the solutions as a function of the salt concentration. The models are accurate in predicting the reduction of the thermal conductivity with salt. Although the hydrogen bond structure of water is significantly distorted at high concentrations, we find that the reduction of the thermal conductivity can be explained in terms of the solution density alone. We have shown that a phenomenological model based on the Bridgman equation, which considers the change in the number density of the solution and the concomitant change in the energy transported per unit volume, provides a quantitative prediction of the dependence of the thermal conductivity with salt concentration.

In addition to the heat transport in aqueous solution, the simulation models predict Soret coefficients of the right order of magnitude and reproduce the correct dependence of the Soret coefficient with concentration and temperature, including the sign reversal at low temperatures. Different authors have suggested a possible connection between the sign reversal in the Soret coefficient and the maximum of density in water. We note that our simulations predict sign reversal at $T \sim 300$ K at a temperature that is much higher than the temperature at which the SPC/E features the density maximum. Hence, our simulation results do not support a correlation between the sign reversal in the Soret coefficient and the dependence of the thermal expansion coefficient of water with temperature.

We have attempted to establish a correlation between the local structure of ions and water molecules and the sign of the Soret coefficient. We have employed as order parameters the radial distribution functions and coordination numbers. We find that changes in temperature equivalent to those needed to induce the sign reversal of the Soret coefficient have a minor impact on the water structure and on the ion average solvation shells. The radial distribution functions do not show a clear correlation between the sign of the Soret coefficient and the ion solvation structure.

It has been suggested that changes in the solvent structure, in particular hydrogen bonding, may influence the thermodiffusive behavior of aqueous solutions. Our results show that the water

dx.doi.org/10.1021/jp403862x | J. Phys. Chem. B 2013, 117, 8209−8222

radial distribution of solutions featuring Soret coefficients of opposite signs are very similar. These results show again the lack of a clear correlation between the sign of the Soret effect and the water structure as measured by the radial distribution function. Hence, we conclude that the radial distribution function, which is widely used to investigate the local structure around ions and water, is not sensitive enough to detect the crucial changes that lead to the peculiar behavior of the Soret effect in ionic solutions. Additional work is therefore needed, possibly exploiting other statistical mechanics variables (e.g., orientational correlations) to establish a correlation between the Soret effect and water structure. Work in this direction using the models discussed in this work is in progress.

■ ASSOCIATED CONTENT

Supporting Information

Experimental and simulation data for thermal conductivities and Soret coefficients. This material is available free of charge via the Internet at http://pubs.acs.org.

■ AUTHOR INFORMATION

Corresponding Author

*E-mail: s.wiegand@fz-juelich.de (S.W.); f.bresme@imperial.ac.uk (F.B.).

Present Address

[‖]F.R.: Forschungszentrum Jülich GmbH, ICS-2 − Theoretical Soft Matter and Biophysics, D-52428 Jülich, Germany.

Notes

The authors declare no competing financial interest.

■ ACKNOWLEDGMENTS

This work has been funded by the Leverhulme Trust and the EPSRC. F.B. would like to thank the EPSRC for the award of a Leadership Fellowship. We thank the Imperial College High Performance Computing Service for providing computational resources. We thank Mounir Bou-Ali, Jean Colombani, and Pablo Blanco for illuminating discussions and comments on thermogravitational column experiments.

■ REFERENCES

(1) Duhr, S.; Braun, D. Thermophoretic Depletion Follows Boltzmann Distribution. *Phys. Rev. Lett.* **2006**, *96*, No. 168301.
(2) Rasauli, S.; Golestanian, R. Soret Motion of a Charged Spherical Colloid. *Phys. Rev. Lett.* **2008**, *101*, No. 108301.
(3) Würger, A. Transport in Charged Colloids Driven by Thermoelectricity. *Phys. Rev. Lett.* **2008**, *101*, No. 108302.
(4) Jiang, H.; Wada, H.; Yoshinaga, N.; Sano, M. Manipulation of Colloids by a Nonequilibrium Depletion Force in a Temperature Gradient. *Phys. Rev. Lett.* **2009**, *102*, No. 208301.
(5) Maeda, Y.; Buguin, A.; Libchaber, A. Thermal Separation: Interplay between the Soret Effect and Entropic Force Gradient. *Phys. Rev. Lett.* **2011**, *107*, No. 038301.
(6) Debuschewitz, C.; Köhler, W. Molecular Origin of Thermal Diffusion in Benzene Plus Cyclohexane Mixtures. *Phys. Rev. Lett.* **2001**, *87*, No. 055901.
(7) Wiegand, S. Thermal Diffusion in Liquid Mixtures and Polymer Solutions. *J. Phys.: Condens. Matter* **2004**, *16*, R357−R379.
(8) Artola, P.; Rousseau, B. Microscopic Interpretation of a Pure Chemical Contribution to the Soret Effect. *Phys. Rev. Lett.* **2007**, *98*, No. 125901.
(9) Mast, C.; Braun, D. Thermal Trap for DNA Replication. *Phys. Rev. Lett.* **2010**, *104*, No. 188102.
(10) Wienken, C.; Baaske, P.; Rothbauer, U.; Braun, D.; Duhr, S. Protein-Binding Assays in Biological Liquids Using Microscale Thermophoresis. *Nat. Commun.* **2010**, *1*, 100.
(11) Bresme, F.; Lervik, A.; Bedeaux, D.; Kjelstrup, S. Water Polarization under Thermal Gradients. *Phys. Rev. Lett.* **2008**, *101*, No. 020602.
(12) Römer, F.; Bresme, F.; Muscatello, J.; Bedeaux, D.; Rubí, J. Thermomolecular Orientation of Nonpolar Fluids. *Phys. Rev. Lett.* **2012**, *108*, No. 105901.
(13) Eisenberg, D.; Kauzmann, W. *The Structure and Properties of Water*; Oxford University Press: Oxford, U.K., 1969.
(14) Putnam, S.; Cahill, D.; Wong, G. Temperature Dependence of Thermodiffusion in Aqueous Suspensions of Charged Nanoparticles. *Langmuir* **2007**, *23*, 9221−9228.
(15) Iacopini, S.; Rusconi, R.; Piazza, R. The "Macromolecular Tourist": Universal Temperature Dependence of Thermal Diffusion in Aqueous Colloidal Suspensions. *Eur. Phys. J. E* **2006**, *19*, 59−67.
(16) Brenner, H. Self-Thermophoresis and Thermal Self-Diffusion in Liquids and Gases. *Phys. Rev. E* **2010**, *82*, No. 036325.
(17) Kita, R.; Wiegand, S.; Luettmer-Strathmann, J. Sign Change of the Soret Coefficient of Poly(ethylene oxide) in Water/Ethanol Mixtures Observed by TDFRS. *J. Chem. Phys.* **2004**, *121*, 3874−3885.
(18) Duhr, S.; Braun, D. Why Molecules Move along a Temperature Gradient. *Proc. Natl. Acad. Sci. U.S.A.* **2006**, *103*, 19678−19682.
(19) Soret, C. Sur L'État D'Équilibre que Prend, du Point de Vue de sa Concentration, une Dissolution Saline Primitivement Homogéne, Dont Deux Parties Sont Portées à des Températures Différentes. *Arch. Sci. Phys. Nat., Geneve* **1879**, *2*, 48−61.
(20) Caldwell, D. Measurement of Negative Thermal-Diffusion Coefficients by Observing Onset of Thermohaline Convection. *J. Phys. Chem.* **1973**, *77*, 2004−2008.
(21) Gaeta, F.; Perna, G.; Scala, G.; Bellucci, F. Non-Isothermal Matter Transport in Sodium-Chloride and KCl Aqueous-Solutions. 1. Homogeneous System (Thermal-Diffusion). *J. Phys. Chem.* **1982**, *86*, 2967−2974.
(22) Longsworth, L. The Temperature Dependence of the Soret Coefficient of Aqueous Potassium Chloride. *J. Phys. Chem.* **1957**, *61*, 1557−1562.
(23) Snowdon, P.; Turner, J. The Soret Effect in Some 0.01 Normal Aqueous Electrolytes. *Trans. Faraday Soc.* **1960**, *56*, 1409−1418.
(24) Snowdon, P.; Turner, J. The Concentration Dependence of the Soret Effect. *Trans. Faraday Soc.* **1960**, *56*, 1812−1819.
(25) Alexander, K. F. Zur Theorie der Thermodiffusion in Flüssigkeiten. *Z. Phys. Chem. (Leipzig)* **1954**, *203*, 213−227.
(26) Platten, J. K.; Bou-Ali, M. M.; Costeseque, P.; Dutrieux, J. F.; Köhler, W.; Leppla, C.; Wiegand, S.; Wittko, G. Benchmark Values for the Soret, Thermal Diffusion and Diffusion Coefficients of Three Binary Organic Liquid Mixtures. *Philos. Mag.* **2003**, *83*, 1965−1971.
(27) Colombani, J.; Bert, J.; Dupuy-Philon, J. Thermal Diffusion in (LiCl,RH2O). *J. Chem. Phys.* **1999**, *110*, 8622−8627.
(28) Gaeta, F. S.; Scala, G.; Brescia, G.; Dichiara, A. Characterization of Macromolecules in Liquid Solutions by Thermal-Diffusion. 1. Dependence of Soret Coefficient on Nature of Dispersing Medium. *J. Polym. Sci., Polym. Phys. Ed.* **1975**, *13*, 177−202.
(29) Ecenarro, O.; Madariaga, J. A.; Navarro, J.; Santamaria, C. M.; Carrion, J. A.; Saviron, J. M. Fickian and Thermal-Diffusion Coefficients from Liquid Thermogravitational Columns. *J. Phys.: Condens. Matter* **1990**, *2*, 2289−2296.
(30) Köhler, W.; Müller, B. Soret and Mass Diffusion-Coefficients of Toluene N-Hexane Mixtures. *J. Chem. Phys.* **1995**, *103*, 4367−4370.
(31) Bou-Ali, M. M.; Ecenarro, O.; Madariaga, J. A.; Santamaria, C. M.; Valencia, J. J. Thermogravitational Measurement of the Soret Coefficient of Liquid Mixtures. *J. Phys.: Condens. Matter* **1998**, *10*, 3321−3331.
(32) Lü, H.; Leaist, D. G. Thermal-Diffusion of Tetrabutylammonium Salts in Aqueous-Solution at 25-degrees-C. *J. Solution Chem.* **1991**, *20*, 199−205.
(33) Polyakov, P.; Luettmer-Strathmann, J.; Wiegand, S. Study of the Thermal Diffusion Behavior of Alkane/Benzene Mixtures by Thermal

Diffusion Forced Rayleigh Scattering Experiments and Lattice Model Calculations. *J. Phys. Chem. B* **2006**, *110*, 26215−26224.
(34) Blanco, P.; Wiegand, S. Study of the Soret Effect in Monosaccharide Solutions. *J. Phys. Chem. B* **2010**, *114*, 2807−2813.
(35) Blanco, P.; Kriegs, H.; Arlt, B.; Wiegand, S. Thermal Diffusion of Oligosaccharide Solutions: The Role of Chain Length and Structure. *J. Phys. Chem. B* **2010**, *114*, 10740−10747.
(36) Wang, Z.; Kriegs, H.; Wiegand, S. Thermal Diffusion of Nucleotides. *J. Phys. Chem. B* **2012**, *116*, 7463−7469.
(37) Stadelmaier, D.; Köhler, W. From Small Molecules to High Polymers: Investigation of the Crossover of Thermal Diffusion in Dilute Polystyrene Solutions. *Macromolecules* **2008**, *41*, 6205−6209.
(38) Ning, H.; Wiegand, S. Experimental Investigation of the Soret Effect in Acetone/Water and Dimethylsulfoxide/Water Mixtures. *J. Chem. Phys.* **2006**, *125*, No. 221102.
(39) Polyakov, P.; Wiegand, S. Systematic Study of the Thermal Diffusion in Associated Mixtures. *J. Chem. Phys.* **2008**, *128*, No. 034505.
(40) Prigogine, I.; Debrouckere, L.; Amand, R. Recherches Sur La Thermodiffusion En Phase Liquide. 2. *Physica* **1950**, *16*, 851−860.
(41) Rousseau, B.; Nieto-Draghi, C.; Avalos, J. The Role of Molecular Interactions in the Change of Sign of the Soret Coefficient. *Europhys. Lett.* **2004**, *67*, 976−982.
(42) Baaske, P.; Wienken, C.; Reineck, P.; Duhr, S.; Braun, D. Optical Thermophoresis for Quantifying the Buffer Dependence of Aptamer Binding. *Angew. Chem., Int. Ed.* **2010**, *49*, 2238−2241.
(43) Nieto-Draghi, C.; Avalos, J.; Rousseau, B. Computing the Soret Coefficient in Aqueous Mixtures Using Boundary Driven Non-equilibrium Molecular Dynamics. *J. Chem. Phys.* **2005**, *122*, No. 114503.
(44) Bresme, F.; Hafskjold, B.; Wold, I. Nonequilibrium Molecular Dynamics Study of Heat Conduction in Ionic Systems. *J. Phys. Chem.* **1996**, *100*, 1879−1888.
(45) Wiegand, S.; Ning, H.; Kriegs, H. Thermal Diffusion Forced Rayleigh Scattering Setup Optimized for Aqueous Mixtures. *J. Phys. Chem. B* **2007**, *111*, 14169−14174.
(46) Groot, S. R. D.; Mazur, P. O. *Non-Equilbrium Thermodynamics*; North-Holland Pub. Co.: Amsterdam, The Netherlands, 1962.
(47) Ikeshoji, T.; Hafksjold, B. Nonequilibrium Molecular-Dynamics Calculation of Heat-Conduction in Liquid and through Liquid-Gas Interface. *Mol. Phys.* **1994**, *81*, 251−261.
(48) Bresme, F. Equilibrium and Nonequilibrium Molecular-Dynamics Simulations of the Central Force Model of Water. *J. Chem. Phys.* **2001**, *115*, 7564−7574.
(49) Hockney, R. W. The Potential Calculation and Some Applications. *Methods Comput. Phys.* **1970**, *9*, 136−211.
(50) Muscatello, J.; Bresme, F. A Comparison of Coulombic Interaction Methods in Non-Equilibrium Studies of Heat Transfer in Water. *J. Chem. Phys.* **2011**, *135*, No. 234111.
(51) Essmann, U.; Perera, L.; Berkowitz, M. L.; Darden, T.; Lee, H.; Pedersen, L. G. A Smooth Particle Mesh Ewald Method. *J. Chem. Phys.* **1995**, *103*, 8577−8593.
(52) Berendsen, H. J. C.; Grigera, J. R.; Straatsma, T. P. The Missing Term in Effective Pair Potentials. *J. Phys. Chem.* **1987**, *91*, 6269−6271.
(53) Miyamoto, S.; Kollman, P. A. Settle: An Analytical Version of the SHAKE and RATTLE Algorithm for Rigid Water Models. *J. Comput. Chem.* **1992**, *13*, 952−962.
(54) Bresme, F.; Chacón, E.; Tarazona, P.; Wynveen, A. The Structure of Ionic Aqueous Solutions at Interfaces: An Intrinsic Structure Analysis. *J. Chem. Phys.* **2012**, *137*, No. 114706.
(55) Dang, L. X. Development of Nonadditive Intermolecular Potentials Using Molecular Dynamics: Solvation of Li^+ and F^- Ions in Polarizable Water. *J. Chem. Phys.* **1992**, *96*, 6970−6977.
(56) Dang, L. X.; Garrett, B. C. Photoelectron Spectra of the Hydrated Iodine Anion from Molecular Dynamics Simulations. *J. Chem. Phys.* **1993**, *99*, 2972−2977.
(57) Smith, D. E.; Dang, L. X. Computer Simulations of NaCl Association in Polarizable Water. *J. Chem. Phys.* **1994**, *100*, 3757−3766.
(58) Dang, L. X. Mechanism and Thermodynamics of Ion Selectivity in Aqueous Solutions of 18-Crown-6 Ether: A Molecular Dynamics Study. *J. Am. Chem. Soc.* **1995**, *117*, 6954−6960.
(59) Deublein, S.; Vrabec, J.; Hasse, H. A Set of Molecular Models for Alkali and Halide Ions in Aqueous Solution. *J. Chem. Phys.* **2012**, *136*, No. 084501.
(60) Allen, M. P.; Tildesley, D. J. *Computer Simulation of Liquids*; Oxford University Press: New York, 1989.
(61) Römer, F.; Lervik, A.; Bresme, F. Nonequilibrium Molecular Dynamics Simulations of the Thermal Conductivity of Water: A Systematic Investigation of the SPC/E and TIP4P/2005 Models. *J. Chem. Phys.* **2012**, *137*, No. 074503.
(62) Bussi, G.; Donadio, D.; Parrinello, M. Canonical Sampling through Velocity Rescaling. *J. Chem. Phys.* **2007**, *126*, No. 014101.
(63) Hess, B.; Kutzner, C.; van der Spoel, D.; Lindahl, E. GROMACS 4: Algorithms for Highly Efficient, Load-Balanced, and Scalable Molecular Simulation. *J. Chem. Theory Comput.* **2008**, *4*, 435−447.
(64) Blanco, P.; Kriegs, H.; Lettinga, M.; Holmqvist, P.; Wiegand, S. Thermal Diffusion of a Stiff Rod-Like Mutant Y21M-fd-Virus. *Biomacromolecules* **2011**, *12*, 1602−1609.
(65) Ning, H.; Datta, S.; Sottmann, T.; Wiegand, S. Soret Effect of Nonionic Surfactants in Water Studied by Different Transient Grating Setups. *J. Phys. Chem. B* **2008**, *112*, 10927−10934.
(66) Arlt, B.; Datta, S.; Sottmann, T.; Wiegand, S. Soret Effect of *n*-Octyl β-D-Glucopyranoside (C_8G_1) in Water around the Critical Micelle Concentration. *J. Phys. Chem. B* **2010**, *114*, 2118−2123.
(67) Wittko, G.; Köhler, W. Precise Determination of the Soret, Thermal Diffusion and Mass Diffusion Coefficients of Binary Mixtures of Dodecane, Isobutylbenzene and 1,2,3,4-Tetrahydronaphthalene by a Holographic Grating Technique. *Philos. Mag.* **2003**, *83*, 1973−1987.
(68) Ning, H.; Kita, R.; Kriegs, H.; Luettmer-Strathmann, J.; Wiegand, S. Thermal Diffusion Behavior of Nonionic Surfactants in Water. *J. Phys. Chem. B* **2006**, *110*, 10746−10756.
(69) Becker, A.; Köhler, W.; Müller, B. A Scanning Michelson Interferometer for the Measurement of the Concentration and Temperature Derivative of the Refractive-Index of Liquids. *Ber. Bunsen-Ges.* **1995**, *99*, 600−608.
(70) Camerini-Otero, R. D.; Franklin, R. M.; Day, L. A. Molecular Weights, Dispersion of Refractive Index Increments, and Dimensions from Transmittance Spectrophotometry. Bacteriophages R17, T7, and PM2, and Tobacco Mosaic Virus. *Biochemistry* **1974**, *13*, 3763−3773.
(71) Sechenyh, V. V.; Legros, J. C.; Shevtsova, V. Experimental and Predicted Refractive Index Properties in Ternary Mixtures of Associated Liquids. *J. Chem. Thermodyn.* **2011**, *43*, 1700−1707.
(72) Muscatello, J.; Römer, F.; Sala, J.; Bresme, F. Water under Temperature Gradients: Polarization Effects and Microscopic Mechanisms of Heat Transfer. *Phys. Chem. Chem. Phys.* **2011**, *13*, 19970−19978.
(73) Bresme, F.; Römer, F. Heat Transport in Liquid Water at Extreme Pressures: A Non Equilibrium Molecular Dynamics Study. *J. Mol. Liq.* **2012**, DOI: 10.1016/j.molliq.2012.09.013.
(74) National Institut of Standards and Technology, NIST Chemistry WebBook. http://webbook.nist.gov/chemistry/.
(75) Ramires, M. L. V.; Nieto de Castro, C. A. Thermal Conductivity of Aqueous Potassium Chloride Solutions. *Int. J. Thermophys.* **2000**, *21*, 671−679.
(76) Ramires, M. L. V.; Nieto de Castro, C. A.; Fareleira, J. M. N. A.; Wakeham, W. A. Thermal Conductivity of Aqueous Sodium Chloride Solutions. *J. Chem. Eng. Data* **1994**, *39*, 186−190.
(77) Chau, P.-L.; Hardwick, A. J. A New Order Parameter for Tetrahedral Configurations. *Mol. Phys.* **1998**, *93*, 511−518.
(78) Bridgman, P. The Thermal Conductivity of Liquids. *Proc. Natl. Acad. Sci. U.S.A.* **1923**, *9*, 341−345.
(79) Vega, C.; Abascal, J. Simulating Water with Rigid Non-Polarizable Models: A General Perspective. *Phys. Chem. Chem. Phys.* **2011**, *13*, 19663−19688.
(80) Harrington, S.; Poole, P.; Sciortino, F.; Stanley, H. Equation of State of Supercooled Water Simulated Using the Extended Simple

Point Charge Intermolecular Potential. *J. Chem. Phys.* **1997**, *107*, 7443−7450.
(81) Wittko, G.; Köhler, W. On the Temperature Dependence of Thermal Diffusion of Liquid Mixtures. *Eur. Phys. Lett.* **2007**, *78*, No. 46007.

Support information

Table 3.1: *Thermal conductivity data from simulations of aqueous KCl and NaCl solutions: Salt concentration, density with respect to water, temperature gradient, heat flux and thermal conductivity.*

c/mol kg^{-1}	$\rho_{\mathrm{ave,H_2O}}$/g cm^{-3}	∇T/K nm^{-1}	J_U / 10^{10} W m^{-2}	λ / W m^{-1} K^{-1}
KCl, DGS ions, T_{ave}/K = 350, p/bar = 500				
1	0.9562	-37.60±0.02	3.12±0.07	0.83±0.02
2	0.9346	-37.00±0.02	2.96±0.07	0.80±0.02
3	0.9115	-36.54±0.02	2.82±0.07	0.77±0.02
4	0.8930	-36.38±0.03	2.72±0.07	0.75±0.02
KCl, DGS ions, T_{ave}/K = 300, p/bar= 1				
1	0.9562	-18.91±0.02	1.51±0.06	0.80±0.03
2	0.9346	-18.65±0.02	1.44±0.06	0.77±0.03
3	0.9115	-18.40±0.02	1.36±0.06	0.74±0.03
4	0.8930	-18.31±0.02	1.32±0.06	0.72±0.03
KCl, DHV ions, T_{ave}/K = 350, p/bar = 500				
1	0.9562	-37.86±0.02	3.14±0.07	0.83±0.02
2	0.9346	-37.37±0.03	3.01±0.07	0.80±0.02
3	0.9115	-36.71±0.02	2.85±0.07	0.78±0.02
4	0.8930	-36.57±0.03	2.77±0.07	0.76±0.02
NaCl, DGS ions, T_{ave}/K = 350, p/bar = 500				
1	0.9692	-37.68±0.02	3.20±0.07	0.85±0.02
2	0.9582	-37.09±0.02	3.11±0.07	0.84±0.02
3	0.9481	-36.73±0.02	3.04±0.07	0.83±0.02
4	0.9394	-36.58±0.02	3.01±0.07	0.82±0.02
NaCl, DGS ions, T_{ave}/K = 350, p/bar = 100				
1	0.9621	-37.91±0.03	3.17±0.09	0.84±0.02
2	0.9531	-37.34±0.03	3.11±0.09	0.83±0.03
3	0.9457	-36.99±0.02	3.02±0.09	0.82±0.03
4	0.9335	-36.73±0.03	2.99±0.09	0.81±0.03

Table 3.2: *The Soret coefficient for NaCl solutions at different concentrations, temperature and pressures from simulations: Average temperature and salt concentration in observed region and Soret coefficient.*

$\frac{T}{\mathrm{K}}$	$\frac{m}{\mathrm{mol\ kg^{-1}}}$	$\frac{s_T}{10^{-3}\mathrm{K^{-1}}}$	$\frac{T}{\mathrm{K}}$	$\frac{m}{\mathrm{mol\ kg^{-1}}}$	$\frac{s_T}{10^{-3}\mathrm{K^{-1}}}$
$p/\mathrm{bar} = 500$			$p/\mathrm{bar} = 100$		
318	1.22±0.02	1.71±0.26	299	1.22±0.02	-1.80±0.59
318	2.31±0.03	1.34±0.34	299	2.43±0.03	-0.08±0.62
318	3.50±0.04	1.61±0.24	299	3.64±0.03	0.68±0.35
318	4.59±0.04	1.27±0.22	299	4.64±0.03	0.67±0.21
328	1.18±0.03	2.54±0.09	309	1.20±0.02	1.08±0.30
328	2.28±0.05	2.38±0.08	309	2.39±0.03	1.40±0.19
328	3.41±0.06	1.70±0.07	309	3.57±0.05	1.55±0.10
328	4.51±0.06	1.45±0.04	309	4.61±0.03	0.79±0.06
339	1.13±0.04	3.06±0.12	318	1.17±0.03	2.23±0.14
339	2.22±0.07	2.68±0.08	318	2.34±0.04	1.65±0.07
339	3.33±0.07	1.61±0.04	318	3.51±0.06	1.56±0.05
339	4.43±0.08	1.44±0.03	318	4.55±0.04	0.83±0.05
348	1.10±0.04	3.46±0.14	328	1.16±0.03	3.44±0.20
348	2.16±0.07	2.68±0.08	328	2.30±0.04	2.05±0.14
348	3.30±0.07	1.93±0.04	328	3.47±0.05	1.81±0.08
348	4.38±0.08	1.61±0.03	328	4.52±0.04	1.00±0.07
358	1.07±0.05	4.00±0.17	338	1.11±0.04	4.34±0.36
358	2.10±0.07	2.87±0.09	338	2.25±0.04	2.14±0.13
358	3.24±0.07	2.02±0.04	338	3.39±0.05	1.95±0.13
358	4.30±0.08	1.77±0.03	338	4.46±0.06	1.56±0.15

Table 3.3: *The Soret coefficient for KCl solutions at different concentrations, temperature, pressures and potential models from simulations: Average temperature and salt concentration in observed region and Soret coefficient.*

$\frac{T}{\mathrm{K}}$	$\frac{m}{\mathrm{mol\ kg^{-1}}}$	$\frac{s_T}{10^{-3}\mathrm{K^{-1}}}$	$\frac{T}{\mathrm{K}}$	$\frac{m}{\mathrm{mol\ kg^{-1}}}$	$\frac{s_T}{10^{-3}\mathrm{K^{-1}}}$	$\frac{T}{\mathrm{K}}$	$\frac{m}{\mathrm{mol\ kg^{-1}}}$	$\frac{s_T}{10^{-3}\mathrm{K^{-1}}}$
DGS ions, p/bar = 500			DGS ions, p/bar = 1			DHV ions, p/bar = 500		
334	1.22±0.05	3.23±0.13	288	1.19±0.02	-2.98±0.11	299	1.35±0.01	-0.80±0.20
334	2.48±0.09	3.15±0.12	288	2.39±0.03	-0.41±0.20	299	1.35±0.01	-0.80±0.20
334	3.71±0.10	2.31±0.07	288	3.67±0.07	1.69±0.26	299	2.69±0.03	-0.36±0.27
334	4.97±0.15	2.25±0.10	288	4.96±0.07	2.16±0.09	299	3.93±0.04	-0.25±0.25
341	1.20±0.05	3.44±0.14	297	1.20±0.02	-1.77±0.17	299	5.16±0.06	0.77±0.30
341	2.43±0.10	3.60±0.15	297	2.39±0.03	1.82±0.16	308	1.34±0.02	0.82±0.22
341	3.64±0.11	2.59±0.08	297	3.62±0.08	3.94±0.14	308	2.63±0.05	1.51±0.22
341	4.89±0.17	2.70±0.11	297	4.84±0.09	3.13±0.11	308	3.86±0.06	1.34±0.19
348	1.17±0.05	3.58±0.15	306	1.20±0.02	0.89±0.24	308	5.07±0.08	1.52±0.14
348	2.37±0.11	3.92±0.17	306	2.33±0.05	3.85±0.13	317	1.31±0.03	1.99±0.16
348	3.57±0.12	2.85±0.10	306	3.54±0.08	3.65±0.15	317	2.57±0.06	2.12±0.13
348	4.81±0.18	3.15±0.12	306	4.68±0.10	3.60±0.12	317	3.78±0.09	2.05±0.12
355	1.15±0.05	3.67±0.16	315	1.18±0.03	4.05±0.20	317	4.99±0.09	1.74±0.07
355	2.31±0.11	4.16±0.19	315	2.25±0.06	4.87±0.14	325	1.31±0.05	6.17±0.71
355	3.49±0.13	3.10±0.12	315	3.40±0.06	3.18±0.12	325	2.54±0.09	5.12±0.89
355	4.71±0.20	3.53±0.14	315	4.52±0.13	5.08±0.15	325	3.73±0.10	3.87±0.24
362	1.12±0.05	3.77±0.17				325	4.91±0.07	1.93±0.25
362	2.24±0.11	4.37±0.21				334	1.26±0.05	4.92±0.27
362	3.41±0.14	3.45±0.14				334	2.47±0.07	3.48±0.25
362	4.60±0.21	3.86±0.16				334	3.63±0.10	3.44±0.14
369	1.08±0.05	3.94±0.18				334	4.82±0.07	1.98±0.07
369	2.17±0.12	4.70±0.24						
369	3.33±0.15	3.85±0.16						
369	4.49±0.22	4.20±0.18						

Table 3.4: *Results from TDFRS experiments of aqueous NaCl and KCl solutions: Soret Coefficient s_T, Diffusion Coefficient D, Thermal Diffusivity D_{th} and Thermal Diffusion Coefficient D_T.*

T/K	$s_T/10^{-3}\text{K}^{-1}$	$D/10^{-5}\text{cm}^2\text{s}^{-1}$	$D_{\text{th}}/10^{-3}\text{cm}^2\text{s}^{-1}$	$D_T/10^{-8}\text{cm}^2\text{s}^{-1}\text{K}^{-1}$
NaCl, $c/\text{mol kg}^{-1} = 4$				
298	1.879±0.007	2.184±0.023	2.101±0.158	4.11±0.06
308	2.097±0.080	2.823±0.136	2.056±0.031	5.93±0.51
318	2.103±0.010	3.322±0.022	2.061±0.060	6.99±0.01
328	2.315±0.127	4.118±0.144	2.204±0.108	9.55±0.87
338	2.358±0.001	4.708±0.110	2.206±0.084	11.11±0.27
NaCl, $c/\text{mol kg}^{-1} = 2$				
298	1.623±0.010	2.104±0.036	2.022±0.027	3.42±0.04
308	1.980±0.045	2.635±0.015	2.053±0.052	5.21±0.09
318	2.219±0.004	3.215±0.010	2.111±0.014	7.13±0.01
328	2.468±0.012	3.862±0.036	2.151±0.007	9.53±0.04
338	2.522±0.027	4.593±0.006	2.208±0.001	11.58±0.14
NaCl, $c/\text{mol kg}^{-1} = 0.5$				
298	1.209±0.107	2.043±0.030	1.987±0.056	2.47±0.25
308	1.828±0.034	2.508±0.088	2.063±0.017	4.59±0.18
318	2.330±0.011	3.027±0.064	2.087±0.005	7.05±0.12
328	2.780±0.051	3.729±0.125	2.156±0.030	10.36±0.16
338	3.155±0.064	4.228±0.142	2.171±0.020	13.35±0.72
KCl, $c/\text{mol kg}^{-1} = 2$				
298	0.947±0.001	2.026±0.004	1.541±0.002	1.92±0.01
308	1.477±0.018	2.414±0.034	1.528±0.010	3.57±0.09
318	1.931±0.018	2.982±0.012	1.609±0.034	5.76±0.08
328	2.199±0.012	3.500±0.016	1.613±0.000	7.70±0.07
338	2.654±0.010	4.004±0.005	1.621±0.009	10.63±0.02
KCl, $c/\text{mol kg}^{-1} = 0.5$				
288	-0.567±0.011	1.648±0.012	1.436±0.023	-0.93±0.02
298	0.494±0.029	1.520±0.120	1.465±0.004	0.78±0.14
308	1.361±0.031	2.073±0.136	1.511±0.036	2.82±0.25
318	2.058±0.053	2.537±0.039	1.549±0.003	5.22±0.21

CHAPTER

FOUR

THERMOPHORESIS OF CHARGED COLLOIDAL RODS

Wang, Z., Kriegs, H., Buitenhuis, J., Dhont, J. K. G. and Wiegand, S., Thermophoresis of charged colloidal rods. *Soft Matter*, 9(36), 8697-8704, 2013. -Reproduced by permission of The Royal Society of Chemistry

Soft Matter

RSC Publishing

PAPER

View Article Online
View Journal | View Issue

Thermophoresis of charged colloidal rods

Cite this: *Soft Matter*, 2013, **9**, 8697

Zilin Wang,[a] Hartmut Kriegs,[a] Johan Buitenhuis,[a] Jan K. G. Dhont*[ab] and Simone Wiegand[a]

The thermal diffusion behavior of dilute solutions of very long and thin, charged colloidal rods (*fd*-virus particles) is studied using a holographic grating technique. The Soret coefficient of the charged colloids is measured as a function of the Debye screening length, as well as the rod-concentration. The Soret coefficient of the *fd*-viruses increases monotonically with increasing Debye length, while there is a relatively weak dependence on the rod-concentration when the ionic strength is kept constant. An existing theory for thermal diffusion of charged spheres is extended to describe the thermal diffusion of long and thin charged rods, leading to an expression for the Soret coefficient in terms of the Debye length, the rod-core dimensions, and the surface charge density. The thermal diffusion coefficient of a charged colloidal rod is shown to be accurately represented, for arbitrary Debye lengths, by a superposition of spherical beads with the same diameter of the rod and the same surface charge density. The experimental Soret coefficients are compared with this and other theories, and are contrasted against the thermal diffusion behaviour of charged colloidal spheres.

Received 24th May 2013
Accepted 18th July 2013

DOI: 10.1039/c3sm51456k

www.rsc.org/softmatter

1 Introduction

Thermal diffusion, which is also known as the Ludwig–Soret effect, is the phenomenon where mass transport is induced by a temperature gradient in a multi-component system. For sufficiently small gradients, the mass flux induced by a temperature gradient ∇T is equal to $-D_T\nabla T$, where D_T is the thermal diffusion coefficient. Thermal diffusion leads to gradients ∇c in concentration, which in turn give rise to a mass flux equal to $-D\nabla c$, where D is the mass diffusion coefficient. The two fluxes counter balance in a stationary state, from which it follows that the ratio of the concentration gradient and the temperature gradient in such a stationary state is equal to the Soret coefficient $S_T = D_T/\rho D$, where ρ is the number density of colloids. The Soret coefficient can be regarded as a response function, which measures the concentration gradient induced per unit of temperature gradient. Note that often a slightly modified definition of the thermal diffusion coefficient is used in experimental contexts,[1] which contains an additional prefactor related to concentration (as discussed by Ning *et al.*,[2] and in Section 4 of the present paper).

In many previous studies, attempts have been made for mixtures of non-polar liquids to relate the Soret coefficient to the mass of the molecules, their moment of inertia, and the viscosity and thermal expansion coefficient.[1] In aqueous systems, where the situation is more complicated, hydrogen bonds and the charge effect are of significant importance.[3,4]

With the advent of new experimental techniques in the last few years, it became possible to investigate the thermal diffusion behaviour of relatively slowly diffusing macromolecules. A number of experimental studies have been performed on charged macromolecules, such as DNA, ionic surfactants, surface modified polystyrene spheres and silica colloids.[2,5–8] For charged silica Ludox particles it was found that the Soret coefficient increases with increasing Debye length and slightly drops at large Debye lengths, of the order of the core-radius of the colloids. For all investigated concentrations at room temperature, a negative Soret coefficient has been observed for this system.[2] Another study reveals an increasing linear dependence of the Soret coefficient with the Debye length for carboxyl-modified polystyrene beads.[5] Here, the Debye length is always very small as compared to the particle radius. Apart from colloids, a study of micellar solutions with the ionic surfactant sodium dedecyl sulphate also shows that raising the Debye length leads to an increase of the Soret coefficient.[7]

To gain a better understanding of the microscopic mechanism of the thermal diffusion process of macromolecules, several theoretical approaches have been developed. The first theory was published by Ruckenstein in 1981,[9] where a connection between thermophoresis of solid colloidal particles and the Marangoni effect is made. Later, models for single spherical particles have been derived in terms of surface potential, independently by Morozov and Piazza.[6,10] A few years later, Bringuier and Bourdon proposed an expression for S_T in terms of the total internal energy of a particle, based on the kinetic theory of Brownian motion.[11] Independently, Fayolle *et al.*[12] and later Duhr and Braun[13] derived an expression for the Soret coefficient for charged colloids with thin double layers,

[a]*ICS-3 Soft Condensed Matter, Jülich, Germany. E-mail: j.k.g.dhont@fz-juelich.de; s.wiegand@fz-juelich.de*

[b]*Institute of Physics, Heinrich-Heine- Universität, D-40225 Düsseldorf, Germany*

which was subsequently generalized by Dhont and Briels[14] to arbitrary Debye lengths. All these theoretical approaches apply only to spherical colloids, while little is known about non-spherical colloids. The present paper is devoted to thermal diffusion of very long and thin, charged colloidal rods.

Fd-virus suspensions are widely used as model systems for colloidal rods. Suspensions of *fd*-virus particles have been shown to exhibit several liquid-crystalline phases (for an overview see ref. 15), and have been used for studies on the response of rod-like colloids to shear flow[16,17] and electric fields.[18] Their suspensions are stable up to 65 °C,[19] and are highly monodisperse. The wild type *fd*-virus has a molecular weight of 1.64×10^7 g mol^{-1}, a contour length L of 880 nm, a radius a of 3.4 nm, and a persistence length L_P of 2.2 μm. The ratio of the persistence length to contour length $L_P/L = 2.5$ indicates that these rods are semi-flexible, which leads to a deviation of isotropic–nematic coexistence concentrations as predicted by Onsager for stiff rods.[15,20] Above pH 4 these particles are negatively charged and interact *via* a combination of electrostatic repulsion and hard-core interactions. The net surface charge can be increased or decreased by increasing or decreasing the solution pH, respectively.[21]

In the present paper we use *fd*-virus suspensions to investigate the thermal diffusion behaviour of very long and thin, charged colloidal rods. The paper is structured as follows. First, we describe the experimental details. In the subsequent section we extend the Dhont–Briels model[14] for spherical colloids to rod-shaped particles. In the results and discussion section we present experimental results for thermal diffusion coefficients and mass diffusion coefficient, where both the ionic strength and concentration are independently and systematically varied. The experimental results are compared to our theory and other theories, and also to former experimental results for spherical colloids. The main conclusions and remarks with respect to possible future work close the paper.

2 Experimental details

2.1 Sample preparation and characterization

The *fd*-virus was prepared following a standard biological protocol using the XL1-Blue strain of *E. coli* as the host bacteria.[22] The obtained virus was purified by repetitive centrifugation (108 000*g*) and then re-dispersed in the chosen buffers. Tris(hydroxymethyl)aminomethane (Tris) with concentrations of 82.15, 15.09, 6.11, 3.29, and 2.05 mM was used as buffer solution. The pHs of all buffer solutions were adjusted to 8.2 by adding concentrated HCl solution. Finally the virus was dialyzed in each chosen buffer and used as stock solutions to prepare the further concentration series for the measurements. The five concentrations of Tris are chosen such that the resulting Debye lengths are varied with equal increments. The studied *fd*-virus concentration is 1 mg ml^{-1} for the fixed-concentration measurements, and in the range of 0.4–1.8 mg ml^{-1} and 0.6–2.2 mg ml^{-1} for the fixed-buffer concentration and the fixed-volume fraction measurements, respectively. Concentrations were determined by UV absorption (NanoDrop ND-1000, Peqlab). All measurements were performed at 20 °C.

2.2 Infrared thermal diffusion forced Rayleigh scattering (IR-TDFRS)

A detailed description of the recently modified IR-TDFRS can be found in the paper by Blanco *et al.*[3] This setup is optimized for aqueous systems and has been used to study the transport properties in different aqueous systems of non-ionic surfactants,[2] saccharide solutions[23] and anisotropic bio-colloids.[3]

The normalized heterodyne scattered intensity $\zeta_{het}^{th}(t)$, assuming an ideal excitation with a step function, is given by,

$$\zeta_{het}^{th}(t) = 1 - \exp\left(-\frac{t}{\tau_{th}}\right) - A(\tau - \tau_{th})^{-1} \left\{\tau\left[1 - \exp\left(-\frac{t}{\tau}\right)\right] - \tau_{th}\left[1 - \exp\left(-\frac{t}{\tau_{th}}\right)\right]\right\} \quad (1)$$

with the steady state amplitude A equal to

$$A = \left(\frac{\partial n}{\partial c}\right)_{p,T}\left(\frac{\partial n}{\partial T}\right)_{p,c}^{-1} S_T c(1-c) \quad (2)$$

where c is the mass fraction, c_{fd} in our particular case, τ_{th} is the heat diffusion time, τ is the equilibration time of the mass diffusion, $(\partial n/\partial c)_{p,T}$ and $(\partial n/\partial T)_{p,c}$ are refractive index contrast factors with respect to mass concentration at constant pressure and temperature, and with respect to temperature at constant pressure and mass concentration, respectively. The refractive index contrast factors are measured independently from the TDFRS measurements. The details about measurement of refractive index contrast factors are described in another paper.[4] Note that the diffusion coefficient can be derived from the equilibration time $D = (\tau q^2)^{-1}$ with the magnitude of the scattering vector q, while S_T can be calculated from amplitude A (*cf.* eqn (2)).

3 Theoretical description

The force on a charged colloidal particle due to the presence of an electric double layer has been shown in ref. 14 to be mainly due to the change of the internal energy of the electric double layer as the ambient temperature changes on moving the colloid. The additional forces due to the temperature-gradient induced deformation of the double layer are relatively small in polar solvents like water.[14] Let F_W denote the force acting on the colloid due to the temperature dependence of the internal energy of the double layer. This force is connected to the work $\mathrm{d}\mathscr{W}$ to reversibly pull the colloid from a box with temperature T over a distance $\mathrm{d}z$ to a box with temperature $T + \mathrm{d}T$, by the relation $F_W \mathrm{d}z = -\mathrm{d}\mathscr{W}$ (see Fig. 1). The work $\mathrm{d}\mathscr{W}$ can be calculated, as far as the contribution from the electric double layer is concerned, by considering the alternative path as depicted in Fig. 1. First the surface of the colloid is reversibly de-charged. The work involved in de-charging the colloid is $-W^{(\mathrm{dl})}(T)$, that is, $W^{(\mathrm{dl})}(T)$ is the reversible work to charge-up the colloidal particle. Then the un-charged colloid is pulled from the box with temperature T to the box with temperature $T + \mathrm{d}T$. As far as the double layer is concerned, there is no work involved, simply because the double layer is

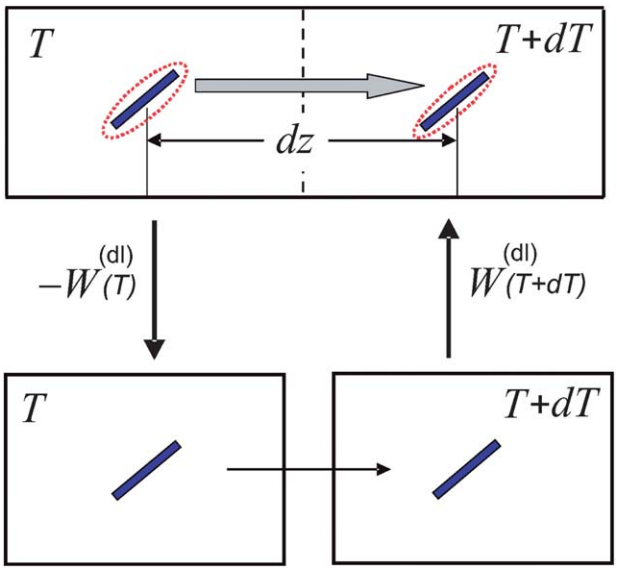

Fig. 1 The alternative path to move the colloid from a box with temperature T over a distance dz to the neighbouring box with temperature T + dT. $W^{(dl)}(T)$ is the reversible work that is required to charge the colloid. The colloid is the blue rod, while the red dashed lines are used to indicate the presence of the double layer.

no longer present for the neutral colloid. Then the colloid is re-charged, which requires the work $+W^{(dl)}(T + dT)$. Hence, $d\mathscr{W} = W^{(dl)}(T + dT) - W^{(dl)}(T) = dT d W^{(dl)}(T)/dT$. It follows that the force is equal to $F_W = -(dT/dz)(dW^{(dl)}/dT)$. The connection of the force to the thermal diffusion coefficient is found from force balance on the diffusive time scale, that is, once the colloid is moving, the friction force $F_{fr} = -\gamma v$ with the solvent balances with F_W, where γ is the friction coefficient and v is the velocity of the colloid. The thermal-gradient induced velocity of the colloid is thus equal to $v = F_W/\gamma$. Substitution of this expression for the velocity into the continuity equation $\partial\rho/\partial t = -d(v\rho)/dz$ (where ρ is the number density of the colloids) and expansion with respect to gradients in temperature and deviations of the temperature from the ambient temperature then lead to $\partial\rho/\partial t = D_T d^2T/dz^2$, where the thermal diffusion coefficient is equal to[14,24]

$$D_T = D_0 \rho \beta \frac{dW^{(dl)}(T)}{dT}, \tag{3}$$

where $D_0 = k_B T/\gamma$ is Einstein's mass diffusion coefficient and $\beta = 1/k_B T$ (where k_B is Boltzmann's constant).

For the calculation of the temperature derivative of the reversible energy to charge the colloidal particle, analytical results can be obtained within the Debye–Hückel approximation. The work required to add a charge dq to the surface of the colloid, homogeneously distributed over its surface, is equal to $\Psi_s(q)dq$, where $\Psi_s(q)$ is the potential at the surface of the colloid with the total charge equal to q. Since within the Debye–Hückel approximation the surface potential is proportional to the charge, the work to charge the colloid up to a total charge equal to Q is given by

$$W^{(dl)} = \int_0^Q dq \Psi_s(q) = \frac{1}{2} Q \Psi_s(Q). \tag{4}$$

This result is valid for arbitrary double-layer thickness.[25] The relationship between the surface potential and the total charge for a *spherical colloid* reads

$$\Psi_s^{(sphere)} = \frac{Q}{4\pi\varepsilon a} \frac{1}{1+\kappa a}, \tag{5}$$

where a is the radius of the sphere, ε is the dielectric constant of the solvent, and κ is the inverse Debye length. Note that both ε and κ are temperature dependent quantities. For a *cylindrical colloid* we have

$$\Psi_s^{(rod)}(Q) = \frac{Q}{2\pi a_c L \varepsilon \kappa} \frac{K_0(\kappa a_c)}{K_1(\kappa a_c)}, \text{ for } \kappa a_c \gtrsim 1, \tag{6}$$

where a_c is the radius of the cylindrical core, L is the length of the core, and $K_{0,1}$ are modified Bessel functions of the second kind of order 0 and 1. The analytical form in eqn (6) is based on the solution of the linearized Poisson–Boltzmann equation for an infinitely long cylinder. For a cylinder of finite length, the analytical form for the infinitely long cylinder is kept here, which amounts to the neglect of end-effects. For Debye lengths that are much larger than the core radius, the potential in eqn (6) varies like $\sim\kappa a_c \ln\{\kappa a_c\}$, and not like that for a sphere. This is an artifact of the originally assumed infinite length of the cylindrical core. The relation (6) is therefore only valid for sufficiently thin double layers, where $\kappa a_c \gtrsim 1$.

Combining the above results it is found that the thermal diffusion coefficient can be written in terms of the surface charge density σ and the Bjerrum length l_B as

$$D_T = A \frac{d \ln \varepsilon}{d \ln T} + B, \tag{7}$$

where for a sphere,

$$\begin{aligned} A^{(sphere)} &= -\mathscr{C} \frac{\kappa a}{(1+\kappa a)^2} \left\{ 1 + \frac{2}{\kappa a} \right\}, \\ B^{(sphere)} &= \mathscr{C} \frac{\kappa a}{(1+\kappa a)^2}, \end{aligned} \tag{8}$$

while for a rod,

$$\begin{aligned} A^{(rod)} &= -\mathscr{C} \frac{L}{\kappa a_c^2} \frac{K_0(\kappa a_c)}{K_1(\kappa a_c)} \left\{ 1 + \frac{1}{2} \kappa a_c \left(\frac{K_0(\kappa a_c)}{K_1(\kappa a_c)} - \frac{K_1(\kappa a_c)}{K_0(\kappa a_c)} \right) \right\}, \\ B^{(rod)} &= \mathscr{C} \frac{L}{2a_c} \left(1 - \frac{K_0^2(\kappa a_c)}{K_1^2(\kappa a_c)} \right), \text{ for } \kappa a_c \gtrsim 1. \end{aligned} \tag{9}$$

where for brevity the constant,

$$\mathscr{C} = \frac{1}{4} D_0 \frac{\rho}{T} \left(\frac{4\pi l_B^2 \sigma}{e} \right)^2 \left(\frac{a}{l_B} \right)^3, \tag{10}$$

is introduced, with $a = a_c$ in the case of a rod, and where D_0 is either the Einstein mass diffusion coefficient $D_0^{(sphere)}$ of a sphere or $D_0^{(rod)}$ of a rod, while $e > 0$ is the elementary charge. We expressed the total charge in terms of the surface charge density σ in order to simplify a comparison between spheres and rods.

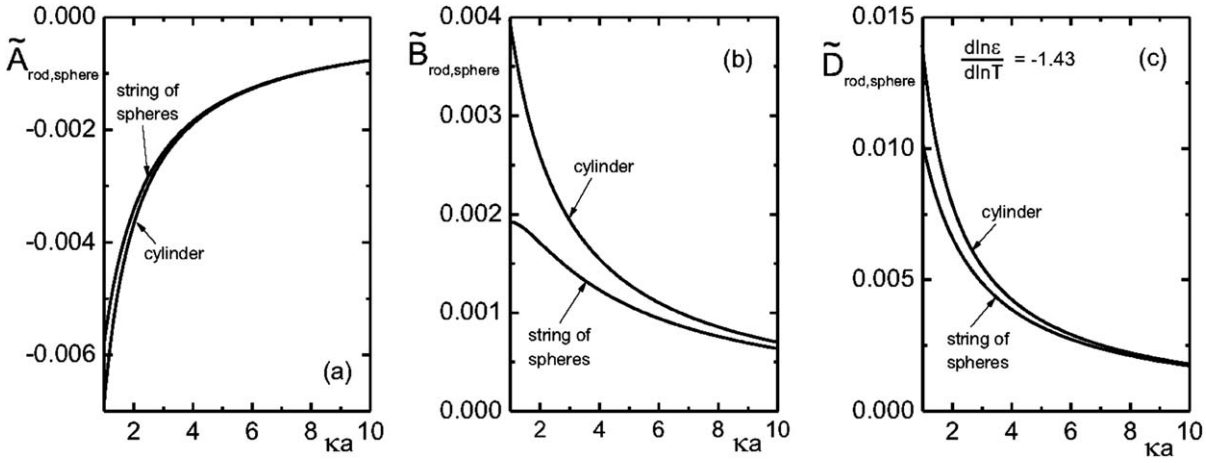

Fig. 2 The dimensionless quantities $\tilde{A} = CA$, $\tilde{B} = CB$ and $\tilde{D}_T = CD_T$, where $C = T16\pi\varepsilon a/\beta D_0 \rho Q^2$ as a function of κa (with $a = a_c$ for the rods), where Q is the monomer charge.

For the cylindrical colloid there are two limiting situations, where either $\kappa a_c \ll 1$ or $\kappa a_c \gg 1$. In the first case of very thick double layers compared to the cylindrical core radius, the core of the rod may be considered as a string of $L/2a_c$ beads of radii a_c. The extended double layer structure of each bead is essentially unaffected by the presence of the relatively small excluded volume of the neighbouring beads, so that within the linearized Poisson–Boltzmann approach the structure of the double layer of the cylinder is well approximated by a sum of the spherical double layers of the beads. Except for the diffusion coefficient D_0, which is different for a sphere and a rod, the thermal diffusion coefficient of the rod is now a sum of the thermal diffusion coefficients of the beads, that is,

$$\frac{A^{(\mathrm{rod})}}{D_0^{(\mathrm{rod})}} = \frac{L}{2a_c}\frac{A^{(\mathrm{sphere})}(a=a_c)}{D_0^{(\mathrm{sphere})}}, \qquad \frac{B^{(\mathrm{rod})}}{D_0^{(\mathrm{rod})}} = \frac{L}{2a_c}\frac{B^{(\mathrm{sphere})}(a=a_c)}{D_0^{(\mathrm{sphere})}}, \ \text{for } \kappa a_c \lesssim 1. \tag{11}$$

The expression for the thermal diffusion coefficient in the other limiting case of thin double layers is given by eqn (9). May be surprisingly, this expression predicts, like for the thick double layers, that the thermal diffusion coefficient of a rod is simply a superposition of the thermal diffusion coefficients of the beads (with radii a_c). This can be analytically verified by substitution of the two leading terms in an asymptotic expansion of the two Bessel functions. Numerical results are given in Fig. 2. Fig. 2a and b show that for $\kappa a_c \gtrsim 2$ the result in eqn (9) is quite accurately approximated by a representation of $2a_c/L$ beads with each having a thermal diffusion coefficient given in eqn (8) with $a = a_c$, where there is an increasing accuracy for thinner double layers. The thermal diffusion coefficient D_T in dimensionless form is plotted in Fig. 2c for a cylinder and the corresponding bead model, with the value $\mathrm{d}\ln\varepsilon/\mathrm{d}\ln T = -1.43$ for water. As can be seen, the approximation of the thermal diffusion coefficient of a rod by that of a string of spheres becomes more accurate on decreasing the Debye length.

The conclusion from the above analysis is that both for thick and thin double layers, the thermal diffusion coefficient of a rod-like colloid can be accurately approximated by $L/2a_c$ times the thermal diffusion coefficient (7) and (8) of a spherical colloid with radius $a = a_c$, with the same surface charge density as the rod. From the above analysis we thus find that the Soret coefficient $S_T^{(\mathrm{rod})} = D^{(\mathrm{rod})}/\rho D_0^{(\mathrm{rod})}$ is equal to

$$S_T^{(\mathrm{rod})} = \frac{1}{4T}\frac{L}{2a_c}\left(\frac{4\pi {l_B}^2\sigma}{e}\right)^2\left(\frac{a_c}{l_B}\right)^3\frac{\kappa a_c}{(1+\kappa a_c)^2} \times\left[1-\frac{\mathrm{d}\ln\varepsilon}{\mathrm{d}\ln T}\left\{1+\frac{2}{\kappa a_c}\right\}\right]. \tag{12}$$

This superposition of thermal diffusion coefficients of spherical beads to approximate the thermal diffusion coefficient of a rod is valid for arbitrary Debye lengths, and will be used in the sequel for a comparison with experimental data for the thermal diffusion coefficient of *fd*-viruses.

4 Experimental results

Measurements of the mass diffusion coefficient and the thermal diffusion coefficient are performed, where the *fd* number concentration (defined as the number of *fd*-virus particles per unit volume) as well as the Debye length are varied independently. The Debye length is tuned by adjusting the concentration of the buffer Tris–HCl solution. Since the acid dissociation constant pK_a of Tris is 8.2 and the pH of all the buffers are adjusted to 8.2, the ionic strength I is half the value of the total molar concentration of Tris. The Debye length κ^{-1} can be calculated from (with N_A Avogadro's number)

$$\kappa^{-1} = \sqrt{\frac{1}{8\pi l_B N_A I}}. \tag{13}$$

An *effective volume fraction* ϕ can be defined, which characterizes the importance of interactions between rods. The effective volume fraction depends on the *fd* number concentration

and the Debye length. Due to inter-particle charge–charge interactions, the apparent radius of the core of the *fd*-virus particles increases by an amount that is approximately given by the Debye length. The effective volume fraction is defined as the volume fraction of rods with a core radius of $a_c + \kappa^{-1}$. Alternatively the apparent radius can be calculated as suggested by Onsager,[20] based on equality of the second virial coefficient of charged rods and the equivalent hard rods with the corresponding apparent core radius. We shall be satisfied with the former simple approximation, as it does not affect our conclusions.

There are thus three parameters of interest: the number concentration of *fd* viruses, the Debye length, and the effective volume fraction. We therefore performed the following set of experiments:

(a) The Debye length is varied with a constant number concentration of *fd*-virus particles (of 1 mg ml^{-1}).

(b) The number concentration of *fd*-virus particles is varied with a fixed Debye length (where the buffer concentration is chosen equal to 6.11 mM).

(c) The effective volume fraction is fixed to 0.0037 with appropriate simultaneous variation of both the *fd*-virus concentration and the Debye length.

These experimental paths are illustrated in Fig. 3a–c, respectively. Although in our suspensions the state of the system is always isotropic, the rods in these figures are sketched with the same orientation for clarity.

The aim of this work is to probe the thermal diffusion behaviour of single *fd*-virus particles as a function of the Debye length, without the intervening effects of inter-particle interactions. In order to probe whether inter-particle interactions affect the measured mass diffusion and thermal diffusion coefficients, we performed a series of experiments as a function of the effective volume fraction. The open symbols in Fig. 4 are experimental data for the Soret coefficient and the mass- and thermal diffusion coefficient at a constant buffer concentration, and thus a fixed Debye length. The effective volume fraction for this series of experiments is changed by only changing the *fd*-virus concentration (path (b)). As can be seen from the lower panel in Fig. 4 (the open symbols), the thermal diffusion coefficient is insensitive to interactions, and is essentially constant up to an effective volume fraction of about 0.0065. The mass diffusion coefficient, however, significantly increases with increasing effective volume fraction, as can be seen from the middle panel (again the open symbols). The blue triangle at low concentration is taken from the literature.[26,27] On the other hand, when the effective volume fraction is increased at a constant *fd*-virus number concentration (1 mg ml^{-1}) by increasing the Debye length (path (a)), significant changes are observed (see the filled symbols in Fig. 4), also for the thermal diffusion coefficient. Since inter-particle interactions are not significant as far as the thermal diffusion coefficient is concerned, its variation with the buffer concentration must be due to the variation of the double-layer thickness. In order to obtain experimental values for the

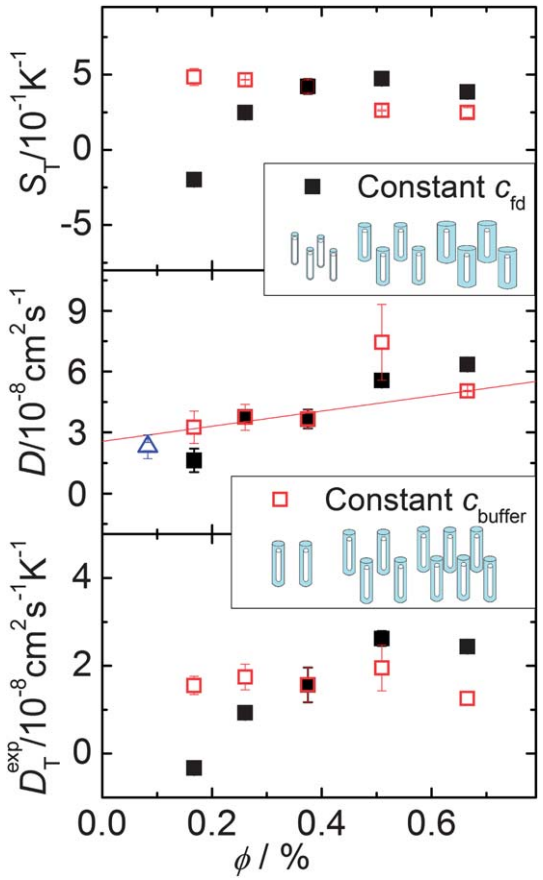

Fig. 4 S_T, D and D_T as a function of the effective volume fraction. Solid squares present measurements with fixed c_{fd} = 1 mg ml^{-1}. Open squares illustrate measurements with constant c_{buffer} = 6.11 mM. The open triangle presents the data of the bulk diffusion coefficient from the literature.[26,27] The red line is a guide to the eye.

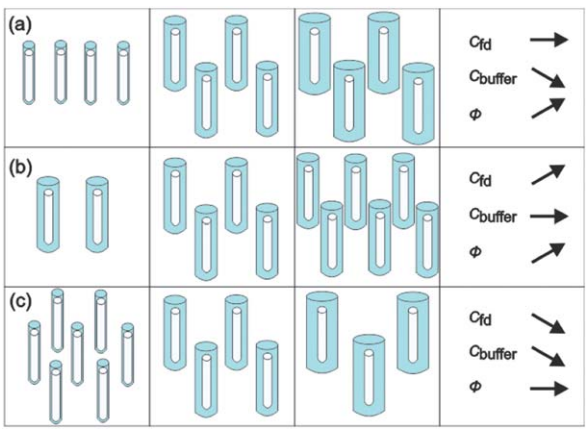

Fig. 3 Illustration of the chosen experimental paths. The white rods present the core of *fd*-viruses and the blue parts are used to indicate the extent of the electric double layers. For clarity the rods have been drawn with the same orientation. In the experiments, however, the systems are isotropic. (a) The number concentration of *fd*-viruses is constant while the Debye length is increased by decreasing the buffer concentration. (b) The number concentration of *fd* viruses is increased at a constant Debye length. (c) Both the number concentration of *fd* viruses and the Debye length are changed in such a way that the effective volume fraction remains constant.

single-particle Soret coefficient S_T^0, we will use the Debye-length dependent thermal diffusion coefficient (filled symbols in the bottom panel in Fig. 5) and the mass diffusion coefficient at infinite dilution $D_0 = 2.3 \times 10^{-8}$ cm^2 s^{-1} from the literature.[26,27] The upper panel in Fig. 5 shows Soret coefficients obtained from the diffraction signal (*cf.* eqn (1) and (2)) corresponding to the ratio of the experimental values for the two diffusion coefficients.

To further establish the Debye-length dependence of the mass- and thermal diffusion coefficients, we performed experiments at a fixed effective volume fraction of 0.0037 (path (c)), by appropriate simultaneous variation of both the *fd* number concentration and the Debye length. The Soret coefficient and the mass- and thermal diffusion coefficients along this path are plotted in Fig. 5 by the open (with center-cross) symbols as a function of the Debye length. The filled symbols in Fig. 5 refer to data obtained along path (a), where the *fd* number concentration is fixed to 1 mg ml^{-1}, and the Debye length is varied by changing the buffer concentration. The two sets of data points in the lower panel for the thermal diffusion coefficient coincide to within experimental error, which again confirms the insignificant inter-particle interactions.

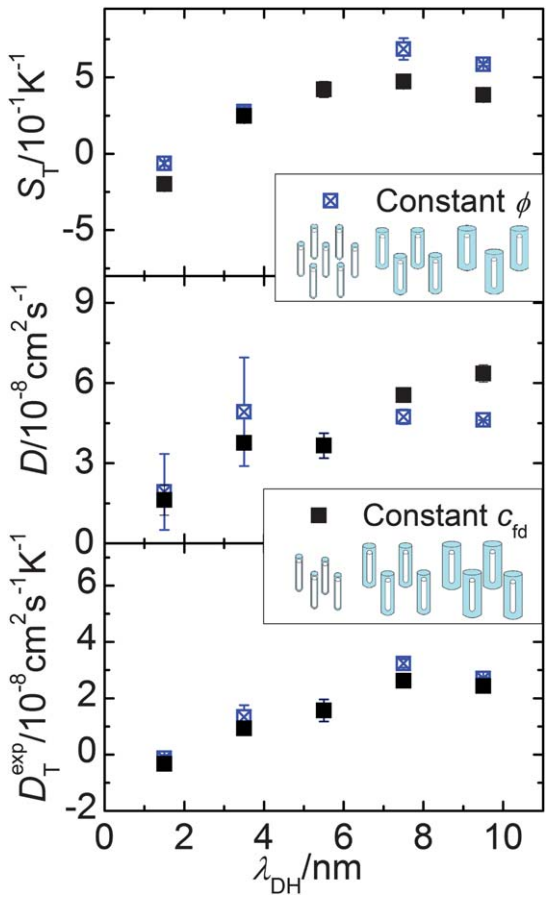

Fig. 5 S_T, D and D_T as a function of the Debye length. Solid squares present measurements with fixed $c_{fd} = 1$ mg ml^{-1}. Empty with center cross-symbols are measurements with constant $\phi = 0.0037$.

5 Comparison of experiments with theory

We compare the single-particle Soret coefficient S_T^0 as a function of the Debye length with the theory that has been developed in Section 3. We note that the thermal diffusion coefficient is sometimes defined differently from the theoretical expressions given in Section 3. The definition of the thermal diffusion coefficient D_T^{exp} in experimental work relates to D_T used in most of the theoretical studies (as in Section 3) through $D_T = \rho c(1-c) D_T^{exp}$, where ρ is the colloid number density and c is the volume fraction of colloids.[2]

In order to asses the importance of the finite extent of the electric double layer, we include a comparison to eqn (12) in the asymptotic limit of very thin double layers, where $\kappa a_c \to \infty$. For such thin double layers we have from eqn (12),

$$S_T^{(rod)} = \frac{1}{4T}\frac{L}{2a_c}\left(\frac{4\pi {l_B}^2 \sigma}{e}\right)^2 \frac{{a_c}^2}{\kappa {l_B}^3} \times \left[1 - \frac{\mathrm{d}\ln\varepsilon}{\mathrm{d}\ln T}\right]. \qquad (14)$$

The corresponding expression for spherical particles (without the factor $L/2a_c$) has been derived independently by Fayolle *et al.*[12] and Duhr and Braun.[13] There is so far no extension of Ruckenstein's theory[9] to rod-like colloids. It is not obvious that we can simply take Ruckenstein's expression for the Soret coefficient for spheres and multiply that with the number of beads to obtain the corresponding expression for rods. We will therefore refrain from a comparison with any possible extension of Ruckenstein's theory to rods.

The result in eqn (12) and the above expression account only for the contribution of the electric double layer to the Soret coefficient. There is an additional "ideal gas" contribution equal to $1/T$, and contributions due to thermal properties of, for example, the solvation layer and the core of the colloids. These contributions are insensitive to salt concentration, so that they determine the "offset" in plots of the Soret coefficient as a function of the Debye length. The offset and the surface charge density σ are used as fitting parameters in a comparison of experiments with theory. Fig. 6 shows the Soret coefficient $S_T^0 = D_T/D_0$ determined from the measured thermal diffusion coefficient D_T and the diffusion at infinite dilution D_0 as a function of the Debye length. The fits are plotted in Fig. 6, while the offset and surface charge density for the best fits to various theories are given in Table 1. The solid line (blue) is a fit to limiting expression (eqn (14)) for very thin double layers. The fit is slightly improved by accounting for the finite extent of the electric double layer, as discussed in Section 3 (the dashed green line). Similar results have been found for charged spherical particles (Ludox silica particles),[2,13] of which the experimental data are presented in Fig. 6 as open circles, which fitted with the model described in Section 3 for spherical colloids.

The question now is whether the surface charge density of $\sigma = (0.050 \pm 0.003)\ e$ nm^{-2} that is found from the fit to our theory is a reasonable value. *Fd*-virus consists of a DNA strand that is covered by 2700 proteins, which carry a bare charge of 9.5 ± 0.5 negative elementary charges per nm. According to a calculation by Buitenhuis,[28] about 90% of these groups at pH = 8.2 are dissociated, so that the total bare charge of an *fd*

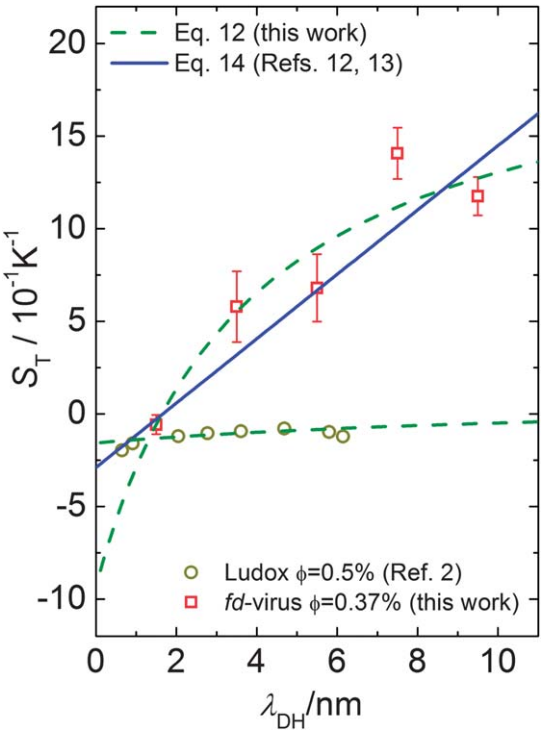

Fig. 6 The Soret coefficient S_T as a function of the Debye length. In contrast to Fig. 4 and 5 the open squares present the calculated $S_T^0 = D_T/D_0$ for the *fd*-virus with an effective volume fraction of $\phi = 0.0037$ and the open circles show S_T of Ludox silica particles. The data of the *fd*-virus are fitted by the two models discussed in the main text. The data of Ludox particle are fitted by Dhont's model for spheres.[2]

Table 1 Parameters obtained by fitting S_T^0 as a function of the Debye length using two models as in Fig. 6

Model	σ/e nm^{-2}	Offset
Eqn (14) (based on ref. 12 and 13)	0.023 ± 0.002	−0.74
Eqn (12) (this work)	0.050 ± 0.003	−1.39
Calculated free surface charge	0.066	

particle is equal to $N = 7500 \pm 400$ e. A large fraction of this surface charge is neutralized by ion-condensation. According to Manning's ion-condensation theory,[29,30] the ratio $b/l_B < 1$ of the typical distance $b = L/N$ between the charges on a cylindrical rod and the Bjrerrum length l_B is equal to the fraction of bare charges that is not neutralized by condensed ions (for monovalent ions). Since $l_B = 0.71$ nm for water at room temperature, it is found that b/l_B is equal to 0.16 ± 0.01. The total number of charges close to the surface of an *fd* particle that determine the structure of the diffuse electric double layer is thus equal to 1239 ± 66, which corresponds to surface charge densities of 0.066 ± 0.004 e nm^{-2} (where the indicated error is certainly much smaller than the actual error that are implicit in the approximations made in the theory on which this estimate is based). This value of the surface charge density is in reasonable agreement with the experimentally found surface charge density of 0.050 ± 0.003. The surface charge density obtained from a fit to the same theory for very thin double layers gives a significantly lower surface charge density (see Table 1).

Within Manning's ion-condensation theory, there is no dependence of the number of condensed ions on the overall ionic strength, which suggests that the contribution of the condensed ions to the thermal diffusion coefficient is independent of the Debye length. The contribution of the condensed ions to D_T is thus incorporated in the offset as introduced earlier, while the Debye-length dependence of D_T is determined by the diffuse electric double layer.

6 Conclusion

In this work we explored the thermal diffusion behaviour of filamentous wild type *fd*-virus. These virus particles are used as a model system for very long and thin, and relatively stiff rod-like colloids. A theory is proposed, which predicts that the thermal diffusion coefficient of a rod is equal to that of a spherical bead with a diameter equal to that of the rod-core, and with the same surface charge density, multiplied by the aspect ratio of the rod (which is equal to the number of beads). Such a superposition of spherical beads to represent the thermal diffusion coefficient of a rod is accurate for arbitrary Debye lengths, including very thin double layers. Thermal diffusion coefficients are measured with Thermal Diffusion Forced Rayleigh Scattering (TDFRS), where an infrared laser is used to create a temperature grating through the excitation of a vibrational mode of the water molecules. In a series of experiments the *fd* concentration and the Debye length were varied independently. We also performed experiments where the *fd* number concentration and the ionic strength are changed in combination, such that the effective volume fraction is fixed. Contrary to the mass diffusion coefficient, the thermal diffusion coefficient is found to be essentially independent of the *fd* concentration. The measured Soret coefficients are well described by the theory that we developed in this paper. Comparing with experiments, there are two adjustable parameters: the ionic-strength independent contribution to the Soret coefficient and the surface charge density. The surface charge density that we find from the fit with theory compares reasonably well with the theoretically predicted value.

Future developments related to charged colloids could include (i) the extension of the theory beyond the Debye–Hückel approximation and (ii) the thermal diffusion of other types of non-spherical colloids, like disks, and of charged rods with varying flexibility.

Acknowledgements

We thank Pavlik Lettinga and Peter Lang for fruitful discussions and we are grateful for experimental advice from Donald Guu. We acknowledge financial support due to the Deutsche Forschungsgemeinschaft grant Wi 1684.

References

1 P. Polyakov, J. Luettmer-Strathmann and S. Wiegand, *J. Phys. Chem. B*, 2006, **110**, 26215–26224.
2 H. Ning, J. K. G. Dhont and S. Wiegand, *Langmuir*, 2008, **24**, 2426–2432.
3 P. Blanco, H. Kriegs, M. P. Lettinga, P. Holmqvist and S. Wiegand, *Biomacromolecules*, 2011, **12**, 1602–1609.
4 Z. Wang, H. Kriegs and S. Wiegand, *J. Phys. Chem. B*, 2012, **116**, 7463–7469.
5 S. Duhr and D. Braun, *Proc. Natl. Acad. Sci. U. S. A.*, 2006, **103**, 19678–19682.
6 R. Piazza and A. Guarino, *Phys. Rev. Lett.*, 2002, **88**, 208302.
7 R. Piazza, S. Iacopini and B. Triulzia, *Phys. Chem. Chem. Phys.*, 2004, **6**, 1616–1622.
8 S. A. Putnam and D. G. Cahill, *Langmuir*, 2005, **21**, 5317–5323.
9 E. Ruckenstein, *J. Colloid Interface Sci.*, 1981, **83**, 77–81.
10 K. Morozov, *J. Magn. Magn. Mater.*, 1999, **201**, 248–251.
11 E. Bringuier and A. Bourdon, *Phys. Rev. E: Stat., Nonlinear, Soft Matter Phys.*, 2003, **67**, 011404.
12 S. Fayolle, T. Bickel, S. Le Boiteux and A. Würger, *Phys. Rev. Lett.*, 2005, **95**, 208301.
13 S. Duhr and D. Braun, *Phys. Rev. Lett.*, 2006, **96**, 168301.
14 J. K. G. Dhont and W. J. Briels, *Eur. Phys. J. E*, 2008, **25**, 61–76.
15 Z. Dogic and S. Fraden, in *Phase Behavior of Rod-Like Viruses and Virus-Sphere Mixtures*, ed. G. Gompper and M. Schick, Wiley-VCH, Weinheim, 2006, vol. 2, pp. 1–78.
16 M. Ripoll, P. Holmqvist, R. G. Winkler, G. Gompper, J. K. G. Dhont and M. P. Lettinga, *Phys. Rev. Lett.*, 2008, **101**, 168302.
17 K. G. Kang, M. P. Lettinga, Z. Dogic and J. K. G. Dhont, *Phys. Rev. E: Stat., Nonlinear, Soft Matter Phys.*, 2006, **74**, 026307.
18 K. Kang and J. K. G. Dhont, *Soft Matter*, 2010, **6**, 273–286.
19 J. X. Tang and S. Fraden, *Biopolymers*, 1996, **39**, 13–22.
20 L. Onsager, *Ann. N. Y. Acad. Sci.*, 1949, **51**, 627–659.
21 K. Purdy, PhD thesis, Brandeis University, 2004.
22 J. Sambrook and D. Russell, *Molecular Cloning: A Laboratory Manual*, Cold Spring Harbor Lab Press, New York, 2001.
23 P. Blanco and S. Wiegand, *J. Phys. Chem. B*, 2010, **114**, 2807–2813.
24 J. K. G. Dhont, S. Wiegand, S. Duhr and D. Braun, *Langmuir*, 2007, **23**, 1674–1683.
25 E. Verwey, J. Overbeek and J. Overbeek, *Theory of the Stability of Lyophobic Colloids*, Dover Publications, 1999.
26 L. Song, U. S. Kim, J. Wilcoxon and J. M. Schurr, *Biopolymers*, 1991, **31**, 547–567.
27 P. Holmqvist, D. Kleshchanok and P. R. Lang, *Langmuir*, 2007, **23**, 12010–12015.
28 J. Buitenhuis, *Langmuir*, 2012, **28**, 13354–13363.
29 G. S. Manning, *Berichte der Bunsengesellschaft für physikalische Chemie*, 1996, **100**, 909–922.
30 G. S. Manning, *J. Phys. Chem. B*, 2007, **111**, 8554–8559.

CHAPTER

FIVE

MOLAR MASS AND TEMPERATURE DEPENDENCE OF THE THERMODIFFUSION OF POLYETHYLENE OXIDE IN WATER/ETHANOL MIXTURES

Molar mass and temperature dependence of the thermodiffusion of polyethylene oxide in water/ethanol mixtures

Zilin Wang,[1,a)] Dzmitry Afanasenkau,[1] Minjie Dong,[1,2] Danni Huang,[1,3] and Simone Wiegand[1,4,b)]

[1]*ICS-3 Soft Condensed Matter, Forschungszentrum Jülich GmbH, D-52428 Jülich, Germany*
[2]*Center for Materials Research, Tallinn University of Technology, Tallinn, Estonia*
[3]*Department of Chemistry, Fudan University, Shanghai 200433, China*
[4]*Chemistry Department – Physical Chemistry, University Cologne, D-50939 Cologne, Germany*

(Received 27 February 2014; accepted 18 July 2014; published online 12 August 2014)

In this work, we study the molar mass dependence of the thermodiffusion of polyethylene oxide at different temperatures in ethanol, water/ethanol mixture ($c_{water} = 0.7$), and water in a molar mass range up to $M_w = 180\,000$ g/mol. Due to the low solubility of polyethylene oxide oligomers in ethanol the measurements are limited up to $M_w = 2200$ g/mol. The specific water/ethanol concentration 0.7 has been chosen, because at this weight fraction the thermal diffusion coefficient, D_T, of water/ethanol vanishes so that the system can be treated as a pseudo binary mixture. The addition of ethanol will degrade the solvent quality, so that we expect a change of the interaction energies between polymer and solvent. The analysis of the experimental data within a theoretical model shows the need of a refined model, which takes specific interactions into account. © *2014 AIP Publishing LLC*. [http://dx.doi.org/10.1063/1.4891720]

I. INTRODUCTION

Thermodiffusion or thermophoresis is a phenomenon where a mass transport is induced by a temperature gradient in a multicomponent system. In the last five years, the effect gained a lot of interest due to applications in biotechnology.[1] The response of molecules, polymers, and colloids to a temperature gradient depends on many parameters such as charge, size, and the hydrophilic and hydrophobic balance. The last plays an important role in the drug discovery process.[2]

For sufficiently small gradients, the mass flux induced by a temperature gradient ∇T is proportional to $-D_T \nabla T$, where D_T is the thermal diffusion coefficient. Thermodiffusion establishes a concentration gradient ∇c, which in turn gives rise to a mass flux equal to $-D \nabla c$, where D is the mass diffusion coefficient. The two fluxes counter balance in the stationary state and the ratio of the established concentration and temperature difference $\Delta c/\Delta T$ is proportional to the Soret coefficient S_T, which is defined as $S_T = D_T/D$.

There have been numerous studies of both organic and aqueous mixtures, trying to explain the mechanism of thermodiffusion.[3–6] Many physical parameters such as molar mass, viscosity, thermal expansion, and moment of inertia have been related to the thermal diffusion coefficient D_T using empirical correlations.[7–9] Apart from the low molar mass mixtures, polymer solutions and colloid suspensions have also been investigated.[10,11] While organic polymers have been studied over a wide concentration and molar mass range,[6,12] the investigation of water soluble polymers is less complete on the molar mass and temperature dependence.[13–15]

Among water soluble polymers, polyethylene oxide (PEO) is of special interest due to its delicate balance of the opposing effects of water-PEO and water-water hydrogen bonding and the resulting complex phase behavior in water.[16,17] Besides a single measurement of poly(vinylalcohol)[18] it was the first polymer with a negative Soret coefficient in ethanol/water mixtures, which had been systematically investigated.[11,13] While PEO is well soluble in water the solubility in ethanol decreases with increasing molar mass.[19,20] Some previous studies of PEO show that the solvent quality has a significant influence on the sign change of S_T. Ethylene oxide oligomers tend to accumulate at the warm side in pure ethanol, which is a bad solvent for high molar mass PEO. If the water content increases, which means the solvent quality improves, the system becomes more thermophobic and ethylene oxide oligomers and also PEO diffuses to the cold region.[11,13,19]

This behavior could be qualitatively understood with a two-chamber lattice model for thermodiffusion in liquid mixtures and dilute polymer solutions.[21,22] The lattice model includes compressibility and directed hydrogen bonding between PEO and water molecules. Within this model the sign change of the Soret coefficient of PEO in the water/ethanol mixture and also the sign change within the binary solvent mixture have been found, in agreement with experimental data. Note that the sign change in the binary mixture could only be reproduced when the mixed water/ethanol interaction parameter had been adjusted to the tabulated density values of the solvent mixture,[22] while a calculation of the mixed interaction according to Berthelot's geometric mean could not reproduce the sign change of the binary mixture. It turns out that the cross interaction has to be stronger than the like-like interaction. This has also been observed in molecular dynamic studies.[23]

a)zil.wang@fz-juelich.de
b)s.wiegand@fz-juelich.de

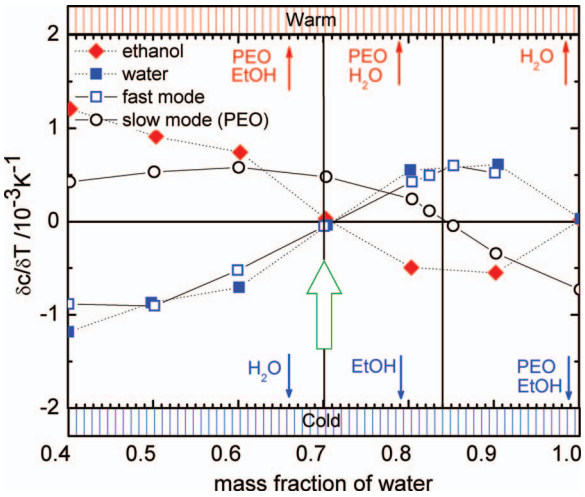

FIG. 1. Overview of the concentration change, δc, per applied temperature difference, δT, in the binary water/ethanol mixture and the ternary of PEO/water/ethanol mixture. Closed and open symbols represent data for the binary and ternary systems, respectively. The block arrow marks the concentration at which the Soret coefficient of the binary mixture water/ethanol vanishes. The dotted lines are guides to the eye. Data are taken from Ref. 13. In the ternary mixture, the cross diffusion of water in ethanol/PEO and ethanol in water/PEO is neglected, and the observed fast process in the diffusion on signal of the Thermal Diffusion Forced Rayleigh Scattering is identified with the diffusion of water in water/ethanol. Further details can be found in the text.

Figure 1 summarizes the results of high molar mass PEO in the water/ethanol mixture and relates it to the binary mixture. The closed and open symbols represent the concentration change as a function of the water content for the binary and ternary systems, respectively. In the ternary mixture, the fast and slow modes are separated signals from the Thermal Diffusion Forced Rayleigh Scattering (TDFRS) measurements.[13] The slow mode reflects the concentration change of PEO in water/ethanol mixture, while the fast mode reflects the concentration change of water within the solvent mixture. In this particular case with a high molar mass PEO ($M_w = 2.65 \times 10^5$ g/mol), the two process are on very different time scales, so that the movement of the solvent components and the polymer can be separated. The data determined from the fast mode of ternary mixture (open square) agree with the results of the binary mixture (solid square). In the measured range, two concentrations are crucial. For systems with a water mass fraction below 0.7, both in the binary and the ternary mixtures, ethanol accumulates at the warm side. When the water concentration increases, ethanol changes its behavior and enriches at the cold side. PEO in ternary system shows a similar behavior. It accumulates at the warm side when the water concentration is below 0.84 and vice versa. The sign change of PEO and ethanol indicates the change of interactions not only between PEO and the solvent, but also within the solvent. We should expect the change of water content i.e., solvent quality is reflected in the interaction parameters.

An already well-established behavior of polymers, both polar and non-polar, at infinite dilution is that the thermal diffusion coefficient D_T becomes independent of molar mass for long enough chains.[19,24,25] Different analytical approaches have been so far employed to explain this behavior.[26–28] Yang and Ripoll[28] make use of a scaling argument and consider the relevance of the hydrodynamic interactions[29] for both the thermophoretic force (proportional to the Soret coefficient) and the friction coefficient. The size dependence of the two quantities results into a precise cancellation, which leads then inevitably to a size-independent D_T. Zhang and Müller-Plathe[30] perform non-equilibrium molecular dynamics simulations with a bead-spring polymer model. Their results show that the chain length for which the plateau value is reached, depends on the flexibility of the chains. In the simulations, more flexible chains reach a constant D_T at shorter chain lengths compared to rigid chains. Describing the chain length in terms of the persistence length l_p, D_T becomes constant when the chain length is of around two to three times l_p. Recent experiments with short ethylene oxide oligomers in ethanol confirmed the simulation results[19] and found that D_T of the ethylene oxide oligomers in ethanol reached the plateau earlier than the D_T in water. This can be expected due to the formation of a hydration shell in water, which should lead to a higher rigidity of the aqueous system.

Several attempts have been made to describe the molar mass dependence with theoretical models. Rauch and Köhler[25] proposed an empirical equation derived from the data of polystyrene in toluene,

$$D_T = \frac{(M - M_e)D_T^{\infty} + M_e D_T^{e}}{M}, \tag{1}$$

here, M_e is the molar mass of the end group, D_T^e is the thermal diffusion coefficient of the end group, D_T^{∞} is the thermal diffusion coefficient at infinite molar mass.

Duhr and Braun[31] developed a model to describe the chain length (L) and charge (σ) dependence of thermodiffusion behavior of DNA. The Soret coefficient is expressed as proportional to the surface area (A) and Debye length (λ_{DH}).[31] Here, the DNA molecules are treated as spheres, so using the scaling behavior of $D \propto L^{-0.75}$, they find $D_T \propto L^{-0.25}$. This model can only describe the charged systems, therefore we cannot apply it to PEO.

Eslamian and Saghir derived a model by considering the solvent as viscous flow surrounding the polymer. They assume that the net heat of transport of the solvent molecules equals the activation energy of viscous flow of the solvent in the pure state. Soret coefficient is expressed in terms of activation energies. This model requires the input data of the heats of transport, which are to our best knowledge not known for our system.

Würger[27,32] assumed that the solvent molecular structure and the Brownian motion of the solute differ with respect to the friction coefficient. He expressed the molar mass dependence of the thermal diffusion coefficient D_T for dilute solutions by

$$D_T = \frac{\beta \varepsilon_p}{6\pi \eta a} - \frac{\beta \varepsilon_s + (\varepsilon_s - \varepsilon_p)/T}{\eta \tilde{\ell} M^{\nu}}, \tag{2}$$

where a is the radius of the monomer, β is the thermal expansion coefficient, η is the dynamic viscosity, $\tilde{\ell}$ is a constant, ε_p and ε_s are the polymer-solvent and solvent-solvent interaction energies, respectively.[27,32] Furthermore, it has been used

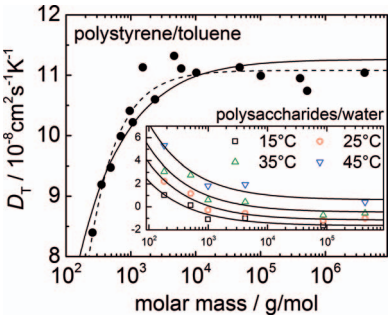

FIG. 2. Molar mass dependence of the thermal diffusion coefficient D_T of styrene oligomers and polystyrene in toluene. The dashed line and solid line present the fits of Eqs. (1) and (2), respectively. The inset shows D_T of saccharide oligomers and polysaccharides in water and the lines correspond to a fit of the molar mass dependence according to Eq. (2). The data have been taken from Refs. 25 and 15.

that in diluted polymer solutions, the diffusion coefficient D depends strongly on the molar mass M and can be described by a scaling law as $D \propto M^{-\nu}$, where $\nu = 0.6$ is a scaling exponent.[33] This approach considers only van der Waals interactions and in the case of an attractive interaction ε_p and ε_s are positive numbers, describing the depth of the potential well. His model has been used by other authors to describe the data of several polymers in different organic solvents. They found that $\beta\varepsilon_p$ is characteristic for the polymer, but independent of the solvent, which means the interaction between polymer and solvent relates only to the thermal expansion coefficient of the solvent.[34]

Fig. 2 shows D_T for styrene oligomers and polystyrene (PS) in toluene as function of the molar mass[25] and the fitted curve according to Eq. (1) (dashed line) and Eq. (2) (solid line). From the model of Würger,[27,32] the interaction energy between polymer and solvent $\varepsilon_p = 1.7 \times 10^{-19}$ J ($\approx 41kT$) can be determined. A determination of the ε_s for this organic system is presently not possible, because there are no temperature dependent measurements. The model from Rauch and Köhler[25] reaches the plateau of D_T earlier than the model of Würger[27,32] and describes the PS data better. But the phenomenological model gives only empirical parameters without physical meaning.

The inset of Fig. 2 shows the molar mass dependence of D_T of saccharide oligomers and polysaccharides in water[15] described by Würger's[27,32] model. It turns out that ε_p lies between -2.4×10^{-19}J ($T = 15\,^\circ$C) and $+0.16 \times 10^{-19}$J ($T = 45\,^\circ$C). The obtained values are in the same order of magnitude as in the case of styrene oligomers and polystyrene in toluene, but the negative interaction energies at low temperatures would imply a repulsive potential, which seems to be unphysical and shows that one needs to be careful, if one applies this model to polar systems.

In order to determine the interaction parameters for PEO in water, ethanol, and the water/ethanol mixture, molar mass and temperature dependent measurements are required. Note that our experimental method works primarily for binary mixtures therefore we have to choose a specific water/ethanol mass fraction in order to be able to identify the diffusion stemming from the low molar mass ethylene oxide oligomers in the solvent mixture. One possible water/ethanol composition is $c_{\text{water}} = 0.7$, where the thermodiffusive contribution from the binary water/ethanol mixture can be neglected. Additionally, we also studied the system in pure water and pure ethanol. Note that PEO with a high molar mass is not soluble in pure ethanol so that the measurements are limited to $M_w \leq 2200$ g/mol. In order to determine both interaction energies, temperature dependent measurements had to be performed.

II. EXPERIMENTAL DETAILS

A. Sample preparation and characterization

Ethylene glycol (≥99.8%), diethylene glycol (≥99%), triethylene glycol (≥99%) were purchased from Sigma Aldrich. PEO with an average molar mass Mw of 240, 660, 2200, 5400, 180 000 g/mol were purchased from Polymer Source and 33 660, 79 565 g/mol were obtained from Max-Planck-Institute for Polymer Research. The polydispersity index (PDI) for all purchased polymers are between 1.07 and 1.2. Solvents were prepared from Milli-Q water and absolute ethanol from Merck. All solutions were filtered through 0.2 μm inorganic membrane filters from Anotop into Hellma quartz cells with an optical path length of 0.2 mm. The filter does not change the concentration, which was validated by measuring the refractive index before and after filtering. For the polymers with low molar mass ($M_w < 6000$ g/mol), the polymer mass concentration was 2% well below the overlap concentration c^*, while c^* is around 0.7% for the $M_w = 180\,000$ g/mol.[35] Therefore, we performed additional measurements for the polymers with $M_w > 30\,000$ g/mol at lower concentrations and extrapolated the measured coefficients to infinite dilution.

B. Infrared thermal diffusion forced Rayleigh scattering (IR-TDFRS)

A detailed description of the recently modified IR-TDFRS can be found in the paper by Blanco *et al.*[36] This setup is optimized for aqueous systems and has been used to study the transport properties in different aqueous systems of non-ionic surfactants,[37] saccharide solutions,[38] nucleotides,[39] and anisotropic bio-colloids.[36]

The normalized heterodyne scattered intensity $\zeta_{\text{het}}^{th}(t)$, assuming an ideal excitation with a step function, is given by

$$\zeta_{\text{het}}^{th}(t) = 1 - \exp\left(-\frac{t}{\tau_{\text{th}}}\right) - A(\tau - \tau_{\text{th}})^{-1} \times \left\{\tau\left[1 - \exp\left(-\frac{t}{\tau}\right)\right] - \tau_{\text{th}}\left[1 - \exp\left(-\frac{t}{\tau_{\text{th}}}\right)\right]\right\},$$

with the steady state amplitude A equal to

$$A = \left(\frac{\partial n}{\partial c}\right)_{p,T}\left(\frac{\partial n}{\partial T}\right)_{p,c}^{-1} S_T c\,(1-c)\,, \tag{3}$$

where c is the mass fraction of the ethylene oxide oligomers or polymers, τ_{th} the heat diffusion time, $(\partial n/\partial c)_{p,T}$ and

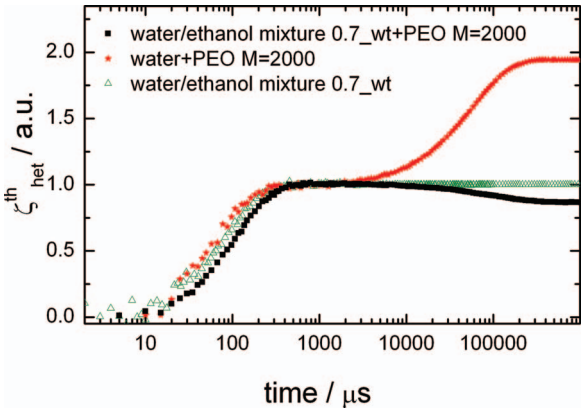

FIG. 3. Heterodyne signal of TDFRS of different solvents. Black square symbols present the signal of PEO 2200 g/mol in a water/ethanol mixture ($c_{water} = 0.7$). Stars show the measurement of PEO 2200 g/mol in pure water and triangles are the signal of the binary water/ethanol mixture ($c_{water} = 0.7$), which shows no concentration plateau. All experiments have been performed at a temperature of T = 25 °C.

$(\partial n/\partial T)_{p,c}$ are refractive index contrast factors with respect to mass concentration at constant pressure and temperature, and with respect to temperature at constant pressure and mass concentration, respectively. The refractive index contrast factors are measured independently from the TDFRS measurements. The details about measuring refractive index contrast factors are described in Ref. 39.

C. Choice of the water/ethanol composition

With our experimental method we determine the thermodiffusion properties from the diffraction efficiency of a refractive index grating. Therefore, the method is primarily for binary systems. Only in special case such as for high molar mass PEO the process stemming from the polymer and the solvent can be separated due to their different time scales.[13] This approach will not be possible in the case of the low molar mass compounds. Only for two specific water/ethanol concentrations, when the concentration signal stemming from the water/ethanol mixture is negligible an investigation of the ternary system is still feasible. At water mass fraction around $c_{water} = 0.19$ the contrast factor $(\partial n/\partial c)_{p,T}$ vanishes, so that the amplitude A of the concentration signal (cf. Eq. (3)) vanishes. Unfortunately, the zero of $(\partial n/\partial c)_{p,T}$ shifts to higher water fractions with increasing temperature,[40] so that for each temperature the water/ethanol composition needs to be adjusted. Another possibility is a water mass fraction of $c_{water} = 0.7$,[3,9,13,40–42] where the Soret coefficient of the water/ethanol mixture vanishes for all temperatures (cf. Fig. 1). Fig. 3 shows the typical signal of the measurements. The black squares and green triangles are the signals of the water/ethanol/PEO mixture with $c_{water} = 0.7$ and water/ethanol mixture with $c_{water} = 0.7$ mass fraction, respectively. The concentration plateau is fairly flat, which shows no contribution of the solvents. The red star symbols present the measurement of PEO in pure water.

III. EXPERIMENTAL RESULTS AND DISCUSSION

A. Results

Fig. 4 shows the Soret coefficient S_T, the diffusion coefficient D, and the thermal diffusion coefficient D_T at $c \to 0$ as function of the molar mass in ethanol, water/ethanol mixture ($c_{water} = 0.7$), and pure water, from left to right. All the samples are measured in the temperature range between 15 °C and 45 °C with a temperature step of 10 °C.

In ethanol, S_T stays rather constant for molar mass below 660 g/mol. Then S_T drops dramatically at 2200 g/mol and changes from positive to negative for all investigated temperatures. No clear trend with temperature can be observed. The Soret coefficient S_T in water/ethanol mixtures decreases monotonically. The values are negative, indicating that PEO accumulates for all temperatures and molar masses at the warm side. The magnitude of S_T also increases with increasing temperature. In pure water, S_T increases as a function of the molar mass, on the contrary to the other two systems. The values are all positive indicating that the ethylene oxide oligomers and polymers are thermophobic. Compared to the water/ethanol mixture the temperature dependence of S_T is less pronounced.

The diffusion coefficient D decreases with increasing molar mass for all solvents and increases with temperature. According to the Stokes-Einstein equation, diffusion coefficient is inversely proportional to the viscosity of the solvent and the temperature. As the viscosity of the water/ethanol mixture ($c_{water} = 0.7$) is higher than pure water,[43] the diffusion coefficients D increases slightly with increasing water content in our concentration range.

In pure ethanol, the thermal diffusion coefficient D_T of ethylene oxide oligomers with low molar masses increases slightly and decreases for higher molar mass. Also the rise of D_T with increasing temperature is more pronounced for low molar masses. For the investigated mass fraction of 2% a sign change from positive to negative occurs for molar mass of 2200 g/mol. In an earlier work by Klein and Wiegand,[19] the sign change of D_T was already observed for the shorter dimer diethylene glycol with $M_w = 200$ g/mol at a higher mass fraction of 20%, which corresponds roughly to the same molar monomer concentration around 4 mM for a mass fraction of 2% of the ethylene oxide oligomer with $M_w = 2200$ g/mol. This observation confirms the picture that the interactions between ethanol, which is a bad solvent, and the individual monomer beads determine D_T. The sign change occurs at a certain molar concentration of the monomer beads. For water/ethanol mixture, D_T increases with increasing molar mass first rapidly and then reaches a plateau around the molar mass of 2200 g/mol. In the previous study of PS/toluene system, a similar molar mass dependence with a plateau around 2000 g/mol has also been observed, although it was in organic solvent and D_T was positive.[25] In another study of polysaccharides in aqueous system, D_T decreases as function of molar mass, but still reaches the plateau in the same range of molar mass.[15] In our study, we also found that for low molar mass D_T decrease with increasing temperature, but for higher molar masses the data agree within the error bars. In pure water, D_T shows a similar molar mass dependence as found for aqueous

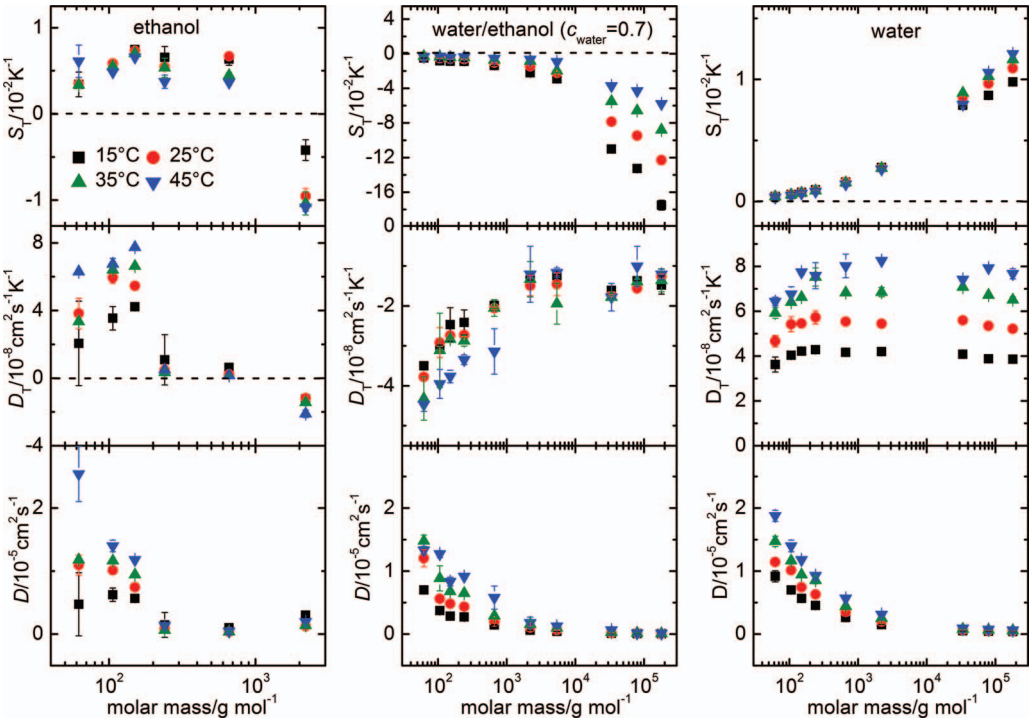

FIG. 4. S_T, D, and D_T of ethylene oxide oligomers and polymers as a function of molar mass in the dilute limit $c \to 0$ in ethanol, water/ethanol mixture ($c_{water} = 0.7$), and water from left to right. All samples are measured at four temperatures in the range between 15 °C and 45 °C presented by square, circle, up triangle, and down triangle symbols, respectively.

and organic polymer solutions.[15,25] Our measurements also show a rise of D_T with increasing temperature.

B. Discussion

In the following, we will analyze the molar mass dependence of D_T at $c \to 0$. We rewrite Eq. (2) in the following form:

$$D_T = A(T) - \frac{B(T)}{M^{\nu}}, \tag{4}$$

with

$$A(T) = \frac{\beta \varepsilon_p(T)}{6\pi\eta a}, \tag{5}$$

$$B(T) = \frac{\beta \varepsilon_s(T) + (\varepsilon_s(T) - \varepsilon_p(T))/T}{\eta \tilde{\ell}}, \tag{6}$$

and determine the temperature dependent quantities $A(T)$ and $B(T)$, which will give us the interaction parameters once the properties such as thermal expansion coefficient β, viscosity η, and the radius a of the monomers are known. Describing the shape of the monomer of PEO by a sphere with radius a can only be a rough estimate. Using the van der Waals volumes of the chemical subunits[44] or the rubber volume of PEO[45] results in $a = 0.25$ nm and $a = 0.21$ nm, respectively. This 20% uncertainty in the radius will also lead to a similar relative error of the interaction parameter $\varepsilon_p(T)$

Fig. 5 shows the thermodiffusion data of ethylene oxide oligomers and polyethylene oxide in pure water, in the water/ethanol ($c_{water} = 0.7$) mixture, and in pure ethanol. Note that the data in pure ethanol due to the low contrast have partially large error bars of more than 50%, so that we excluded the measurements of the tri-mer from the data analysis. There are two reasons that the signal amplitude A (cf. Eq. (3)) for the measurements in ethanol are so low: first, the scattering of the low mass monomers and oligomers is weak and additionally the contrast factor $(\partial n/\partial c)_{p,T}$ is 30%–60% lower in comparison with the solvent mixture and pure water.

The inset shows the interaction parameter ε_p, which has been determined directly from $A(T)$ using the literature data for the thermal expansion coefficient[46] and the viscosity.[47] For the two solvents containing ethanol ε_p is negative and in the order of 10^{-20} J, which is close to the interaction parameters used in the lattice model by Luettmer-Strathmann.[22] In the case of the aqueous system, ε_p is up to one order of magnitude larger and shows a stronger temperature dependence.

The parameter $\varepsilon_s(T)$ and $\tilde{\ell}$ can be determined from the temperature dependence of $B(T)$. It turns out that this procedure gives only reasonable results for the aqueous system, while for the other systems the uncertainties in the parameters are very high and $\varepsilon_s(T)$ is orders of magnitude too large. In a second approach, we used Eq. (6) at different temperatures and solved the linear equation system in order to determine $\varepsilon_s(T)$ and $\tilde{\ell}$. We found that $\varepsilon_s(T)$ also spreads over a wide range and we were not able to identify a temperature trend of $\varepsilon_s(T)$. Therefore, we plotted in the insets of Figure 5 only the average value of $\varepsilon_s(T)$ as solid line. The double arrow marks one standard deviation indicated by the dotted line.

Figures 6(a) and 6(b) show an overview of the determined interaction parameters according to Eq. (4) as function of the water/ethanol mass fraction. Part (a) enlarges the

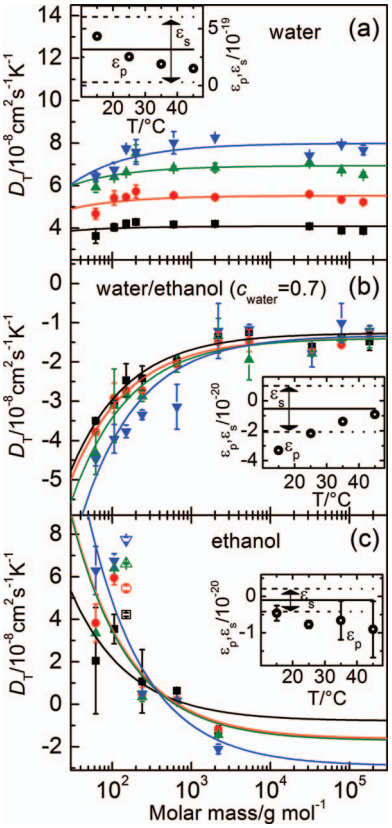

FIG. 5. Molar mass dependence of the thermal diffusion coefficient D_T with $c \to 0$ at 15, 25, 35, and 45 °C in (a) pure water, (b) the ethanol/water (c_{water} = 0.7) mixture, and in (c) pure ethanol. The symbols for different temperatures are used as in Fig. 4. The open symbols have been excluded from the data analysis. Lines are fits according to Eq. (4). The inset shows the determined interaction parameters ε_p as function of temperature and the range of ε_s. For further details see text.

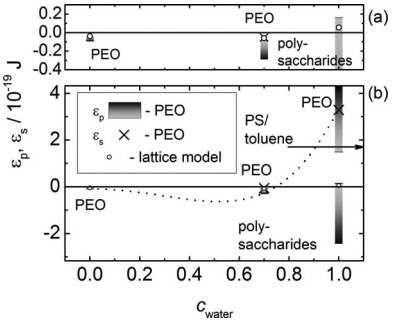

FIG. 6. Interaction parameters according to Eq. (4) for PEO and polysaccharides as function of the water/ethanol content. The filled areas show the variation of $\varepsilon_p(T)$ as function of temperature, whereas the blue part denotes the values at the lower temperatures. The cross marks the average value of $\varepsilon_s(T)$. The dotted line is a guide for the eye. Part (a) enlarges the area around $\varepsilon_s(T) = \varepsilon_p(T) = 0$ from part (b).

area around $\varepsilon_p = \varepsilon_s = 0$. The temperature dependence found for $\varepsilon_p(T)$ is indicated by the gradient filled areas, whereas the dark and light grey parts refer to cold and warm temperatures, respectively. For comparison, we also show the values for the two systems mentioned in the Introduction. In this plot, it becomes obvious that the change of $\varepsilon_p(T)$ is more pronounced in pure water than in the solutions containing ethanol. The cross marks are the average values of $\varepsilon_s(T)$, which are always in the same order of magnitude as $\varepsilon_p(T)$. In contrast to the observations found for aqueous mixtures,[23] where the cross interaction, in this case $\varepsilon_p(T)$, was always stronger than the like-like interaction, $\varepsilon_s(T)$, we cannot identify a clear trend, although the determined interaction energies are in the same range as the interaction parameters used in the lattice model by Luettmer-Strathmann.[22] The most striking point is the sign change with solvent composition. While the interaction parameters are positive for pure water, they become negative for the solutions containing ethanol. The observed trend looks very similar to the change of the Soret coefficient as function of the solvent composition as it has been measured before.[13] Another general trend, although hard to see for pure ethanol, is that the absolute value of $\varepsilon_p(T)$ becomes smaller with increasing temperature. This also holds for polysaccharides in pure water, although here $\varepsilon_p(T)$ is in contrast to the PEO system negative, which cannot be understood, because water should be a good solvent for the polysaccharides, so that we would expect attractive interactions as in the case of the PS/toluene system.

For the organic polymer solution of polystyrene in toluene, we find $\varepsilon_p(T) = 0.17 \times 10^{-19}$ J at 22 °C, which is indicated by an arrow in Figure 6(b). This finding agrees with the ε-values found for the system PEO/water.

IV. CONCLUSION

In this paper, we presented the molar mass dependence of thermodiffusion of polyethylene oxide in ethanol, water/ethanol mixture (c_{water} = 0.7), and water in a temperature range between 15 °C and 45 °C. We found that in pure ethanol, S_T, D, and D_T all decrease as function of molar mass, with a sign change from positive to negative in S_T and D_T at a molar mass around 2200 g/mol. In water/ethanol mixture (c_{water} = 0.7), S_T and D decrease and D_T increases monotonically with increasing molar mass. S_T and D_T are negative for all the molar masses, indicating that ethylene oxide oligomers and polymers are thermophilic in water/ethanol mixture. In pure water system, S_T increases and D decreases as function of molar mass. D_T increases and then reaches a plateau.

For all compositions studied in this work, the molar mass dependence can be described with a theoretical model derived by Würger.[32] The determined interaction energies ε_s and ε_p are positive under good solvent conditions (water) and negative otherwise. It needs to be pointed out that the theoretical model has been derived for organic polymer solutions with short range van der Waals interactions and not for polymers in solvents with specific interactions, so that the model will not be capable to describe the investigated mixtures in detail. Nevertheless, the determined interaction parameters lie in a reasonable range and compare well with other literature results.[22] The deficiency of the model becomes evident if we look at the analysis of polysaccharides in water. Although water is a good solvent for polysaccharides negative interaction energies are found indicating bad solvent conditions. Here, a refined model needs to be developed which takes specific interactions such as hydrogen bonds into account.

ACKNOWLEDGMENTS

The authors thank Marisol Ripoll, Gerhard Nägele, Kousaku Maeda, and Alois Würger for inspiring discussions. We gratefully acknowledge the gracious support of Jan Dhont for this work. Additionally, we thank the Deutsche Forschungsgemeinschaft (DFG) for financial support due to Grant No. Wi 1684.

[1]C. J. Wienken, P. Baaske, U. Rothbauer, D. Braun, and S. Duhr, Nat. Commun. **1**, 1 (2010).
[2]C. A. Lipinski, F. Lombardo, B. W. Dominy, and P. J. Feeney, Adv. Drug Delivery Rev. **64**, 4 (2012).
[3]G. Wittko and W. Köhler, EPL **78**, 46007 (2007).
[4]P. Polyakov, E. Rossinsky, and S. Wiegand, J. Phys. Chem. B **113**, 13308 (2009).
[5]R. Kita, P. Polyakov, and S. Wiegand, Macromolecules **40**, 1638 (2007).
[6]J. Rauch and W. Köhler, J. Chem. Phys. **119**, 11977 (2003).
[7]C. Debuschewitz and W. Köhler, Phys. Rev. Lett. **87**, 4 (2001).
[8]P. Blanco, P. Polyakov, M. M. Bou-Ali, and S. Wiegand, J. Phys. Chem. B **112**, 8340 (2008).
[9]P. Polyakov and S. Wiegand, J. Chem. Phys. **128**, 034505 (2008).
[10]H. Ning, J. Buitenhuis, J. K. G. Dhont, and S. Wiegand, J. Chem. Phys. **125**, 204911 (2006).
[11]B.-J. de Gans, R. Kita, S. Wiegand, and J. Luettmer Strathmann, Phys. Rev. Lett. **91**, 245501 (2003).
[12]D. Stadelmaier and W. Köhler, Macromolecules **41**, 6205 (2008).
[13]R. Kita, S. Wiegand, and J. Luettmer Strathmann, J. Chem. Phys. **121**, 3874 (2004).
[14]R. Kita and S. Wiegand, Macromolecules **38**, 4554 (2005).
[15]Y. Kishikawa, H. Shinohara, K. Maeda, Y. Nakamura, S. Wiegand, and R. Kita, Phys. Chem. Chem. Phys. **14**, 10147 (2012).
[16]J. Israelachvili, Proc. Natl. Acad. Sci. U.S.A. **94**, 8378 (1997).
[17]E. E. Dormidontova, Macromolecules **35**, 987 (2002).
[18]M. Giglio and A. Vendramini, Phys. Rev. Lett. **38**, 26 (1977).
[19]M. Klein and S. Wiegand, Phys. Chem. Chem. Phys. **13**, 7090 (2011).
[20]J. Chan, J. J. Popov, S. Kolisnek-Kehl, and D. G. Leaist, J. Sol. Chem. **32**, 197 (2003).
[21]J. Luettmer-Strathmann, J. Chem. Phys. **119**, 2892 (2003).
[22]J. Luettmer-Strathmann, Int. J. Thermophys. **26**, 1693 (2005).
[23]C. Nieto-Draghi, J. B. Avalos, and B. Rousseau, J. Chem. Phys. **122**, 114503 (2005).
[24]M. E. Schimpf and J. C. Giddings, Macromolecules **20**, 1561 (1987).
[25]J. Rauch and W. Köhler, Macromolecules **38**, 3571 (2005).
[26]F. Brochard and P. G. Degennes, C. R. Acad. Sci., Ser. II **293**, 1025 (1981).
[27]A. Würger, Phys. Rev. Lett. **102**, 078302 (2009).
[28]M. C. Yang and M. Ripoll, J. Phys.: Condens. Matter **24**, 195101 (2012).
[29]M. Doi and S. Edwards, *The Theory of Polymer Dynamics* (Oxford Science Publications, 1986).
[30]M. Zhang and F. Müller-Plathe, J. Chem. Phys. **125**, 124903 (2006).
[31]S. Duhr and D. Braun, Proc. Natl. Acad. Sci. U.S.A. **103**, 19678 (2006).
[32]A. Würger, Rep. Prog. Phys. **73**, 126601 (2010).
[33]G. Strobl, *The Physics of Polymers* (Springer, 2007).
[34]D. Stadelmaier and W. Khler, Macromolecules **42**, 9147 (2009).
[35]J. Brandrup, *Polymer Handbook*, 2nd ed. (Wiley, New York, NY, 1975).
[36]P. Blanco, H. Kriegs, M. P. Lettinga, P. Holmqvist, and S. Wiegand, Biomacromolecules **12**, 1602 (2011).
[37]H. Ning, S. Datta, T. Sottmann, and S. Wiegand, J. Phys. Chem. B **112**, 10927 (2008).
[38]P. Blanco and S. Wiegand, J. Phys. Chem. B **114**, 2807 (2010).
[39]Z. Wang, H. Kriegs, and S. Wiegand, J. Phys. Chem. B **116**, 7463 (2012).
[40]A. Königer, B. Meier, and W. Köhler, Philos. Mag. **89**, 907 (2009).
[41]P. Kolodner, H. Williams, and C. Moe, J. Chem. Phys. **88**, 6512 (1988).
[42]S. Wiegand, H. Ning, and H. Kriegs, J. Phys. Chem. B **111**, 14169 (2007).
[43]I. Khattab, F. Bandarkar, M. Fakhree, and A. Jouyban, Korean J. Chem. Eng. **29**, 812 (2012).
[44]J. T. Edward, J. Chem. Educ. **47**, 261 (1970).
[45]D. van Krevelen, *Properties of Polymers*, 3rd ed. (Elsevier, Amsterdam, 1997).
[46]N. Osborne, E. McKelvy, and H. Bearce, *Density and Thermal Expansion of Ethyl Alcohol and of its Mixtures with Water* (National Bureau of Standards, 1913), Vol. 9, pp. 327–474.
[47]E. Bingham and R. Jackson, *Standard Substances for the Calibration of Viscometers* (National Bureau of Standards, 1918), Vol. 14.

CHAPTER

SIX

THERMOPHORESIS OF A COLLOIDAL ROD: STERIC AND CHARGE CONTRIBUTIONS

In this study we investigated the thermodiffusion behavior a colloidal model system consisting of fd-virus grafted with polyethylene oxide (M_w= 5000 g/mol) as a function of the ionic strength, which corresponds to different Debye lengths. The results are compared with recent measurements of the bare fd-virus. The diffusion coefficient agrees within the error bars and increases with increasing Debye length, λ_{DH}. The thermal diffusion coefficient, D_T, of the grafted fd-virus does not change with ionic strength, while D_T of the bare virus decrease with increasing ionic strength. Therefore the Soret coefficient, S_T, of the grafted fd-virus shows a decay with increasing λ_{DH}. At high λ_{DH} corresponding to low ionic strength the S_T-values of both colloidal model systems approach each other. The steric and the charge contributions correspond to different Debye length. For the short Debye lengths we find a clear contribution from the polymer chain,

which fades out for the longer Debye lengths, when the polymer chains fit into the electrostatic layer.

6.1 Introduction

In the last five years the thermodiffusion or thermophoretic motion of molecules in a temperature gradient gained a lot of interest due to applications in biotechnology [90] and as one key parameter in the origin of life puzzle [55]. Due to the complexity of interactions as hydrogen bonds and long range charge effects the behavior of aqueous system can often not be foreseen. Even in non-polar mixtures there is still a lack on a deep microscopic understanding of thermodiffusion although for those systems the thermophoretic behavior can be predicted by using thermodynamic concepts such as heats of transfer or empirical equations [20, 40, 70]. The thermophoretic motion in aqueous systems depends on a number of properties such as size, charge, hydration shell and conformation .

The rod-like *fd*-virus have been widely used as model systems in soft matter physics due to their high monodispersity in terms of both size and shape [27, 44, 78]. The wild type *fd*-virus has a molecular weight of 1.64×10^7 g/mol, a contour length L of 880 nm, a radius a of 3.4 nm, and persistence length L_P of 2.2 μm. The *fd*-virus consist of single-strand DNA with amino groups and acidic residues, which determines the surface properties of *fd*-virus. Above pH 4 they are negatively charged and interact via a combination of electrostatic repulsion and hard-core interactions. The net surface charge can be increased or decreased by increasing or decreasing the solution pH, respectively [74]. Therefore the *fd*-virus can be electrostatically stabilized by adjusting the pH value or the ionic strength of their solution. However, involving electric double layer the change of ionic strength always has an influence on the effective volume of *fd*-virus themselves. One way to turn the *fd*-virus into charge independent is to graft neutral polymer polyethylene oxide (PEO) with large enough molar mass to the surface of the virus, so the polymer coatings stabilize the rods sterically.

In this work PEO ($Mw = 5000$ g/mol) with an active *N*-hydroxysuccinimide (NHS) end was chosen for the surface modification. We expect a sterically dominant interparticle interaction for high ionic strength because the electric double layer is deeply confined within the grafted polymers and in the opposite case the interaction is determined by the electric double layer for very low ionic strength, as intuitively illustrated by Figure 6.1. By changing the ionic

strength we focus on the investigation of the steric and charge contribution of the colloidal model system.

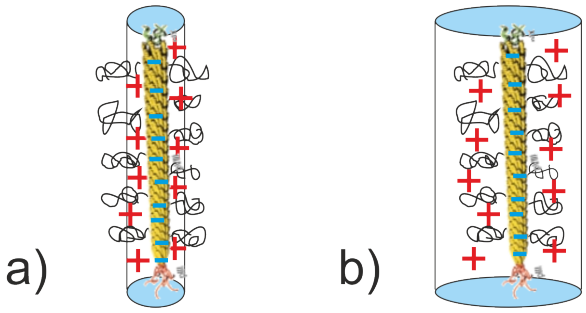

Figure 6.1: *Illustration of steric and electrostatic contributions at different Debye length. a) At high ionic strength the polymer chains exceed the electrostatic range. The system is dominated by steric repulsion. b) For low salt contant and long range electrostatic interaction the thermophoretic behavior is dominated by charge effects.*

6.2 Experimental Details

6.2.1 Sample Preparation and Characterization

The *fd*-virus was prepared following a standard biological protocol using XL1-Blue strain of *E. coli* as the host bacteria [81]. The obtained virus was purified by repetitive centrifugation (108000 *g*) and then re-dispersed in the Tris(hydroxymethyl)aminomethane (Tris) buffer solution of 2 mM.

PEO grafted *fd*-viruses (PEO-*fd*) were prepared using PEO with an activated succinimidyl end-group (Methoxypolyethylene glycol 5000 propionic acid N-succinimidyl ester (*m*PEO-SPA) obtained from Fluka) which reacts with the amino groups on the surface of the virus following Dogic *et al.* [26] with some minor modifications. As the succinimidyl-groups would also react with the amine group of the Tris buffer, the virus described above was transferred to a 20 mM phosphate buffer at pH 8.5 with 15% ethanol to prevent the growth of micro-organisms. The virus solution was diluted with buffer to obtain about 215 mL *fd* solution of 4 mg/mL. Then 4.1 g of solid *m*PEO-SPA polymer was added to the stirring solution of the viruses and the reaction was allowed to proceed for a few hours. After that the viruses

were purified from the excess unreacted PEO by three centrifugation/redispersion cycles at 30000 rpm (about 108000 *g* at the bottom of the tubes) to obtain a stock solution of PEO-*fd* in a 2 mM Tris/1 mM HCl buffer (pH 8.1).

The successful PEO grafting on the *fd* virus was demonstrated by the difference of the concentration at which the isotropic nematic (IN) phase transition takes place for PEO-*fd* as compared to bare *fd* at an ionic strength of 100 mM [26]. Therefore a small amount of bare as well as PEO-*fd* virus was redispersed in a 200 mM Tris/100 mM HCl buffer (pH 8.3, ionic strength 100 mM) by repeated centrifugation/redispersion cycles as described above. The concentrated virus dispersion was diluted by the buffer drop by drop until the permanent birefringence was just lost. From these solutions the concentration was determined by the UV absorption at 269 nm using an absorption coefficient of 3.84 $\mathrm{cm^2 mg^{-1}}$. The PEO itself was found not to contribute significantly to the absorption at 269 nm, so that for PEO-*fd* the concentration of the *fd* core is obtained. In this way an IN phase transition concentration of 9 mg/mL was obtained for the PEO-*fd*, whereas for bare *fd* the corresponding concentration was found to be 19 mg/mL. This large difference in concentration indicates a higher grafting density as compared to the original results from Dogic [26].

To characterize the grafting density more quantitatively, the concentration obtained from the solid content was compared to the concentration from the UV absorption. Because the solid content includes the weight of the PEO whereas the UV absorption only measures the corresponding concentration of the *fd* cores (PEO does not absorb significantly) the amount of PEO grafted to the virus can be determined from the difference of solid content to the "UV-concentration". Because PEO continuous to lose weight if dried at higher temperatures the solid content was determined at only 35 °C under vacuum. All weights were obtained by drying to constant weight, drying bottles were pre-dried to obtain their empty weight and the small contribution of the buffer was determined and subtracted. In this way the solid content was determined twice using about 13 mg dry PEO-*fd* per determination. Doing so resulted in an approximate value of 22_wt% PEO relative to the *fd* part of PEO-*fd*, or 18_wt% PEO relative to the weight of PEO-*fd*. Using a molecular weight of 16.4×10^6 g/mol for the *fd* virus, 5000 g/mol for the PEO and 2700 major coat proteins per virus, this corresponds to about 27% of all coat proteins being grafted with a PEO molecule.

Tris with concentrations of 82.15, 29.57, 15.09, 6.11, 3.29, and 2.05 mM were used as buffer solutions. The pH of all buffer solutions were adjusted to 8.2 by adding concentrated HCl solution. The stoke solution of PEO-*fd* virus was dialyzed in each chosen buffer and then the

concentration was adjusted to 1 mg/ml. Concentrations were determined by UV absorption (NanoDrop ND-1000, Peqlab). All measurements have been performed at 20 °C.

6.3 Results and Discussion

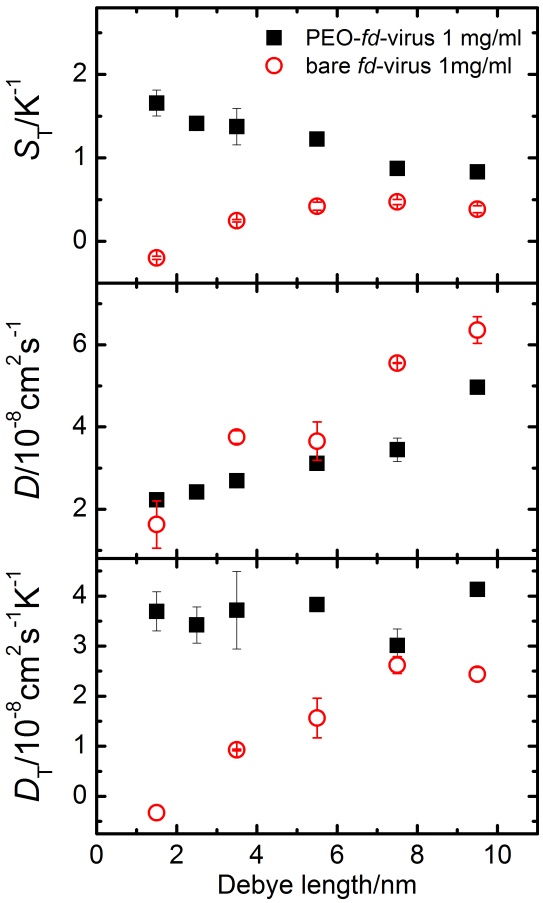

Figure 6.2: *S_T, D and D_T of the PEO-fd-virus (c_{PEO-fd} = 1mg/ml), represented by the black squares and bare fd-virus (c_{fd} = 1mg/ml), represented by the red circles as a function of the Debye length.*

Soret coefficient, S_T, diffusion coefficient, D, and thermal diffusion coefficient, D_T of PEO grafted *fd*-virus are investigated as a function of ionic strength from the range of 1 mM and 41 mM. According to Zhang *et al.* [98], for grafting PEO with molar mass of 5000 g/mol the phase behavior of PEO-*fd*-virus starts to become ionic strength independent at an ionic strength above 20 mM corresponding to the Debye length of 2.15 nm, because the

electric double layer is confined within the PEO layer at high ionic strength. Below the ionic strength of 20 mM the dominant interaction should be electrostatic. One can expect at low ionic strength the behavior of PEO-*fd* should be similar as the bare *fd*. The obtained values are compared with the values of bare *fd*-virus in Figure 6.2. S_{T} of grafted and bare *fd*-virus show opposite trends as a function of Debye length. As increasing Debye length S_{T} of two systems approach each other. The values of D are in a comparable range. D_{T} of bare *fd* increases with Debye length, while D_{T} of PEO-*fd* shows no dependence of Debye length.

The next questions to ask are how is the interaction between PEO-*fd*-virus at low ionic strength and how much does the polymer contribute above the electric double layer. To answer these questions further investigations at different concentrations of PEO-*fd* have to be performed. To be able to separate the effect of PEO and the electric double layer, PEO should also be investigated as a function ionic strength.

CHAPTER

SEVEN

CONCLUSION AND OUTLOOK

The relevance of thermodiffusion in biological system has drawn increasing attention in recent years. Thermodiffusion or thermophoresis is the mass transport phenomena of a multi-component system due to a temperature gradient. The main quantity to characterize thermodiffusion is the Soret coefficient, S_{T}, which describes the separation of a mixture under a temperature gradient. It equals to the ratio of the thermal diffusion coefficient, D_{T}, and the diffusion coefficient, D. By convention, a positive Soret coefficient indicates that the molecules enrich at the cold side and *vice versa*.

In the class of biological systems two very important examples are the determination of binding constant of proteins, and the effect in the 'origin of life' scenario due to the existence of large temperature gradients in the early oceans [3, 90]. A microscopic understanding of the thermal diffusion process of liquids in general and particularly for aqueous and biological systems is lacking. The latter systems are often more complicated due to the capability to form hydrogen bonds and many biological molecules contain hydrophobic and hydrophilic groups, so that their behavior changes depending on the environment such as solvent quality, pH and ionic strength. Proteins are often stabilized in buffers containing salts and surfactants so that many components are present and for the charged components long range interactions

need to be taken into account. A full analysis of a complete biological system is too complex at the moment, so that we concentrated on four simpler biological relevant model systems.

In the present thesis we investigated the thermodiffusion behavior of various biological and synthetic bio-compatible systems. Most of our investigations have been performed by a holographic grating technique, the so-called Infrared Thermal Diffusion Forced Rayleigh Scattering (IR-TDFRS). This technique is especially suitable for studies of aqueous system, because the energy of the IR laser can be directly absorbed and converted into the temperature grating, so that no extra dye is required. Computer simulations have been also employed to compare the experimental data and to advance in the microscopic understanding of the thermodiffusion phenomena. As illustrated in figure 7.1 a typical biological system such as a virus in a buffer solution is complex and contains many components like proteins, polymers, ions and DNA-strands, which are formed by nucleotides. We have focused our studies on four of the components including nucleotides, alkali halides, a water soluble polymer and a charged rod-like colloid. The goal is to identify the relevant properties, which influence the thermodiffusion of aqueous systems.

In Chapter 2 we investigated the thermodiffusion behavior of nucleotides. These small-biomolecules are the building blocks of macromolecules like DNA or RNA, which are the most fundamental molecules for life. Each nucleotide molecule is composed by a nitrogenous base, a five-carbon sugar, and one or more phosphate groups. We studied five nucleotides, cyclic adenosine- and guanosine- monophosphate (cAMP and cGMP), 5'-adenosine- and 5'-cytidine-monophosphate (AMP and CMP) and adenosine diphosphate (ADP) at different temperatures. These nucleotides were chosen in a systematic way considering the progressive variation of their structures such that the thermophoretic properties can be systematically investigated. The thermodiffusion behavior of nucleotides is studied as a function of various physical properties. In contrast to organic mixtures, we have shown that nucleotides do not vary significantly their Soret coefficient with molar mass and the asymmetry of the molecule. This is a reflection of the different solvent molecule interactions, which are intrinsically different between organic mixtures and nucleotides due to for instance the presence of hydrogen bonds or electrostatic interactions. The influence of hydrophobicity/hydrophilicity has been analyzed through the partition coefficient $\log p$, which can be calculated from the structure of nucleotide and describes ratio of concentrations of a compound in a mixture of octanol and water. As a nucleotide molecule contains both a polar and a non-polar part, the hydrophobicity/hydrophilicity of nucleotides is related to their capabilities to form hydrogen bonds

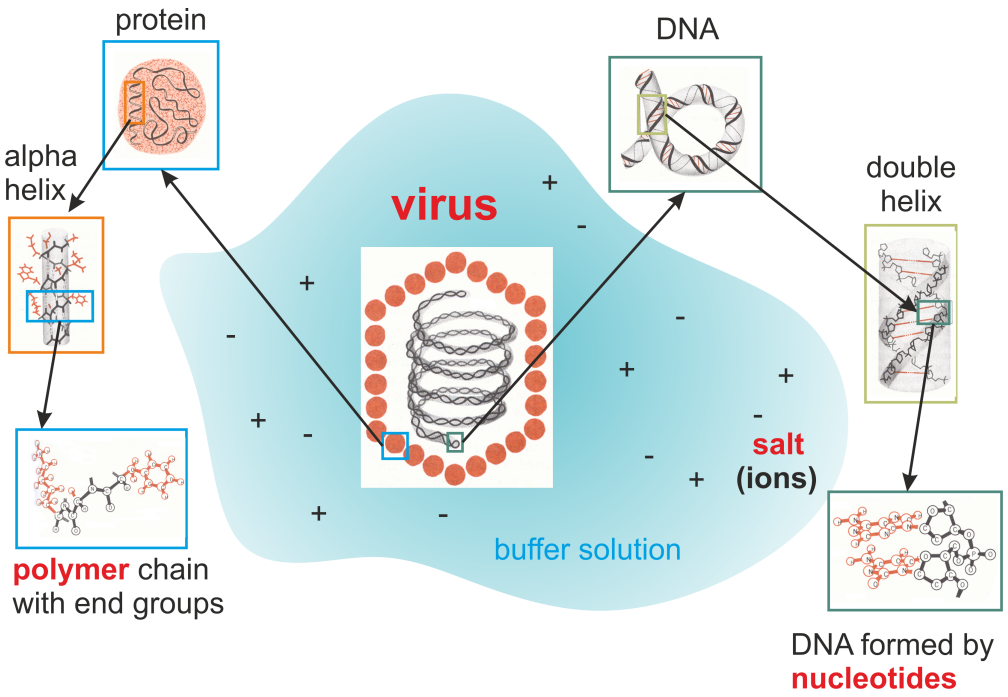

Figure 7.1: *Schematic drawing of a virus in a buffer solution and its building blocks. The coat proteins consist of an alpha helix, which is formed by a polymer backbone with side groups, The inner of the virus consists of a DNA double helix strand formed by nucleotides. The components marked in red such as simple salt ions, nucleotides, a water soluble polymer and a charged virus have been investigated.*

and their interactions with water molecules. In the studied temperature range, nucleotides with higher degree of hydrophobicity accumulate more effectively at the cold side. The increase of the repulsion between the nucleotides and the water molecules enhances then their separation.

For one nucleotide, cAMP, we also investigated the influence of the pH value. The surface charge of the nucleotides vary drastically with the surrounding pH value since nucleotides have both proton donor (phosphate) and acceptor (amino) sites. The measured Soret coefficient shows a clear decay with increasing pH value, *i. e.* increasing ionic strength. The charge influence is further investigated in later chapters.

Interestingly, compared to other aqueous systems with a similar molar mass, such as oligosaccharide, the obtained thermal diffusion coefficients of the nucleotides are one order of magnitude larger. This means that nucleotides have a much larger tendency to separate from water than oligosaccharides under a temperature gradient. This is certainly a factor that

has favored the prebiotic evolution to provide a high concentration of nucleotide monomers for the formation of DNA and RNA. Furthermore, in the measured temperature range, increasing the average temperature S_T of the nucleotides also increases. This dependence of temperature can be described with an empirical equation (Eq. 1.4). This empirical equation has shown to be valid as well in many aqueous solutions of proteins and polymers [46].

Additionally, we have studied the variation of the thermal diffusion coefficient of nucleotides with the thermal expansion coefficient and the kinematic viscosity, which are tabulated properties. We verified a direct proportionality of S_T with the ratio of the thermal expansion coefficient and the kinematic viscosity, as also found in the case of alkanes and monoscaccharides [5, 69].

In Chapter 3 the biological relevant aqueous alkali halide solutions ($Na^+/K^+ - Cl^-$) were investigated by both non-equilibrium molecular dynamics simulations and TDFRS measurements. We studied the role of pressure, average temperature and salt concentration on the determination of the Soret coefficient. The experimental data correspond to 1 bar pressure, whereas the simulation results were obtained at 100 and 500 bar. Our simulation results show that the pressure has a small impact on the Soret coefficient, which increases slightly going from 100 to 500 bar. This effect is more noticeable at lower salt concentrations. Anyhow, the qualitative dependence of the Soret coefficient with salt concentration overall is not affected by the pressure. We found that both the experimental and simulated Soret coefficients agree in the order of magnitude. Furthermore, we observed experimentally that the thermal conductivity decreases as a function of salt concentration. This dependence was accurately reproduced by the simulation.

The Soret coefficient has been studied as function of salt concentration and average temperature. We found experimentally that the Soret coefficient decreases with concentration at temperatures higher than 315 K, whereas it increases at lower temperatures. Similar as nucleotides, the temperature dependence of Soret coefficient of salts can also be described by Eq. 1.4. The Soret coefficient for both salts NaCl and KCl changes the sign from positive to negative with decreasing temperature. The sign change temperature depends on the salt composition, 283 K for NaCl and 293 K for KCl at the concentration of 0.5 M. For solutions with higher concentration we did not observe the sign inversion due to the limited temperature range that can be achieved experimentally. The extrapolation from Eq. 1.4 indicates that the sign inversion temperature of high concentration solutions should be lower than that of low concentration solutions. In previous studies, the origin of the sign inversion

has been linked to the unusual behavior of the thermal expansion coefficient in water *i. e.* water density maximum, which changes sign at about 277 K [87]. However, our simulation results do not support this correlation, as the density maximum found for the water model that we have used is at much lower temperature, 241K. This temperature is well below the sign inversion temperature we observed. We discussed the sign inversion in the framework of free energy. At low temperatures, the formation of hydrogen bonds is favored and the system would minimize its free energy by accumulating water at the cold side. On the other hand, at high temperatures, the hydrogen bond formation is more perturbed and becomes less important. Hence an increasing of the number of water molecules at the warm side will increase the entropy and therefore reduce the free energy. We have performed additional simulations to compute the water-water radial distribution function for ionic solutions. The results show that changes in temperature have a minor impact on the water structure and on the ion average solvation shells. The reason might be the radial distribution function is not sensitive enough to detect the crucial changes that lead to the unusual behavior of the Soret coefficient in ionic solutions.

Based on some results of small molecules mentioned in Chapter 2 and 3, we investigated the charge influence on the thermodiffusion behavior systematically. In Chapter 4 we studied very long (800 nm) and thin (3.4 nm as radius) virus so called *fd*-virus as a stiff colloidal rod model system with a persistence length of approximately 1 μm. The thermodiffusion behavior of dilute solutions of *fd*-virus was measured as function of the ionic strength and the rod-concentration. The ionic strength was varied by adjusting the concentration of buffer. It is inversely proportional to the Debye screening length, *i. e.* the thickness of the electric double layer. The Soret coefficient of the rods increases with increasing Debye length, with either fixed and varied rod-concentration. Meanwhile, it shows almost no dependence on the rod-concentration when the ionic strength is kept constant. When the volume fraction of the rods is fixed and we vary both the ionic strength and rod-concentration, the Soret coefficient still shows an increasing dependence of Debye length. The all above facts indicate that the contribution of the electric double layer dominates compared to the influence of the inter-particle interaction between rods.

We extended the theory to describe the thermodiffusion of charged spheres to long and thin charged rods. An expression for the Soret coefficient in terms of the Debye length, the rod-core dimension, and the surface charge density was given. The theory shows that the Soret coefficient of rod-like colloids can be presented by a superposition of spherical beads with the

same diameter of the rod and the same surface charge density for arbitrary Debye lengths. The number of beads was calculated as the ratio of the rod length and the rod diameter.

The Soret coefficients obtained from experiment are well described by our theory. To compare with the experimental data, the ionic-strength dependent contribution to the Soret coefficient and the surface charge density were used as adjustable parameter in the theory. These two parameters can be obtained by fitting Soret coefficient as a function of Debye length using our model. The surface charge density obtained from the fitting is about 3% lower than the calculated value. According to Manning's ion-condensation theory, a fraction of the surface charge is neutralized by ion-condensation. The contribution of the condensed ions to the Debye length dependence of Soret coefficient is incorporated. Therefore, the surface charge density we obtained from the model is only the part from the diffuse electric double layer.

In Chapter 5 we investigated the solvent quality influence and molar mass dependence of thermodiffusion using a bio-compatible macromolecule polyethylene oxide (PEO). PEO can form hydrogen bonds with water and is soluble in both water and ethanol. Water is a good solvent for PEO, and the addition of ethanol degrades the solvent quality. The thermodiffusion behavior of PEO was investigated at different temperatures in water, ethanol and in a water/ethanol mixture ($c_{\mathrm{water}} = 0.7$) in a molar mass range from monomer up to $M_{\mathrm{w}} = 180000$ g/mol. We observed a sign change of the Soret coefficient from positive to negative in pure ethanol at a molar mass around 2200 g/mol, indicating that polyethylene oligomers accumulate at the cold side and higher molar mass PEO enrich at the warm side. In pure water PEO of all molar masses accumulate at the cold side. By adding ethanol to pure water, the thermophoretic motion of PEO changes the direction, so that the polymer accumulates at the warm side. We analyzed the observed behavior within a theoretical model derived by Würger [92] and calculated the interaction energy between solvent molecules ε_s and the interaction energies between the solvent and the polymer ε_p. The obtained values for ε_s and ε_p are positive at good solvent conditions, which shows that the interaction between water and PEO is attractive. The interaction energies become negative when the solvent quality is degraded. All determined values for ε_s and ε_p are reasonable and comparable with the data from computer simulations of a two chamber lattice model [54].

For both pure water and water/ethanol mixture thermal diffusion coefficient of PEO increases with increasing molar mass of PEO and reach a plateau. This behavior has been described by Brochard and de Gennes [13] using a scaling concept. For long enough chains, the long-range interactions between monomers can be neglected in the calculation of the thermal diffusion

coefficient, D_T, and therefore a polymer chain moves under a temperature gradient with the same velocity as the individual monomers. The size dependence of the thermophoretic force and the friction force results into a precise cancellation, which leads then inevitably to a size-independent thermal diffusion coefficient.

In the last chapter some thermodiffusion measurements of a *fd*-virus grafted with PEO ($M_w = 5000$ g/mol) are discussed. The grafted *fd*-virus has been investigated as a function of the ionic strength, which varies the charge contribution relative to steric contributions as illustrated in Figure 6.1. The Soret coefficient decreases with increasing Debye length, which is opposite to the trend observed for the bare *fd*-virus with the same rod number concentration discussed in Chapter 4. For large Debye lengths the polymer chains are confined within the electric double layer and we found the same Soret coefficient as for the bare virus. In contrast to the bare *fd*-virus, the thermal diffusion coefficient, D_T, of the grafted *fd*-virus shows no Debye length dependence, which might be an indication that the thermal diffusion coefficient is less sensitive to interactions compared to the Soret coefficient, whereas the concentration dependence of $S_T = D_T/D$ is caused by the diffusion coefficient, D.

In this work we investigated the thermophoresis of four aqueous systems, which serve as biological relevant model systems. We found no correlation between thermodiffusion behavior and the structures of the solute molecules, but it turned out that the hydrophobic/hydrophilic balance and the quality of solvent play important roles. For all investigated systems we found that the Soret coefficient increases with increasing temperature. The analysis of the thermophoretic measurement of the polymer PEO in ethanol/water mixtures showed a clear correlation between the solvent quality and solvent-solvent and polymer-solvent interaction parameters. Good solvents lead to attractive interaction parameters and for bad solvents we found repulsive interactions. The thermophoretic behavior of the two investigated charged systems the aqueous alkali halide solutions and the charged colloidal rods dispersion can be described by computer simulation and a theoretical model, respectively. The fact that we observed only for the salt system a concentration dependence of the Soret coefficient and not for the *fd*-virus is related to the low *fd*-virus concentration. Compared to other effects such as the hydrophobic/hydrophilic balance or the chemical structure of the solute molecules the charge influence can be better reproduced by theory and simulations. Preliminary experiments of the grafted *fd*-virus indicate that the situation becomes more complicated, if the electrostatic interactions are screened by steric interactions. In order to understand

this behavior more experiments with grafted PEO chains of different lengths need to be performed.

BIBLIOGRAPHY

[1] P. A. Artola and B. Rousseau. Thermal diffusion in simple liquid mixtures: what have we learnt from molecular dynamics simulations? *Mol. Phys.*, 111(22-23):3394–3403, 2013.

[2] P. A. Artola, B. Rousseau, and G. Galliero. A new model for thermal diffusion: Kinetic approach. *J. Am. Chem. Soc.*, 130:10963–10969, 2008.

[3] P. Baaske, F. M. Weinert, S. Duhr, K. H. Lemke, M. J. Russell, and D. Braun. Extreme accumulation of nucleotides in simulated hydrothermal pore systems. *Proc. Natl. Acad. Sci. USA*, 104:9346–9351, 2007.

[4] P. Blanco, H. Kriegs, M. P. Lettinga, P. Holmqvist, and S. Wiegand. Thermal diffusion of a stiff rod-like mutant Y21M *fd*-virus. *Biomacromolecules*, (12):1602–1609, 2011.

[5] P. Blanco and S. Wiegand. Study of the Soret effect in monosaccharide solutions. *J. Phys. Chem. B*, 114(8):2807–2813, 2010.

[6] M. M. Bou-Ali and J. K. Platten. Metrology of the thermodiffusion coefficients in a ternary system. *J. Non-Equilib. Thermodyn.*, 30(4):385–399, 2005.

[7] D. Braun, N. L. Goddard, and A. Libchaber. Exponential DNA replication by laminar convection. *Phys. Rev. Lett.*, 91(15):158103, 2003.

[8] D. Braun and A. Libchaber. Thermal force approach to molecular evolution. *Phys. Biol.*, 1:P1–P8, 2004.

[9] S. L. Brimhall, M. N. Myers, K. D. Caldwell, and J. C. Giddings. High temperature thermal field-flow fractionation for the characterization of polyethylene. *Sep. Sci. Technol.*, 16:671–689, 1981.

[10] E. Bringuier. Simple ideas about thermodiffusion in a binary liquid mixture. *C.R. Mec.*, 341(4-5):365–371, 2013.

[11] E. Bringuier and A. Bourdon. Colloid transport in nonuniform temperature. *Phys. Rev. E*, 67:011404, 2003.

[12] E. Bringuier and A. Bourdon. Kinetic theory of colloid thermodiffusion. *Physica. A.*, 385:9–24, 2007.

[13] F. Brochard and P. G. de Gennes. Soret effect of flexible macromolecules. *Cr. Acad. Sci. II*, 293:1025–1027, 1981.

[14] H. Cabrera, L. Marti-Lopez, E. Sira, K. Rahn, and M. Garcia-Sucre. Thermal lens measurement of the Soret coefficient in acetone/water mixtures. *J. Chem. Phys.*, 131(3):Art. No. 031106, 2009.

[15] J. Chan, J. J. Popov, S. Kolisnek-Kehl, and D. G. Leaist. Soret coefficients for aqueous polyethylene glycol solutions and some tests of the segmental model of polymer thermal diffusion. *J. Solution Chem.*, 32(3):197–214, 2003.

[16] S. Chapman. The kinetic theory of a gas constituted of spherically symmetrical molecules. *Phil. Trans. Roy. Soc. London*, 211:433–483, 1912.

[17] K. Clusius and G Dickel. Zur trennung der chlorisotope. *Naturwissenschaften*, 27:148–149, 1939.

[18] H. Cölfen and M. Antonietti. Field-flow fractionation techniques for polymer and colloid analysis. In *New Developments in Polymer Analytics I*, volume 150 of *Advances in Polymer Science*, pages 67–187. 2000.

[19] J. Colombani, J. Bert, and J. Dupuy-Philon. Thermal diffusion in (LiCl,RH_2O). *J. Chem. Phys.*, 110(17):8622–8627, 1999.

[20] D. A. De Mezquia, M. M. Bou-Ali, M. Larranaga, J. A. Madariaga, and C. Santamaria. Determination of molecular diffusion coefficient in n-alkane binary mixtures: Empirical correlations. *J. Phys. Chem. B*, 116:2814–2819, 2012.

[21] C. Debuschewitz and W. Köhler. Molecular origin of thermal diffusion in benzene plus cyclohexane mixtures. *Phys. Rev. Lett.*, 87:4, 2001.

[22] J. K. G. Dhont. Thermodiffusion of interacting colloids. i. a statistical thermodynamics approach. *J. Chem. Phys.*, 120(3):1632–1641, 2004.

[23] J. K. G. Dhont. Thermodiffusion of interacting colloids. ii. a microscopic approach. *J. Chem. Phys.*, 120:1642–1653, 2004.

[24] J. K. G. Dhont and W. J. Briels. Single-particle thermal diffusion of charged colloids: Double-layer theory in a temperature gradient. *Eur. Phys. J. E*, 25:61–76, 2008.

[25] J. K. G. Dhont, S. Wiegand, S. Duhr, and D. Braun. Thermodiffusion of charged colloids: Single-particle diffusion. *Langmuir*, 23:1674–1683, 2007.

[26] Z. Dogic and S. Fraden. Development of model colloidal liquid crystals and the kinetics of the isotropic-smectic transition. *Phil. Trans. R. Soc. Lond. A*, 359(1782):997–1014, 2001.

[27] Z. Dogic and S. Fraden. Ordered phases of filamentous viruses. *Curr. Opin. Colloid Interface Sci.*, 11(1):47–55, 2006.

[28] S. Duhr, S. Arduini, and D. Braun. Thermophoresis of DNA determined by microfluidic fluorescence. *Eur. Phys. J. E*, 15:277–286, 2004.

[29] S. Duhr and D. Braun. Why molecules move along a temperature gradient. *P. Natl. Acad. Sci. USA*, 103:19678–19682, 2006.

[30] M. Eslamian and M. Z. Saghir. Dynamic thermodiffusion model for binary liquid mixtures. *Phys. Rev. E*, 80(1):11, 2009.

[31] M. Eslamian and M. Z. Saghir. Microscopic study and modeling of thermodiffusion in binary associating mixtures. *Phys. Rev. E*, 80(6):Art. No. 061201, 2009.

[32] B. Faissat, K. Knudsen, E. H. Stenby, and F. Montel. Fundamental statements about thermal-diffusion for a multicomponent mixture in a porous-medium. *Fluid Phase Equilib.*, 100:209–222, 1994.

[33] S. Fayolle, T. Bickel, and A. Würger. Thermophoresis of charged colloidal particles. *Phys. Rev. E*, 77, 2008.

[34] A. Firoozabadi, K. Ghorayeb, and K. Shukla. Theoretical model of thermal diffusion factors in multicomponent mixtures. *AlChE J.*, 46:892–900, 2000.

[35] F. S. Gaeta, G. Perna, G. Scala, and F. Bellucci. Nonisothermal matter transport in sodium chloride and potassium chloride aqueous solutions. 1. homogeneous system (thermal diffusion). *J. Phys. Chem.*, 86(15):2967–2974, 1982.

[36] J. C. Giddings, V. Kumar, P. S. Williams, and M. N. Myers. Polymer separation by

thermal field-flow fractionation - high- speed power programming. *Adv. Chem. Ser.*, (227):3–21, 1990.

[37] R. Haase. *Thermodynamics of irreversible Processes*. Dover, New York, 1990.

[38] B. Hafskjold. *Computer Simulations of Thermal Diffusion in Binary Fluid Mixtures*, volume 584, page 3. Springer, 2002.

[39] S. Hartmann, W. Köhler, and K. Morozov. The isotope Soret effect in molecular liquids: a quantum effect at room temperatures. *Soft Matter*, 8(5):1355–1360, 2012.

[40] S. Hartmann, G. Wittko, W. Kohler, K. I. Morozov, K. Albers, and G. Sadowski. Thermophobicity of liquids: Heats of transport in mixtures as pure component properties. *Phys. Rev. Lett.*, 109:065901–1–065901–4, 2012.

[41] M. Hartung, J. Rauch, and W. Köhler. Thermal diffusion of dilute polymer solutions: The role of solvent viscosity. *J. Chem. Phys.*, 125(21):214904, 2006.

[42] S. Iacopini and R. Piazza. Thermophoresis in protein solutions. *Europhys. Lett.*, 63(2):247–253, 2003.

[43] J. Janca, V. Kasparkova, V. Halabalova, L. Simek, J. Ruzicka, and E. Barosova. Microthermal field-flow fractionation of bacteria. *J. Chromatogr. B.*, 852:512–518, 2007.

[44] K. Kang and J. K. G. Dhont. Electric-field induced transitions in suspensions of charged colloidal rods. *Soft Matter*, 6:273–286, 2010.

[45] L. J. T. M. Kempers. A comprehensive thermodynamic theory of the Soret effect in a multicomponent gas, liquid, or solid. *J. Chem. Phys.*, 115:6330–6341, 2001.

[46] Y. Kishikawa, S. Wiegand, and R. Kita. Temperature dependence of Soret coefficient in aqueous and nonaqueous solutions of pullulan. *Biomacromolecules*, 11(3):740–747, 2010.

[47] R. Kita, S. Wiegand, and J. Luettmer Strathmann. Sign change of the Soret coefficient of poly(ethylene oxide) in water/ethanol mixtures observed by tdfrs. *J. Chem. Phys.*, 121(8):3874–3885, 2004.

[48] M. Klein and S. Wiegand. The Soret effect of mono-, di- and tri-glycols in ethanol. *Phys. Chem. Chem. Phys.*, 13(15):7059–7063, 2011.

[49] W. Köhler and R. Schäfer. *Polymer analysis by thermal-diffusion forced Rayleigh scattering*, volume 151 of *Advances in Polymer Science*, pages 1–59. 2000.

[50] P. Kolodner, H. Williams, and C. Moe. Optical measurement of the Soret coefficient of ethanol water solutions. *J. Chem. Phys.*, 88(10):6512–6524, 1988.

[51] A. Königer, B. Meier, and W. Köhler. Measurement of the Soret, diffusion, and thermal diffusion coefficients of three binary organic benchmark mixtures and of ethanol-water mixtures using a beam deflection technique. *Philos. Mag.*, 89(10):907–923, 2009.

[52] A. Königer, H. Wunderlich, and W. Köhler. Measurement of diffusion and thermal diffusion in ternary fluid mixtures using a two-color optical beam deflection technique. *J. Chem. Phys.*, 132(17):–, 2010.

[53] C. Ludwig. Diffusion zwischen ungleich erwärmten orten gleich zusammengesetzter lösungen. *Sitz. ber. Akad. Wiss. Wien Math.-naturw. Kl*, 20:539, 1856.

[54] J. Luettmer-Strathmann. Lattice model for thermodiffusion in polymer solutions. *International Journal of Thermophysics*, 26:1693–1707, 2005.

[55] C. B. Mast, N. Osterman, and D. Braun. Thermal solutions for molecular evolution. *Int. J. Mod. Phys. B*, 26:1230017–1–1230017, 2012.

[56] C. B. Mast, S. Schink, U. Gerland, and D. Braun. Escalation of polymerization in a thermal gradient. *Proc. Natl. Acad. Sci. USA*, 110(20):8030–8035, 2013.

[57] K. I. Morozov. Thermal diffusion in disperse systems. *J. Exp. Theor. Phys.*, 88(5):944–946, 1999.

[58] P. Naumann, A. Martin, H. Kriegs, M. Larranaga, M. M. Bou-Ali, and S. Wiegand. Development of a thermogravitational microcolumn with an interferometric contact less detection system. *J. Phys. Chem. B*, 116(47):13889–13897, 2012.

[59] C. Nieto-Draghi, J. B. Avalos, and B. Rousseau. Computing the Soret coefficient in aqueous mixtures using boundary driven nonequilibrium molecular dynamics. *J. Chem. Phys.*, 122, 2005.

[60] H. Ning, S. Datta, T. Sottmann, and S. Wiegand. Soret effect of nonionic surfactants in water studied by different transient grating setups. *J. Phys. Chem. B*, 112(35):10927–10934, 2008.

[61] H. Ning, J. K. G. Dhont, and S. Wiegand. Thermal-diffusive behavior of a dilute solution of charged colloids. *Langmuir*, 24:2426–2432, 2008.

[62] H. Ning and S. Wiegand. Experimental investigation of the Soret effect in acetone/water

and dimethylsulfoxide/water mixtures. *J. Chem. Phys.*, 125(22):221102, 2006.

[63] K. Okabe, N. Inada, C. Gota, Y. Harada, T. Funatsu, and S. Uchiyama. Intracellular temperature mapping with a fluorescent polymeric thermometer and fluorescence lifetime imaging microscopy. *Nat. Commun.*, 3, 2012.

[64] A. Parola and R. Piazza. Particle thermophoresis in liquids. *Eur. Phys. J. E*, 15:255–263, 2004.

[65] R. Piazza and A. Guarino. Soret effect in interacting micellar solutions. *Phys. Rev. Lett.*, 88(20):208302, 2002.

[66] R. Piazza, S. Iacopini, and B. Triulzia. Thermophoresis as a probe of particle-solvent interactions: The case of protein solutions. *Phys. Chem. Chem. Phys.*, 6:1616–1622, 2004.

[67] R. Piazza and A. Parola. Thermophoresis in colloidal suspensions. *J. Phys. Condens. Mat.*, 20:153102, 2008.

[68] J. K. Platten. The Soret effect: A review of recent experimental results. *J. Appl. Mech-T. Asme.*, 73:5–15, 2006.

[69] P. Polyakov, J. Luettmer-Strathmann, and S. Wiegand. Study of the thermal diffusion behavior of alkane/benzene mixtures by thermal diffusion forced Rayleigh scattering experiments and lattice model calculations. *J. Phys. Chem. B*, 110(51):26215–26224, 2006.

[70] P. Polyakov, E. Rossinsky, and S. Wiegand. Study of the Soret effect in hydrocarbon chain/aromatic compound mixtures. *J. Phys. Chem. B*, 113:13308–13312, 2009.

[71] P. Polyakov and S. Wiegand. Systematic study of the thermal diffusion in associated mixtures. *J. Chem. Phys.*, 128(3):034505, 2008.

[72] P. Polyakov, M. Zhang, F. Müller-Plathe, and S. Wiegand. Thermal diffusion measurements and simulations of binary mixtures of spherical molecules. *J. Chem. Phys.*, 127(1):014502, 2007.

[73] I. Prigogine, L. Debrouckere, and R. Amand. Recherches sur la thermodiffusion en phase liquide .1. *Physica*, 16(7-8):577–598, 1950.

[74] K. Purdy. *Liquid Crystal Phase Transitions of Monodisperse and Bidisperse Suspensions of Rodlike Colloidal Virus.* PhD thesis, Brandeis University, 2004.

[75] S. A. Putnam, D. G. Cahill, and G. C. L. Wong. Temperature dependence of thermodiffusion in aqueous suspensions of charged nanoparticles. *Langmuir*, 23(18):9221–9228, 2007.

[76] J. Rauch and W. Köhler. On the molar mass dependence of the thermal diffusion coefficient of polymer solutions. *Macromolecules*, 38(9):3571–3573, 2005.

[77] B. C. Reed. Liquid thermal diffusion during the manhattan project. *Phys. Perspect.*, 13:161–188, 2011.

[78] M. Ripoll, P. Holmqvist, R. G. Winkler, G. Gompper, J. K. G. Dhont, and M. P. Lettinga. Attractive colloidal rods in shear flow. *Phys. Rev. Lett.*, 101:168302–1–168302–4, 2008.

[79] P. Rossmanith and W. Köhler. Polymer polydispersity analysis by thermal diffusion forced Rayleigh scattering. *Macromolecules*, 29(9):3203–3211, 1996.

[80] W. M. Rutherford. Effect of mass distribution on the isotopic thermal diffusion of substituted benzenes. *J. Chem. Phys.*, 81(12):6136–6139, 1984.

[81] J. Sambrook and D. Russell. *Molecular Cloning: A Laboratory Manual*. Cold Spring Harbor Lab Press: New York, 2001.

[82] M. E. Schimpf and J. C. Giddings. Characterization of thermal diffusion in polymer solutions by thermal field-flow fractionation: effects of molecular weight and branching. *Macromolecules*, 20(7):1561–1563, 1987.

[83] M. E. Schimpf and J. C. Giddings. Characterization of thermal diffusion in polymer solutions by thermal field-flow fractionation: dependence on polymer and solvent parameters. *J Polym. Sci. Pol. Phys.*, 27:1317–1332, 1989.

[84] M. E. Schimpf and S. N. Semenov. Mechanism of polymer thermophoresis in nonaqueous solvents. *J. Phys. Chem. B*, 104:9935–9942, 2000.

[85] S. A. I. Seidel, P. M. Dijkman, W. A. Lea, G. Van Den Bogaart, M. Jerabek-Willemsen, A. Lazic, J. S. Joseph, P. Srinivasan, P. Baaske, A. Simeonov, I. Katritch, F. A. Melo, J. E. Ladbury, G. Schreiber, A. Watts, D. Braun, and S. Duhr. Microscale thermophoresis quantifies biomolecular interactions under previously challenging conditions. *Methods*, 59(3):301–315, 2013.

[86] G. H. Thompson, M. N. Myers, and J. C. Giddings. An observation of a field-flow fractionation effect with polystyrene samples. *Sep. Sci.*, 2:797–800, 1967.

[87] C. Vega and J. L. F. Abascal. Simulating water with rigid non-polarizable models: A general perspective. *Phys. Chem. Chem. Phys.*, 13:19663–19688, 2011.

[88] S. Villain-Guillot and A. Würger. Thermal diffusion in a binary liquid due to rectified molecular fluctuations. *Phys. Rev. E*, 83(3):030501, 2011.

[89] S. Wiegand. Thermal diffusion in liquid mixtures and polymer solutions. *J. Phys.: Condens. Matter*, 16:R357–R379, 2004.

[90] C. J. Wienken, P. Baaske, U. Rothbauer, D. Braun, and S. Duhr. Protein-binding assays in biological liquids using microscale thermophoresis. *Nat. Commun.*, 1:100, 2010.

[91] G. Wittko and W. Köhler. Universal isotope effect in thermal diffusion of mixtures containing cyclohexane and cyclohexane-d(12). *J. Chem. Phys.*, 123(1), 2005.

[92] A. Würger. Molecular-weight dependent thermal diffusion in dilute polymer solutions. *Phys. Rev. Lett.*, 102:078302, 2009.

[93] A. Würger. Thermal non-equilibrium transport in colloids. *Rep. Prog. Phys.*, 73:126601, 2010.

[94] M. Yang and M. Ripoll. Simulations of thermophoretic nanoswimmers. *Phys. Rev. E*, 84(6):061401, 2011.

[95] K. J. Zhang, M. E. Briggs, R. W. Gammon, and J. V. Sengers. Optical measurement of the Soret coefficient and the diffusion coefficient of liquid mixtures. *J. Chem. Phys.*, 104(17):6881–6892, 1996.

[96] M. Zhang and F. Müller-Plathe. The Soret effect in dilute polymer solutions: Influence of chain length, chain stiffness, and solvent quality. *J. Chem. Phys.*, 125:124903, 2006.

[97] M. M. Zhang and F. Müller-Plathe. Reverse nonequilibrium molecular-dynamics calculation of the Soret coefficient in liquid benzene/cyclohexane mixtures. *J. Chem. Phys.*, 123(12):124502, 2005.

[98] Z. Zhang, J. Buitenhuis, A. Cukkemane, M. Brocker, M. Bott, and J. K. G. Dhont. Charge reversal of the rodlike colloidal *fd* virus through surface chemical modification. *Langmuir*, 26(13):10593–10599, 2010.

[99] K. Zillner, M. Jerabek-Willemsen, S. Duhr, D. Braun, G. Laengst, and P. Baaske. *Microscale Thermophoresis as a Sensitive Method to Quantify Protein: Nucleic Acid Interactions in Solution*, volume 815 of *Methods in Molecular Biology*, pages 241–252.

2012.

ACKNOWLEDGEMENT

It would not have been possible to write this doctoral thesis without the help and support of the kind people around me, to only some of whom it is possible to give particular mention here.

First and foremost I would like to thank Prof. Jan K. G. Dhont, my scientific idol, for giving me the chance to do my PhD in the wonderful group ICS-3. He is always there for the group, patient and helpful, providing us perfect working conditions and strong theoretical support.

I would like to express my gratitude to Prof. Annette Schmidt. Without her it would be impossible to proceed my PhD defense in University of Cologne. I would like also to thank Prof. Hans-Günther Schmalz for taking the chair of my examination committee.

I wish to express my special appreciation and thanks to my supervisor Dr. Simone Wiegand for her inspiring advice and selfless help. I will never forget the time we spent together in front of her computer, improving my papers or practising my presentations. The knowledge and experience I learned from her is the priceless wealth for my life.

I thank Prof. Wim Briels, Dr. Fernando Bresme, Dr. Frank Römer and Dr. Mounir Bou-Ali for the international collaborations and discussions.

My sincere thanks also go to Dr. Hartmut Kriegs. He spent a lot of time in the dark lab and in front of computer to help me with the alignment of the setup and data evaluation. I would like to thank Dr. Johan Buitenhuis for the instruction of the chemistry lab and preparing PEO coated *fd*-virus. Further I want to thank Dr. Peter Lang and Prof. Pavlik Lettinga for their fruitful discussions. I would also like to thank Dr. Marisol Ripoll and Karl Flören for correcting my thesis.

I would like to thank all the people in ICS-3, especially Philipp and Dzmitry for the pleasant time working together, Manolis for his companion always in the late working hours and wise life tips, Jonas and Rafael for their help on Latex and of course Yunfei, Silvia and Yi for all the laughs. I would also like to thank the senior students Bastian, Christoph and Donald for their useful experience and kind help. And I should not forget to thank Danni and Minjie for their contribution in the PEO work.

At the end I want to thank my beloved parents for the unconditional love and care. I thank my boyfriend for the support and encouragement for the years.

PUBLICATIONS

• **Wang, Z.**, Afanasenkau, D., Dong, M., Huang, D. and Wiegand, S., Molar mass and temperature dependence of the thermodiffusion of polyethylene oxide in water/ethanol mixtures. *J. Chem. Phys.*, 141(6), 064904, 2014.

• Alonso de Mezquia, **Wang, Z.**, Lapeira, E., Klein, M., Wiegand, S. and Bou-Ali, M. M., Thermodiffusion, molecular diffusion and Soret coefficient of binary and ternary mixtures of *n*-Hexane, *n*-dodecane and toluene. *Eur. Phys. J. E*, accepted.

• **Wang, Z.**, Kriegs, H., Buitenhuis, J., Dhont, J. K. G. and Wiegand, S., Thermophoresis of charged colloidal rods. *Soft Matter*, 9(36), 8697-8704, 2013.

• Römer, F., **Wang, Z.**, Wiegand, S. and Bresme, F., Alkali halide solutions under thermal gradients: Soret coefficients and heat transfer mechanisms. *J. Phys. Chem. B*, 117(27), 8209-8222, 2013.

• **Wang, Z.**, Kriegs, H. and Wiegand, S., Thermal diffusion of nucleotides. *J. Phys. Chem. B*, 116(25), 7463-7469, 2012.

DECLARATION OF INDIVIDUAL CONTRIBUTION

Article no. 1

Title: Thermal diffusion of nucleotides

Corresponding Thesis Chapter: Chapter 2

Status: Published

Wang, Z., Kriegs, H. and Wiegand, S., Thermal diffusion of nucleotides, *J. Phys. Chem. B*, 116(25), 7463-7469, 2012.

The independent contribution of the candidate:
I have worked on thermal diffusion of nucleotides with guidance from PD Dr. Simone Wiegand. All the experiments and data analysis have been done 100 % by me. The interpretation of the data and preparation of the manuscript in majority (~ 80%) has been done by me with guidance from PD Dr. Simone Wiegand.

Article no. 2

Title: Alkali halide solutions under thermal gradients: Soret coefficients and heat transfer mechanisms

Corresponding Thesis Chapter: Chapter 3

Status: Published

Römer, F., **Wang, Z.**, Wiegand, S. and Bresme, F., Alkali halide solutions under thermal gradients: Soret coefficients and heat transfer mechanisms, *J. Phys. Chem. B*, 117(27), 8209-8222, 2013.

The independent contribution of the candidate:
This collaborative project on alkali halide solutions under thermal gradients has been initiated by Dr. Frank Römer and Dr. Fernando Bresme. The experiments and analysis of the experimental data have been done 100% by me. The experimental section and part of the discussion section have been written by me. Figure 1 and 7 have been prepared by me.

Article no. 3

Title: Thermophoresis of charged colloidal rods,

Corresponding Thesis Chapter: Chapter 4

Status: Published

Wang, Z., Kriegs, H., Buitenhuis, J., Dhont, J. K. G. and Wiegand, S. Thermophoresis of charged colloidal rods, *Soft Matter*, 9(36), 8697-8704, 2013.

The independent contribution of the candidate:
I have worked on thermal diffusion of charged colloidal rods with guidance from PD Dr.

Simone Wiegand and Prof. Jan Dhont. All the experiments and data analysis have been done 100 % by me. The theory development has been done by Prof. Jan Dhont. The preparation of the manuscript has been done ~ 60% by me.

Article no. 4

Title: Molar mass and temperature dependence of the thermodiffusion of polyethylene oxide in water/ethanol mixtures

Corresponding Thesis Chapter: Chapter 5

Status: Submitted

Wang, Z., Afanasenkau, D., Dong, M., Huang, D. and Wiegand, S., Molar mass and temperature dependence of the thermodiffusion of polyethylene oxide in water/ethanol mixtures. *J. Chem. Phys.*, submitted.

The independent contribution of the candidate:
The project aims at the molar mass and solvent dependence of thermodiffusion of biocompatible polymer. The design of this project was initiated by PD Dr. Simone Wiegand. I have done ~ 50% of the experiments. The rest of experiments have been done by Danni Huang and Minjie Dong, who were supervised by me. ~ 80% of the data analysis has been done by me. The interpretation of experimental data and preparation of the manuscript has been done ~ 60% by me.

ERKLÄRUNG

Ich versichere, dass ich die von mir vorgelegte Dissertation selbständig angefertigt, die benutzten Quellen und Hilfsmittel vollständig angegeben und die Stellen der Arbeit - einschließlich Tabellen, Karten und Abbildungen -, die anderen Werken im Wortlaut oder dem Sinn nach entnommen sind, in jedem Einzelfall als Entlehnung kenntlich gemacht habe; dass diese Dissertation noch keiner anderen Fakultät oder Universität zur Prüfung vorgelegen hat; dass sie - abgesehen von angegebenen Teilpublikationen - noch nicht veröffentlicht worden ist sowie, dass ich eine solche Veröffentlichung vor Abschluß des Promotionsverfahrens nicht vornehmen werde. Die Bestimmungen dieser Promotionsordnung sind mir bekannt. Die von mir vorgelegte Dissertation ist von Prof. Dr. A. Schmidt betreut worden.

1. **Wang, Z.**, Kriegs, H., Buitenhuis, J., Dhont, J. K. G. and Wiegand, S.
   Thermophoresis of charged colloidal rods,
   Soft Matter, 9(36), 8697-8704, 2013.

2. Römer, F., **Wang, Z.**, Wiegand, S. and Bresme, F.,
   Alkali halide solutions under thermal gradients: Soret coefficients and heat transfer mechanisms,
   J. Phys. Chem. B, 117(27), 8209-8222, 2013.

3. **Wang, Z.**, Kriegs, H. and Wiegand, S.,
   Thermal diffusion of nucleotides,
   J. Phys. Chem. B, 116(25), 7463-7469, 2012.